2019

# Nutritional Transporter Mediated Drug Delivery for Cancer

Siddharth S. Kesharwani
*South Dakota State University*

# NUTRITIONAL TRANSPORTER MEDIATED DRUG DELIVERY FOR CANCER

BY

SIDDHARTH S. KESHARWANI

A dissertation submitted in partial fulfillment of the requirements for the

Doctor of Philosophy

Major in Pharmaceutical Sciences

South Dakota State University

2019

NUTRITIONAL TRANSPORTER MEDIATED DRUG DELIVERY FOR CANCER

BY

SIDDHARTH S. KESHARWANI

This dissertation is approved as a creditable and independent investigation by a candidate for the Doctor of Philosophy in Pharmaceutical Sciences degree and is acceptable for meeting the dissertation requirements for this degree. Acceptance of this does not imply that the conclusions reached by the candidate are necessarily the conclusions of the major department.

Hemachand Tummala, Ph.D. Date
Dissertation Advisor

Omathanu Perumal, Ph.D. Date
Head, Department of Pharmaceutical Sciences

Dean, Graduate School Date

THIS DISSERTATION IS DEDICATED TO MY PARENTS AND SISTER

# ACKNOWLEDGEMENTS

There have been so many individuals who have positively contributed throughout my graduate education and research at South Dakota State University (SDSU). I would like to thank and show my heartfelt gratitude to all those people for their assistance, support, guidance, and motivation.

First, I would like to express my sincere appreciation and thank you to Dr. Hemachand Tummala for his support, guidance, motivation, and supervision during my Ph.D. I will be grateful to him for giving me the opportunity to pursue a Ph.D. in his laboratory, learn various techniques, as well as work on multiple projects during my Ph.D. training. My sincere appreciation and heartfelt gratitude to Dr. Jayarama Bhat Gunaje for his constant motivation, support, advice, guidance, and contribution to my personal and professional development. I am thankful to my Ph.D. advisory committee members; Dr. Wenfeng An, Dr. Xiangming Guan, Dr. Keith Miskimins, and Dr. Lloyd Metzger for their valuable suggestions, continued support and motivation. I would also like to thank Dr. Michael Wimberly and Dr. Lara Prihodko my previous graduate faculty representatives for their contributions.

I am also thankful to Dr. Dennis D. Hedge, the former Dean of the College of Pharmacy & Allied Health Professions, Dr. Jane Mort, the current Dean of the College of Pharmacy and Allied Health Professions, Dr. Omathanu Perumal, Professor and Head of the Department of Pharmaceutical Sciences and the staff (especially Emily Trias, Sarah Vaa, Vickie Prussman and Jolene Landmark) at the College of Pharmacy & Allied Health Professions, SDSU for the opportunity to pursue my graduate education, help and support. I will always be grateful to all the faculty members and course instructors who helped me to gain advanced knowledge and skills in the pharmaceutical sciences at SDSU. I am also

thankful to Dr. Komal Raina for helping with intravenous injections for mice study. In addition, I am also thankful to our collaborators Dr. Samir Mitragotri (Harvard University), Dr. Amar Singh (University of Nebraska Medical Center) and Dr. Abhay T. Sangamwar (NIPER, Mohali-India) and their lab members for their contribution and support. I would like to thank the Animal Resource Wing at SDSU, Sanford Research, and the Regional Blood Bank, Sioux Falls, SD for their help with animal research, flow cytometry, and blood samples.

Further, I am thankful to my past and current fellow graduate students, all my previous and current lab members including Mr. Pratik Muley, Dr. Mrigendra Rajput, Dr. Mohit Tyagi, Dr. Mohammed Ali Bakkari, Mr. Chaitanya Valiveti, Ms. Addyson Rosa, and Ms. Susmitha Narisetty for their help and support. I would like to especially thank and acknowledge Mr. Pratik Muley for his help, support, guidance, and training on experimental techniques during my initial years of Ph.D.

Finally, I am expressing my sincere gratitude and utmost respect to my parents, Mr. Shivkumar D. Kesharwani, and Mrs. Sushma S. Kesharwani, and my elder sister Dr. Pooja Kesharwani for their continuous motivation, support, encouragement, advice, affection, love and well wishes to pursue my higher education. I am always fortunate to have great friends (Swagat, Sonali, Foram, Suswara, Nishidh, Nisarg, Shegan, Nilkanth, and Aakash) around me who supported me through thick and thin of my life.

I will always remain grateful to the Department of Pharmaceutical Sciences, College of Pharmacy & Allied Health Professions at SDSU for providing me assistantship and research facility to support my graduate education and research.

TABLE OF CONTENTS

# LIST OF ABBREVIATIONS

| | |
|---|---|
| US | United States |
| NPs | Nanoparticles |
| EPR | Enhanced permeability and retention |
| VEGF | Vascular endothelial growth factor |
| MPS | Mononuclear phagocytic system |
| HER-2 | Human epidermal growth factor receptor 2 |
| TfR | Transferrin receptor |
| EGFR | Epidermal growth factor receptor |
| FGF | Fibroblast growth factors |
| SR | Sigma receptors |
| BnR | Bombesin receptor |
| NMB | Neuromedin B receptor |
| GRP | Gastrin-releasing peptide |
| SSTR | Somatostatin receptor |
| ETR | Endothelin receptor |
| LDL | Low-density lipoprotein |
| FSHR | Follicle-stimulating hormone receptor |
| BR | Biotin receptor |
| CLR | C-type lectin receptor |
| ASGPR | Asialoglycoprotein receptor |
| NRP-1 | Neuropilin 1 |

| | |
|---|---|
| RES | Reticuloendothelial system |
| PEG | Polyethylene glycol |
| RBCs | Red blood cells |
| HPMA | N-(2-hydroxypropyl) methacrylamide |
| P-gp | P-glycoprotein |
| MRP1 | Multidrug resistance-associated protein 1 |
| BCRP | Breast cancer resistance protein |
| ADME | Absorption, distribution, metabolism, and excretion |
| ABC | ATP binding cassette transporters |
| SLC | Solute carrier transporters |
| ATP | Adenosine triphosphate |
| PET | Positron emission tomography |
| FDG | 2-[fluorine-18]-fluoro-2-deoxy-D-glucose |
| SGLTs | Sodium-dependent glucose transporters |
| MFS | Major facilitator superfamily |
| (HIF-1) | Hypoxia-inducible factor-1 |
| HCC | Hepatocellular carcinoma |
| PSA | Prostate-specific antigen |
| ABC | Accelerated blood clearance |
| HA | Hydroxylamine |
| EDC | 1-Ethyl-3-(3-dimethylaminopropyl) carbodiimide |
| GLU | 2-amino-2-deoxy-D-glucose |
| ATCC | American Type Culture Collection |

| | |
|---|---|
| RPMI-1640 | Roswell Park Memorial Institute |
| FBS | Fetal bovine serum |
| IACUC | Institutional Animal Care and Use Committee |
| DLS | Dynamic Light Scattering |
| SEM | Scanning electron microscope |
| PAGE | Polyacrylamide gel electrophoresis |
| Ig | Immunoglobulin |
| THF | Tetrahydrofuran |
| PBS | Phosphate buffered saline |
| IR | Infrared |
| Pa | Pascal |
| WHO | World Health Organization |
| PDI | Polydispersity index |
| NHS | N-Hydroxysuccinimide |
| PFA | Paraformaldehyde |
| DAPI | 4′,6-diamidino-2-phenylindole |
| PMSF | Phenylmethylsulfonyl fluoride |
| Lamp1 | Lysosomal associated membrane protein 1 |
| GFP | Green fluorescent protein |
| FTIR | Fourier transform infrared |
| NMR | Nuclear magnetic resonance |
| PXRD | Powder X-ray diffraction |
| DCM | Dichloromethane |

LIST OF FIGURES

**CHAPTER I**



**CHAPTER II**

**CHAPTER III**

# LIST OF TABLES

**CHAPTER I**



**CHAPTER II**



**CHAPTER III**

# ABSTRACT

NUTRITIONAL TRANSPORTER MEDIATED DRUG DELIVERY FOR CANCER

SIDDHARTH S. KESHARWANI

2019

Recent advancements in nanotechnology have unfolded novel opportunities in medicine, especially in targeted therapeutics and imaging for cancer. However, the majority of the existing nanotechnologies for cancer suffer from shortcomings such as (i) rapid elimination from the systemic circulation before reaching the cancer tissue. (ii) poor tumor accumulation, targeting, and penetration due to inadequate vasculature and extensive extracellular matrix in the tumor. Thus, overcoming these two limitations of nanotechnology is of considerable interests for cancer researchers.

In this dissertation, we demonstrate the feasibility of glucose-modified nanoparticles (GLU-NPs) as an efficient cancer targeted-delivery system for enhancing the systemic circulation time and tumor accumulation.

In **chapter II**, using a natural physiological interaction between glucose on the GLU-NPs and the surface glucose transporter GLUT1 on the RBCs, we have demonstrated the enhancement of systemic circulation time and thereby, improved tumor accumulation. GLU-NPs interaction with GLUT1 is non-covalent, reversible and importantly, established *in-vivo*. GLU-NPs enhanced the circulation time by hitchhiking on RBCs and reducing opsonization.

In **chapter III**, we have demonstrated the ability of GLU-NPs to differentiate breast cancer versus noncancer cells based on the expression levels of GLUT1. GLUT1 is

overexpressed in multiple cancer types, and the level of expression is correlated with the invasiveness of cancer. GLU-NPs were able to deliver significantly large amounts of encapsulated cargo to breast cancer cells potentially through caveolae-mediated endocytosis. The *in-vivo* tumor imaging results depict that the GLU-NPs highly accumulated into tumors compared to state-of-art technology PEGylation.

In summary, we have demonstrated the ability of GLU-NPs as a smart drug delivery system for *in-vivo* enhancement of systemic circulation time and tumor accumulation, which will have applications beyond cancer therapy and imaging, such as sustained drug delivery and targeting to other organs.

# CHAPTER I

# INTRODUCTION

### 1.1. Cancer: Current Therapies and Challenges

Cancer, the second leading cause of mortalities in the United States (US), is a heterogeneous group of diseases involving complex molecular alterations at the cellular level and the exact causes of which are difficult to deduce [1, 2]. It occurs in a wide range of tissues with different outcomes. For example, in the US, there are approximately 200 types of cancers, with lung, breast, prostate and colon cancer accounting for the majority of the mortalities. The number of cancer patients being diagnosed is expected to be doubled by the next two decades [1-4]. One out of three people will develop malignancies in their lifetime, with half of the people diagnosed with cancer dying within the five years of the occurrence of the disease [5]. It is predicted that approximately 1.5-1.9 million new cancer cases will be diagnosed in the U.S. in 2019 [1-5].

The current clinical management of cancer involves surgery, radiotherapy, chemotherapy, targeted drug therapies and more recently immunotherapy and gene therapy. Chemotherapy has been widely utilized for the clinical management of cancer mainly affecting cell cycle arrest and/or apoptosis [6-8]. The clinical therapy of cancer using traditional drugs is not satisfactory due to their high toxicity and occurrence of drug resistance [3, 4, 9, 10]. Chemotherapy fails to distinguish between normal and cancer tissues to a significant level to avoid severe toxicity [11, 12]. One of the primary goals of the current research in cancer therapeutics is to either identify cancer-specific targets *(targeted therapies)* or to deliver the chemotherapeutic drugs specifically to the cancer cells *(targeted drug delivery)* [13, 14]. Discovering new cancer targets and developing new drugs that specifically act on these targets is an expensive, time-consuming and cumbersome process [15, 16]. This is further complicated by the high mutation rates of

cancer cells that quickly alter the drug target to develop drug resistance [12, 17-20]. However, several barriers to cancer drug delivery complicate the efforts for targeted drug delivery [21]. Figure 1-1 provides various biological, physiological, physiochemical, and clinical barriers towards the development of therapeutics to cancers. Nanomedicine provides unique advantages in overcoming some of the listed challenges for cancer drug delivery [9, 10, 17, 22-30].

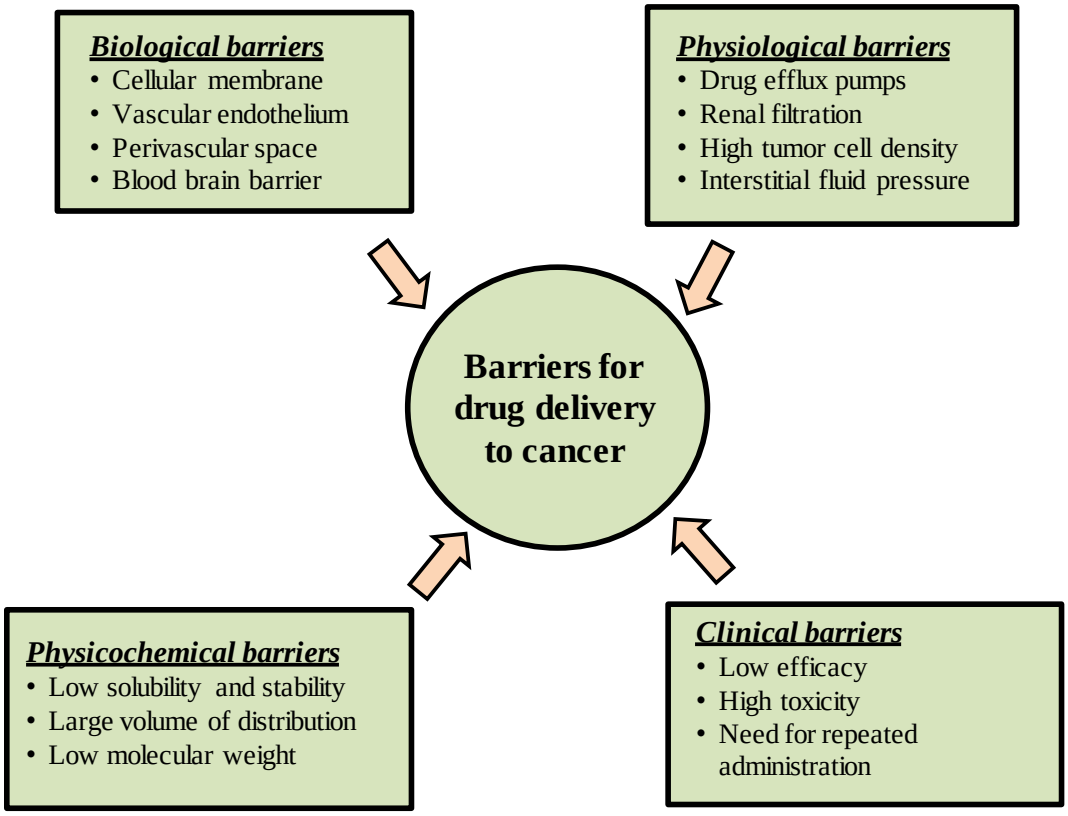


**Figure 1-1:** Various biological, physiological, physiochemical, and clinical barriers towards the delivery of therapeutics to cancers [17, 28, 30].

### 1.2. Nanomedicine and its Application for Cancer-targeted Drug Delivery

Effective drug delivery is a critical factor in developing treatments for cancer. Restricted accessibility to tumor tissues due to excess extracellular matrix, poor vasculature along with the limited systemic circulation time, and non-specific distribution of anti-cancer drugs poses a unique challenge to deliver therapeutic levels of cancer drugs to the target tissues. Inefficient delivery of anti-cancer drugs lead to poor tumor response, causes severe side effects, and promotes the development of cancer drug resistance. Due to the development of drug resistance, drugs that show favorable initial response are often rendered ineffective following repeated administrations, and the relapsed cancer becomes much more difficult to treat. Furthermore, due to the cytotoxic nature of chemotherapeutic drugs on both cancer and healthy cells, the drug dosage should be restricted to cancer cells to avoid adverse effects on healthy cells [6, 7, 9, 10, 13, 14, 17, 22-25, 28, 31-33]. To effectively treat cancers and minimize the effect of developing resistance, high doses of potent therapeutics are needed to be safely delivered to cancer sites. Nanotechnology offers unique physical and chemical properties that are beneficial in the targeted delivery of chemotherapeutic agents to the cancer tissue.

Nanotechnology is at the forefront of drug delivery research, providing innovative approaches for the diagnosis, treatment, prevention and the management of various diseases, including cancer [3, 4, 22, 26, 34]. Nanotechnology provides nanoscale drug delivery vehicles including organic, polymeric, metallic and solid–lipid nanoparticles, micelles, liposomes, dendrimers, etc. Several of these are either currently approved or undergoing investigations for the delivery of a variety of small and macromolecular drugs [28, 34]. Nanoparticles (NPs) are 1-100 nm in diameter; however, submicron particles are

also often included in this category. Nanocarriers provide unique advantages for cancer drug delivery such as improved cancer targeting, reduced non-specific cellular uptake, controlled drug release, ability to carry multiple drugs, protection of the cargo (drugs/imaging agents) from the adverse biological environments during their transit and delivery to cancer tissues [33].

**Characteristics of an ideal cancer-targeted nanomedicine:** [17, 28, 30]

i. An ability to carry therapeutic levels of the drug.
ii. Provide an injectable form (intravenous) for a poorly soluble drug either by improving its solubility or dispersibility.
iii. Biodegradable and biocompatible.
iv. Avoid premature clearance from the circulation.
v. Minimal drug leakage from the nanocarrier during its transit to the target tissue.
vi. Protect the drug from degradation during storage and transit to the target after injection.
vii. Increase the localization of the drug to the target tissue while minimizing off-target distribution/toxicity (drug targeting).
viii. Enhance cellular uptake and promote intracellular trafficking to deliver the drug to the target molecule.
ix. Low rate of aggregation (physical stability).

In nanomedicine, targeting refers to designing nanocarriers that take advantage of the differences between cancer and the normal cells, with the intention of increasing the accumulation and penetration in cancer tissues as compared to healthy tissues. There are two different ways for the delivery of drugs: *passive targeting* (nanomedicine equipped

without any targeting ligand) and *active targeting* (nanomedicine equipped with a targeting ligand) [14, 28, 30, 31, 33, 35-38].

### *1.2.1. Passive Targeting to Cancer*

Passive targeting essentially refers to preferential accumulation of drug/nanomedicine in the cancer tissues due to the unique physicochemical properties of nanomedicine combined with the altered anatomical structures in cancer contributing to enhanced permeation and retention (EPR effect) [17, 30, 32, 33, 39].

#### *1.2.1.1. Enhanced Permeability and Retention (EPR) Effect*

The normal tissues are characterized by continuous capillaries with the small pore radii being 6-7 nm and the large pore radii being 20-28 nm. To serve the needs of the rapidly growing cancerous tissues, through the release of vascular endothelial growth factor (VEGF) and other factors by the cancer cells, rapid vascularization is promoted. Such rapid vascularization often leads to a leaky and defective vascular architecture devoid of the basement membrane and impaired lymphatic drainage. The abnormal fenestrations in the cancer vasculature allow nanocarriers to leak into cancerous tissues, sparing the normal tissues [40, 41]. Since cancer tissues lack a well-developed lymphatic drainage capability, NPs that enter are retained within the tissues for prolonged periods of time. This phenomenon is called as the enhanced permeability and retention (EPR) effect and Matsumura *et al.* were the first to describe it [42].

EPR effect is applicable to all solid tumors. It is observed in almost all types of human cancers with the exception of prostate and pancreatic cancer [17]. Passive targeting through EPR effect is seen in small and well-vascularized cancers; however, accumulation

is often inadequate in poorly vascularized cancer tissues. Moreover, vessel permeability might differ within a single solid tumor, resulting in non-uniform drug profusion and incomplete cancer treatment. Moreover, passive targeting suffers from certain limitations such as: (i) the extent of passive targeting depends on angiogenesis and the degree of tumor vasculature which usually varies between patients and the tumor types. (ii) In the case of solid tumors, the high interstitial fluid pressure avoids the entry and homogeneous drug distribution into the tumors [43, 44].

To exploit the EPR effect, it requires the NPs to have a specific size range and shape (physiochemical properties). In addition, the NPs must be in circulation for a significant duration for them to pass through leaky vasculature of cancer. However, the immune system perceives exogeneous NPs as foreign and eliminates them quickly through mononuclear phagocytic systems (MPS). Studies in mouse xenograft have shown that the vasculature can permit extravasation of particles 10-200 nm in diameter with limited studies showing EPR effect up to 500 nm in diameter [45, 46]. Various approaches have been reported to enhance the circulation time of NPs, which is discussed in detail in section 1.4. We have also addressed this challenge through a unique approach using red blood cells (chapter II). Some of the clinically approved nanomedicine technologies using passive targeting are listed in Table 1-1.

**Table 1-1:** List of clinically approved passively targeted nanomedicines [35].

| Nanocarrier | Name | Drug | Indication/Cancer | References |
|---|---|---|---|---|
| **Liposomes** | Doxil® | Doxorubicin | Breast, ovarian, Kaposi sarcoma and multiple myeloma | [47] |
| | Myocet® | Doxorubicin | Breast | [48, 49] |
| | Onco-TCS® | Vincristine | Non-Hodgkin lymphoma | |
| | DaunoXome® | Daunorubicin | Kaposi sarcoma | [50] |
| | DepoCyt® | Cytosine Arabinoside (cytarabine) | Neoplastic meningitis | [51] |
| | Marqibo® | Vincristine | Acute lymphoid leukemia | [52] |
| | Mepact® | Mifamurtide | Osteosarcoma | [53, 54] |
| **Nanoparticles** | Abraxane® | Albumin-paclitaxel | Breast, pancreatic and non-small cell lung cancer | [49] |
| | Transdrug® | Doxorubicin | Hepatocarcinoma | |
| **Micelles** | Genexol-PM® | Paclitaxel | Breast, lung and ovarian cancer | [55] |
| **PEG-L-asparaginase** | Oncaspar® | Asparagine specific enzyme | Acute lymphoblastic leukemia | [56] |

### 1.3. Active Targeting to Cancer

Active targeting involves attachment of a ligand that acts as a homing device for nanomedicine that binds with high affinity to proteins (receptors) that are over-expressed on the diseased tissues such as cancer compared to healthy tissues [17, 30, 32, 33, 39]. It is also known as *ligand-mediated or receptor-mediated targeting*. Active targeting includes three components: drug, delivery system (NPs), and the targeting ligand. The drug is often encapsulated or conjugated to the delivery system. The targeting ligand is attached on the surface of the NPs by covalent or non-covalent interactions. Targeting ligands include biological molecules such as folic acid, carbohydrates, antibodies, antibody fragments, aptamers, oligonucleotides and peptides, etc. (Table 1-2). Multiple targeting ligands could be attached to enable multivalent targeting, thus enhancing the binding efficiency and overcoming the mutations in the targets. This has been termed as *"synaphic" targeting*. There is enhanced cellular internalization in case of actively targeted nanomedicine rather than increased accumulation as observed in passive targeting.

The most common approach in the preparation of actively targeted NPs takes advantage of well-known molecular recognition in the antibody-antigen binding. For example, human epidermal growth factor receptor 2 (HER-2) is highly overexpressed in a certain population of breast cancers [57, 58-60]. Liposomes conjugated with antibodies to HER-2 yielded 700-fold higher drug uptake as compared to the non-targeted liposomes in HER2-positive breast cancers [61, 62]. Some of the other examples related to NP cancer-targeting include CC52 antibody-modified liposomes against colon adenocarcinoma, anti-CD19 for B-cell lymphoma, and 34A antibody for metastatic lung cancer [63, 64].

**Table 1-2:** Common receptors and ligands for cancer drug targeting [17, 65, 66].

| Receptors | Targeting ligands |
|---|---|
| Transferrin receptors (TfRs)-TfR1 and TfR2 | Transferrin |
| Folate receptors | Folate |
| Integrin receptor | $\alpha_v\beta3$ |
| Epidermal growth factor receptor (EGFR): EGFR (ErbB1, HER1), ErbB2 (HER2), ErbB3 (HER3) and ErbB4 (HER4) | Epidermal growth factor |
| Fibroblast growth factors (FGFRs) | Fibroblast growth factor |
| Sigma receptors | S1R and S2R receptors |
| Bombesin receptors (BnR) | The gastrin-releasing peptide (GRP) receptor; neuromedin B receptor (NMB) and orphan receptor (BRS-3) |
| Somatostatins (SSTRs) receptors | SSTR1-5 |
| Endothelin receptors (ETRs) | ETRA and ETRB, Endothelin's (ET-1-3). |
| Low-density lipoprotein (LDL) receptor | Low-density lipoprotein |
| Asialoglycoprotein receptor | Glycosylated polylysine |
| Galactose/Glucose/Mannose receptors | Galactose/Glucose/Mannose |
| Others | Follicle stimulating hormone receptors (FSHRs); Biotin receptors (BRs); C-type lectin receptors (CLRs); Asialoglycoprotein receptor (ASGPR); and Neuropilin 1 (NRP-1). |

However, antibodies are relatively large (~150 kDa in molecular weight), and their conjugation often results in poor size control and reduced stealth capability (evasion by the immune system) [67, 68]. These shortcomings led to the emergence of alternative targeting ligands. Such ligands include variations of whole antibodies such as Fab fragments and single-chain variable fragments, growth factors and nutrients whose receptors are over-expressed in cancer cells, RNA-based aptamers and peptides such as RGD and LyP-1 that target tumor vasculatures [69, 70, 71]. The small physical dimension of these alternatives enables high ligand density and more effective multivalent targeting without compromising the particle's circulation time.

Active targeting to receptors has some drawbacks which limit its potential clinical usage. One of the crucial factors to be considered is the availability and the capacity of the receptors to be targeted by the probe. It is essential since the number and the availability of cell surface receptors determines the ability/efficiency of specific binding of the targeting ligand. Several clinically approved actively targeted systems are listed in Table 1-3. The efficiency of the active targeting is also determined by the elimination of the drug delivery system from the circulation and degradation of the ligand while in circulation. Short *in-vivo* circulation half-life could be an advantage in imaging because it quickly eliminates the background caused by the excess probe. However, in drug targeting, short half-life gives the targeted delivery system less time to penetrate into the target tissue. Long circulation times are especially important when the target is outside the vasculature [72, 73]. In summary, for both passive and active targeting of nanomedicine, short circulation time in the blood is a major challenge. The current approaches to enhance the circulation time of nanomedicine are discussed under section 1.4 and also in chapter II.

**Table 1-3:** List of clinically approved actively targeted nanomedicines [34].

| Name | Targeting moiety | Drug | Cancer |
|---|---|---|---|
| Tositumomab (Antibody-radioactive element conjugate) | Mouse anti-CD20 antibody | $^{131}$Iodine | Non-Hodgkin's lymphomas |
| Denileukin diftitox (Fusion protein of targeting agent and therapeutic protein) | Interleukin 2 | Diphtheria toxin fragment | Cutaneous T-cell lymphoma |
| Gemtuzumab (Antibody-drug conjugate) | Humanized anti-CD33 antibody | Calicheamicin | Acute myeloid leukemia |
| Ibritumomab (Antibody-radioactive element conjugate) | Mouse anti-CD20 antibody | $^{90}$Yttrium | B-cell non-Hodgkin’s lymphoma |

### 1.4. Enhancing the Systemic Circulation Time of Nanomedicines

Majority of chemotherapeutics are given intravenously. When delivered intravenously, irrespective of the therapeutic objective of the NPs, their circulation time in the blood is a key determinant for efficient accumulation in the target tissues [74, 75]. However, majority of the existing technologies for nanomedicine suffer from two major shortcomings in drug accumulation in cancer tissues: (i) rapid elimination from the systemic circulation before reaching the cancer tissue (ii) poor tumor accumulation and penetration due to inadequate vasculature and extensive extracellular matrix in the tumor [40, 41, 74, 76]. NPs are commonly eliminated from the body via a two-step process. The first step involves adsorption of the serum proteins of the complement system on the surface of NPs, which is termed as opsonization. Following opsonization, the NPs are engulfed by the circulating macrophages or the macrophages of the liver and spleen or the reticuloendothelial system (RES) of the liver [77-79]. More specifically, hydrophobic and/or charged NPs suffers from high opsonin mediated immune clearance [80]. It is very critical to enhance the circulation time of nanomedicine for clinical advancement.

Currently, there are three major strategies proposed for enhancing the circulation time of NPs: (i) modifying the physicochemical characteristics such as size and shape of the NPs, (ii) altering the surface of the particles to reduce opsonization, and (iii) mimicking blood cells and/or closely attaching on them to evade immune recognition. The size of a nanocarrier is a crucial factor that determines the circulation in the blood which in turn is related to tumor accumulation, retention and drug release. For example, liposomes > 200 nm in diameter do not extravasate into tumors [81]. The same study showed that PEGylated unilamellar liposomes between 5 to 150 nm have increased blood

circulation (half-life ~50-55 h) and thus, increased tumor accumulation and anti-tumor efficacy. In general, smaller sized particles are less likely to be taken up by macrophages than the larger ones. However, the smaller particles demonstrate widespread accumulation in other organs and are also rapidly excreted through glomerular filtration. In general, the recommended size of the NPs is larger than 20 nm to avoid glomerular filtration, but smaller than 100 nm to minimize uptake by mononuclear phagocytic cells [82-84].

There are a variety of techniques employed for the surface modification of NPs to prevent and/or reduce the opsonization. The surface modification could be accomplished either by incorporating the surface modifying agent during the preparation of particles or attaching on to the surface of prepared particles by a covalent bond or passive adsorption [85-87]. The surface of the NPs is altered to become hydrophilic to prevent the uptake and clearance by macrophages. Hydrophilic coating of the surface further provides protection against plasma protein adsorption (opsonization) [78]. Polyethylene glycol (PEG) is currently the gold standard for the stealth surface coating, and it is present in many FDA-approved products. The process of coating the surface of NPs with PEG is called PEGylation. PEGylation enhances the surface hydrophilicity of NPs without adding a charge to it [39, 79, 88-92]. However, concerns and limitations of PEG such as its non-biodegradability, immunological responses, and the toxic side products that accompany its synthesis, have motivated the search for safer and more compatible substitutes. Of the utmost concern is the emergence of anti-PEG antibodies that have been observed in approximately 25% of patients and normal humans, which leads to accelerated blood clearance of the particles in subsequent injections. Such observations raise concern over the ubiquitous use of PEG and demonstrate the need for novel, non-immunogenic

approach in prolonging NP circulation half-life [93-99]. More details on PEGylation and its limitations are described in detail in Chapter II. Other polymers used for stealth coating of NPs include Polyoxazolines, Poly (amino acids) such as poly (hydroxyethyl L-glutamine) or poly (hydroxyethyl-L-asparagine), N-(2-hydroxypropyl) methacrylamide (HPMA), Polybetaines, Polyglycerols, Polysaccharides, Poloxamers and Poloxamines [74, 100].

Recently, several biomimetic approaches have been proposed to enhance the systemic circulation time of NPs [75, 76, 101, 102]. For instance, blood cells (like erythrocytes) are known to remain in the circulation for months. Red blood cells (RBCs) have gained attention as alternatives to PEG for enhancement of the circulation time and tumor targeting of NPs [76, 80, 103-118]. RBCs have been investigated as drug carriers since they possess intrinsic biocompatibility and non-immunogenicity, enhanced circulation and ability to be cleared from the circulation. RBCs express various surface markers such as receptor/transporter proteins, glycans and acidic sialyl moieties [113]. RBC-targeted nanoparticulate delivery systems have demonstrated superior circulation half-life and better tumor penetration than PEGylated NPs as observed in mouse models. The most common RBC-based strategies to enhance the circulation time of NPs include [76, 80, 103, 104, 106-111, 118, 119]: (i) *preparing nanocarriers with RBC membranes*- This involves coating or preparing nanocarriers using RBC membranes. This approach is highly biocompatible, prolongs circulation time and/or tumor targeting. (ii) *coating the surface of the polymeric-NPs with RBC membrane*- This approach involves camouflaging the NPs surface with the erythrocyte exterior for long circulation while keeping the applicability of the polymeric core and (iii) *attaching the NPs on to the surface of RBCs*-

Coupling or attaching to the RBC surface represents an alternative strategy to the other two mentioned above. This is possible since the RBC membrane provides a surface area that could be utilized to couple proteins or therapeutics molecules [120].

RBCs express various surface markers such as receptor/transporter proteins, glycans and acidic sialyl moieties for conjugation to NPs. In this dissertation (chapter II), we have designed a unique strategy based on the physiological interaction between nutritional transporters (glucose transporters-GLUT1) present on the RBCs membrane with their natural ligands. We hypothesize that by conjugating glucose on the surface of NPs enables them to bind to GLUT1 on the membrane of RBCs to travel along for enhanced circulation time. Stealth coated RBC-NPs also reduce the *in-vitro* macrophage uptake as seen with the solid gold nanospheres [121]. They could be employed either for continuous release of drugs in the circulatory systems or for targeted delivery to specific organs. Hence, developing biomimetic approaches for the enhancement of the circulation time of NPs of considerable interest in the field of medical nanotechnology. Moreover, it would require not one but an amalgamation of available strategies [100], such as employing appropriate size, shape, surface and mechanical properties, exploitation of natural cells to achieve an enhancement of circulation time for particulate delivery systems [121-126].

### 1.5 Receptors versus Transporters as Targets for Active Targeting for Cancer

To qualify as a target for active targeting for cancer, the target molecule has to be differentially expressed in cancer tissue compared to the healthy tissue. Various receptors have been reported over the years as targets for cancer-drug targeting (Table 1-2). The

current targeting strategies primarily focus on modifying ligands on the surface of the nano-based drug delivery system to recognize and interact with specific receptors on the surface of the cell membrane. However, the targeting efficiency has been limited by the variability and heterogeneity of the receptors. It has been found that different patients with the same disease have differential expression levels of receptors and differential expression of the same receptors at different stages of the disease for the same patient. Thus, receptor-based targeting strategies have not been brought to clinics and there is a need to develop alternative targeting strategies [65, 127].

Recently, transporters have become emerging targets for the development of targeted drug delivery systems. Transporters are membrane proteins that have specificity to a group of structurally similar ligands. The ligands, once bound, are transported into the cell through a channel within the protein structure of the transporter. The ligands for transporters are usually small molecules, such as glucose or amino acids, that could pass through a small transporter channel. It would not be possible for larger molecules or NPs to transport through the channel to enter the cell. In contrast, receptors transport the ligands or NPs with the ligand into the cell through endocytosis. The endocytotic vesicles are large enough to carry NPs along with the ligand. However, in the last few years transporters have been explored to deliver drugs specifically to cancer cells as they have also been shown to induce endocytosis. The advantages of utilizing transporters as targets for nano-based cancer drug targeting compared to receptors could be categorized into two different aspects (i) *pathological differences* and (ii) *delivery related advantages*. The pathological differences include: (i) A strong positive correlation exists between the transporter expression versus invasiveness of the cancer cells and poor prognosis in multiple cancer

types. (ii) The expression levels of transporters are less variable than the receptors. (iii) The variability and heterogeneity in terms of expression of transporters in patients, and within the same patient during the various stages of diseases, are less as compared to the receptors. The delivery advantages of transporters as compared to receptors include: (i) Most of the targeting moieties for receptors are macromolecules, whereas in the case of transporters they are small molecules. (ii) Lack of potential immune reactivity is a unique advantage of ligands for transporters as opposed to receptors. (iii) The ligands for transporters are usually stable and could be structurally modified, as opposed to those for the receptors. [65, 127].

Nutritional transporters are a group of influx transporters that transport hydrophilic nutrients such as sugars or amino acids across the membrane. Cancer cells are known for their uncontrolled rapid growth and proliferation, therefore, are in high demand for nutrients (glucose, amino acids, fatty acids, vitamins) [128]. To meet the demand for high nutrients, cancer cells usually express high levels of nutritional transporters compared to normal cells [129]. Similarly, cancer cells also express high levels of efflux transporters such as P-glycoprotein (P-gp), multidrug resistance-associated protein 1 (MRP1) and breast cancer resistance protein (BCRP), which play a role in drug resistance and survival. This would enable to either inhibit or use the endogenous over-expression of these transporters as potential targets for the development of strategies for cancer. Since the cancer cells induce these specific transporters to fulfill their increased demand of nutrients and metabolic needs, it is expected that normal cells would not be expressing or their expression would be relatively low, thus reducing undesirable side effects [65, 127, 129].

## 1.6. Transporters in Drug Delivery for Cancer

Hydrophilic molecules are unable to readily diffuse across the membrane. For this, they depend upon channels, pumps and/or transporters to move in and out of the cells and organelles [130]. The transporter's primary function is to regulate the influx and efflux of various essential endogenous compounds such as nutrients, amino acids, sugars, and inorganic ions, etc. [131]. Drugs that possess structural similarity to these substrates are recognized and transported into the cell by transporters [132]. Transporters often work in tandem for the regulation of the transport of compounds across the barriers throughout the body, thus playing a crucial role in the absorption, distribution, metabolism, and excretion (ADME) of structurally and pharmacologically diverse molecules [130]. Approximately 10% of the human genome encodes for proteins with transporter-related functions, [122] which emphasizes their complex role in transporting molecules across the tissues. Furthermore, there has been considerable interest in transporters as major targets for developing new drugs [122].

### *1.6.1. Classification of Transporters*

Transporters could be classified into broadly four ways: (i) ***efflux vs influx transporters*** (ii) ***secretory vs absorptive transporters*** (iii) ***ATP binding cassette transporters (ABCs) vs solute carrier (SLCs) transporters*** and (iv) ***Passive vs active transporter*** [133]. ***Efflux transporter*** pumps the substrates out of the cells while the ***influx transporters*** are responsible for the uptake of substrates into the cells. Transporters that transfer their substrates into the systemic circulation are ***absorptive*** and those that excrete substances from blood circulation are ***secretory*** transporters. Membrane transporters can be further

classified as ***ABC transporters*** *and* ***SLC transporters***. The ABC transporters are primary active transporters, that efflux out wide range of substrates. The SLC family includes transporters that function by secondary active transport and facilitative diffusion. They are located on the cell membrane as well as on the intracellular membrane of organelles. ***Active transporters*** utilize adenosine triphosphate (ATP) to pump the molecules against the concentration gradient. They are further classified as primary or secondary active transporters according to the mechanism of energy coupling. ***Passive transport*** is the movement of molecules down the concentration gradient without the need for energy [132] [134].

### *1.6.2. Membrane Transporters*

Membrane transporters are integral membrane proteins that facilitate the transport of drugs or macromolecules via the processes of facilitated diffusion or active transport [95]. They exist within and span the membrane across which they transport exogenous and endogenous substances including major nutrient metabolites [95, 135]. Identification of various genes has made it possible to classify the transporters into two distinct superfamilies', namely: *ATP binding cassette proteins (ABC) transporters* and *solute carrier proteins (SLC)* transporters [135].

#### *1.6.2.1. ABC Transporters*

ABC transporters are ATP binding cassette proteins. They are the largest superfamily of transport proteins found in humans. They utilize energy from hydrolysis of ATP to carry out the function of translocation of various substrates across the membranes [132]. There are 40 ABC transporters classified into 7 subfamilies based on their amino acid sequence

identity from A to G subfamily as: *ABCA, ABCB, ABCC, ABCD, ABCE, ABCF and ABCG* [95, 135, 136]. Numerous clinical studies have revelated that multi-drug resistance phenotype in tumors is associated with over-expression of *P-gp, MRP1, MRP2, MRP3, MRP4, MRP5 and BCRP*, which primarily mediate the efflux of xenobiotics and drugs. Therefore, to develop an effective chemotherapeutic regimen, thorough knowledge about the mechanisms of multi-drug resistance caused by ABC transporters is required [135, 136].

*1.6.2.2. SLC Transporters*

SLC transporters comprise both the facilitated and secondary active transporters. They utilize electrochemical gradient for facilitating the movement of substrates across the membranes or ion-gradients generated by the ATP-dependent pumps to transport substrate across the concentration gradient [130]. The SLC transporters either work by passive diffusion along the concentration gradient of the substrate or by co-transport against the concentration gradient of another solute. These transporters do not possess ATP-binding sites. They constitute the largest family of membrane transporter proteins in the human genome with approximately 400 SLC transporter genes that have been identified and grouped into 55 families [133]. The SLC transporters function as influx transporters for nutrients and other essential substances for cell survival [95, 137].

## 1.7. Nutritional Transporters as Targets for Cancer-targeted Drug Delivery

One of the hallmarks of cancer cells has been uncontrolled growth and proliferation, which increases the demand of nutrients that are required for the synthesis of DNA, RNA and/or

as a source of metabolic energy [129]. The nutrient demand is fulfilled by glucose, amino acids, vitamins, and fatty acids, etc. Most of these nutrients are hydrophilic in nature and cannot permeate across the plasma membrane in mammalian cells. The uptake of these hydrophilic nutrient molecules occurs through nutritional transporters that are located on the plasma membrane. Such a high demand for nutrients for their rapid growth coupled with poor availability of nutrients due to inefficient development of tumor vasculature propel cancer cells to highly express nutritional transporters for their survival [138]. Therefore, it is imperative to understand the changes in the function and expression of nutritional transporters in cancer cells as compared to the normal cells. Identification of specific nutrient transporters upregulated in cancer cells as compared to normal cells would enable to either inhibit the cellular signaling pathways that are responsible for their induction to specifically block the function of that transporter to impair the growth of the tumor. Nutritional transporters have become targets for new anti-cancer drug discovery [65, 129, 133].

Numerous nutrient transporters are implicated in cell growth, of which the *glucose transporters*, *amino acid transporters (includes both amino acid exchangers and amino acid importers) and the monocarboxylate transporters* have been extensively studied for their association with cancer (Table 1-4) [138]. The increased demand for glucose by the cancer cells is regulated via the induction of GLUT1 and SLGT1 transporters. This increased entry of glucose is well-coordinated with increased glycolysis, which leads to higher lactate production. Cancer cells upregulate MCT4 transporters to expel lactate out of the cells. Similarly, the increased demand for amino acids is meet by cancer cells by induction of LAT1, ASCT2, xCT/4F2hc, and $ATB^{0,+}$. Evidence exists on the

pharmacological inhibition of these transporters to control the cancer cell growth. Hence, these transporters possess the ability as targets for cancer therapy [129, 138].

Recently, nutritional transporters have been explored as alternatives to deliver drugs, diagnostic markers or nano-drug delivery systems across cancer cells for active drug targeting (Table 1-7 and 1-8) [65, 129, 133]. Examples of this include, tumor-specific delivery of positron emission tomography (PET) imaging agent, 2-[fluorine-18]-fluoro-2-deoxy-D-glucose (FDG) that utilizes glucose transporter activity that arises due to the enhanced requirement of glucose and other sugars by the cancer cells [139]. $^{131}$Iodine therapy has been utilized in patients with thyroid cancers due to the ability of the thyroid to accumulate iodine [140].

### *1.7.1. Glucose Transporter Family and their Role in Cancer*

Glucose is one of the essential metabolic substrates which cannot diffuse across the lipid bilayer due to its hydrophilicity [122]. The transport of glucose into the cytosol is mediated by two families of hexose transporters: the ***sodium-dependent glucose transporters (SGLTs)*** delivers glucose against the concentration gradient utilizing the sodium-electrochemical gradient, whereas the ***GLUT family of transporters*** translocates glucose along the concentration gradient using a facilitative diffusion. The GLUT proteins belong to the solute carrier 2A family SLC2A (SLC2A1–SLC2A14). To date, 14 forms of GLUTs have been sequenced in humans, which have been categorized into three distinct classes based on the sequence similarity: *class 1 (GLUTs 1-4 and 14), class 2 (GLUTs 5, 7, 9 and 11)* and *class 3 (GLUTs 6, 8, 10, 12 and HMIT)* (Table 1-5) [122, 141]. As a member of the major facilitator superfamily (MFS) of the membrane transporters, GLUTs possess

some common structural similarities such as presence of ~500 amino acids, 12-transmembrane helices, an N-linked glycosylation site, and intracellular -$NH_2$ and –COOH terminus including several conserved residues and motifs [129, 133] [141].

**Table 1-4:** Nutrient transporters implicated in cancer [65, 129].

| Common Name | SLC Designation | Tissues Over-expressing Transporter |
|---|---|---|
| ***Glucose Transporters*** | | |
| GLUT1 | SLC2A1 | Brain, breast, pancreatic, lung, prostate, head and neck, gastric, colorectal, renal, thyroid, and hepatocellular |
| GLUT3 | SLC2A3 | Breast, ovarian, lung, stomach, oral squamous cell, bladder |
| GLUT4 | SLC2A4 | Lung, gastric, thyroid, multiple myeloma |
| GLUT12 | SLC2A12 | Prostate and breast |
| SGLT1 | SLC5A1 | Prostate, lung pancreatic, head and neck |
| ***Amino Acid Exchangers*** | | |
| ASCT2 | SLC1A5 | Glioma, hepatoma |
| xCT/4F2hc | SLC7A11/SLC3A2 | Brain, pancreatic, hepatocellular, leukemia |
| LAT1/4F2hc | SLC7A5/SLC3A2 | Prostate, brain, colon, liver, lung, and skin |

| | | |
|---|---|---|
| LAT3 | SLC43A1 | Prostate |
| CAT-1 | SLC7A1 | Glioma |
| ***Net Amino Acid Importers*** | | |
| SNAT 1-5 | SLC38 A1-A5 | |
| $ATB^{0,+}$ | SLC6A14 | Colorectal, cervical, breast |
| EAAT2 | SLC1A2 | |
| PAT1/LYAAT-1 | SLC36A1 | |

**Table 1-5:** Classification of GLUTs with respective details about the transporters.

| **Transporter** [142] | **Gene Name** | **Predominant Substrates** | **Tissue and Cellular Expression** | **Role and Properties** |
|---|---|---|---|---|
| ***SGLT Transporters*** | | | | |
| SGLT1 | SLC5A1 | Glucose, galactose | The small intestine, salivary gland, heart, and kidney. | Intestinal and renal absorption of glucose. |
| SGLT2 | SLC5A1 | Methyl-α-D-glucopyranoside | Kidney. | Renal absorption of glucose from the glomerular filtrate. |
| ***Class I GLUT Transporters*** | | | | |
| GLUT1 | SLC2A1 | Glucosamine, glucose, galactose and mannose. | Brain, erythrocytes, blood-brain barrier, fetal tissues. | Basal level glucose uptake. |
| GLUT2 | SLC2A2 | Glucosamine, glucose, galactose, fructose and mannose. | Liver, kidney, brain, pancreatic islet cells and intestine. | It is a high capacity and low-affinity glucose transporter, trans-epithelial glucose and |

| | | | | |
|---|---|---|---|---|
| | | | | fructose transport. Glucose sensing in the pancreatic $\beta$-cells. |
| GLUT3 | SLC2A3 | Glucose, galactose, mannose, and xylose. | Neurons of brain and testis. | Neuronal glucose transporter. |
| GLUT4 | SLC2A4 | Glucose and glucosamine | Skeletal and cardiac muscle, adipose tissues. | It is expressed in tissues which have insulin-stimulated acute glucose transport. |
| GLUT14 | SLC2A14 | -- | Testis | -- |
| ***Class II GLUT Transporters*** | | | | |
| GLUT5 | SLC2A5 | Fructose | Kidney, testis, muscle and small intestine. | Fructose transporter. |
| GLUT7 | SLC2A7 | Glucose and fructose | The small intestine, colon, prostate, and testis. | -- |

| | | | | |
|---|---|---|---|---|
| GLUT9 | SLC2A9 | Glucose and fructose | Kidney, liver, small intestine, placenta, lung, and leucocytes. | -- |
| GLUT11 | SLC2A11 | Glucose and fructose | Heart and muscle. | Possess three different isoform GLUT11a, GLUT11b, GLUT11c with distinct tissue distribution. |
| ***Class III GLUT Transporters*** | | | | |
| GLUT6 | SLC2A6 | Glucose | Spleen, brain and leucocytes | -- |
| GLUT8 | SLC2A8 | Glucose, fructose, and galactose | Brain, testis, adrenal gland, liver, spleen. | -- |
| GLUT10 | SLC2A10 | Glucose and galactose | Heart, brain, liver, placenta, lung, kidney, pancreas. | It is associated with causation of arterial tortuosity syndrome. |

| | | | | |
|---|---|---|---|---|
| GLUT12 | SLC2A12 | Glucose | Prostate, placenta, adipose tissue heart, skeletal muscle. | Similar to GLUT4, it is transported to the plasma membrane in response to insulin. |
| GLUT13 | SLC2A13 | Myo-inositol | Brain and adipose tissue | -- |

*1.7.1.1. GLUT1 Transporter*

GLUT1 is the most ubiquitous and extensively studied glucose transporter. Its properties have been extensively studied in human RBCs. GLUT1 corresponds to 10% of the total integral membrane protein in RBCs [143]. Through this, glucose equilibrates between the serum and red cell cytoplasm. It is primarily present in the plasma membrane. Substrates of GLUT1 are glucose, mannose, galactose, glucosamine, etc. It has multiple substrates but possesses a high affinity for glucose (Table 1-5). The structural requirement for binding of 2-amino-2-deoxy glucose to GLUT1 transporters requires the presence of free hydroxyl groups at the carbon 1, 4 and 6 in the 2-amino-2-deoxy glucose molecule. The amino group at the carbon 2 of glucose is most suitable for recognition and binding to GLUT1 transporter on the RBCs membrane (Figure 1-2). It is actively inhibited by cytochalasin B and phloretin. It also plays a critical role in cerebral glucose uptake since it is highly expressed on the brain endothelial cells (Table 1-5) [129, 141].

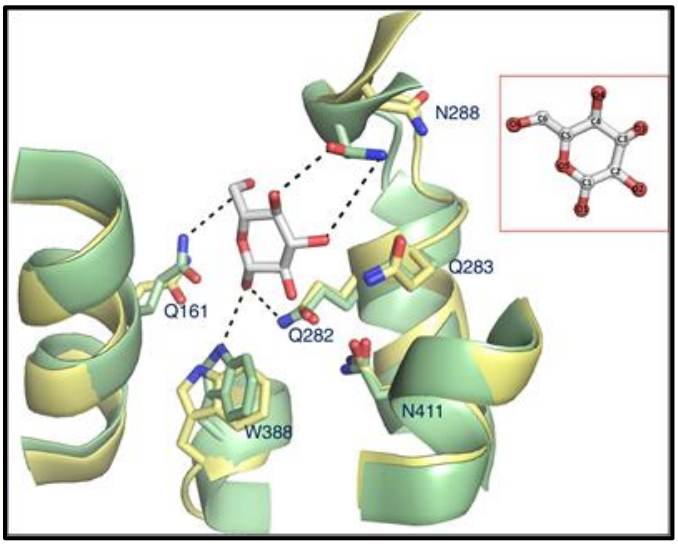


**Figure 1-2:** Glucose binding to GLUT1 transporter. Modified and adopted from [141].

GLUT1 is highly expressed in the majority of cancer types. This could be due to the aggressive nature of cancers, which demonstrates an increased demand for metabolic energy, especially through glycolysis using glucose. Switching the metabolic pathway from mitochondrial oxidative phosphorylation to aerobic glycolysis under hypoxic conditions is a hallmark of the cancer cells. This switch of the metabolic pathways is an energetically efficient process that requires excessive amounts of glucose [143, 144]. This phenomenon is termed the *Warburg effect*. This increased dependence of glucose gives rise to enhanced expression and surface transport of GLUTs more specifically GLUT1 [145]. The factors that are responsible for the up-regulation of GLUT1 include hypoxia-inducible factor-1 (HIF-1), c-MYC, AKT, Ras and p53, etc. Oncogenesis also plays a critical role in the induction of GLUT1 [11, 144].

*1.7.1.2. GLUT1 Expression in Various Cancers*

GLUT1 is a key rate-limiting factor in the transport and metabolism of glucose in cancer cells. GLUT1 is overexpressed in a number of cancer types including breast, brain, ovarian, hepatic, pancreatic, esophageal, renal, lung, cutaneous, colorectal, endometrial, bladder, cervical, hepatocellular, head and neck and gastric cancers [146-149] (Table 1-6). This overexpression of GLUT1 in various cancers is utilized for tumor diagnosis, imaging, therapy, and disease management. An increased level of expression is observed in cancers of high grade and high proliferative index. The survival of cancer patients is related reciprocally to the expression level of GLUT1 [65, 150]. GLUT1 is expressed in 42% of breast tumors with increased expression in cancers of higher grade and proliferative activity as compared to non-cancerous tissues. Subsequent studies also reported ~47% and

51% expression levels of GLUT1 in breast cancer [151]. Godoy *et al.* have reported as high as 91% positive staining of the invasive ductal carcinoma analysis as compared to control [152, 153, 154, 155, 156]. This clearly indicates the consistency of GLUT1 overexpression in ductal carcinoma [155, 157].

In addition, the levels of GLUT1 protein expression correlates to poor prognosis in a wide range of solid tumors [158, 159]. For example, high levels of GLUT1 in breast cancer correlates with poor survival, aggressive biological behavior and more malignant potential in patients. GLUT1 expression is associated with increased malignant potential, poor prognosis and invasiveness in the lung, colorectal, gastric and ovarian cancers [160 161, 162]. A thorough systematic review and meta-analysis of a total of 26 studies including 2948 patients revealed that overexpression of GLUT1 correlated with poor 3-year overall survival and 5-year overall survival of tumors [150]. *Haber et al.* through their studies have shown that the risk of dying from colon cancer was 2.3 times higher in patients with high GLUT1 expression, as compared with low expression and correlated to poor prognosis [163]. *Reis et al.* utilized a scoring system and demonstrated that GLUT1 is correlated with increasing malignant potential in non-invasive and invasive urothelial carcinomas of the bladder [164]. *Chen et al.* report that Sirtuin 1 increases the transcription activity and expression of GLUT1, therefore, promoting the cell proliferation and glycolysis in bladder cancer cells. *Nemejcove et al.* study confirm high expression of GLUT1 in endometrioid carcinomas. Among 184 cases studied, 160 (87%) cases demonstrated increased expression of GLUT1 [165]. The combined studies of *Younes et al.*, *Yamamoto et al.*, *Noguchi et al*. report increased expression of GLUT1 in the stomach and esophageal cancer and its relation to progression in Barrett's metaplasia [166, 167,

168]. These studies suggest that GLUT1 is a prognostic indicator and a potential therapeutic target in tumors [145]. Similar increased GLUT1 expression patterns have been found in thyroid, lung, ovarian, and cutaneous cancers as shown in Table 1-6 [158, 169].

**Table 1-6:** GLUT1 expression in various cancers.

| Cancer Type | Results/ Expression Patterns | Reference |
|---|---|---|
| Hepatocellular carcinoma (HCC) | The results of mRNA and protein expression in 152 patients revealed that ~68.2% of human HCC tissues demonstrated higher GLUT1 expression as compared to noncancer tissue. Increased GLUT1 expression affected the proliferation and invasiveness, promoting tumorigenesis of HCC. | [170] |
| Gastric cancer | GLUT1 is upregulated in gastric cancer and is related to unfavorable clinical survival and first progression survival | [171] |
| Prostate cancer | The results reveal that GLUT1 expression is considerably higher in prostate cancer tissues than the normal tissues as well as positively | [172] |

| | | |
|---|---|---|
| | correlates with the prostate-specific antigen (PSA) level and Gleason score. | |
| Head and neck squamous cell carcinoma | Through immunohistochemical analysis on 135 human samples of cancer, author report significantly higher (~96% cases) expression of GLUT1 in neoplastic vs non-neoplastic samples. GLUT1 is expressed in basal/parabasal epithelial cells and in oral carcinoma | |
| Cervical cancer | Mendez *et. al.* through histologic analysis in 31 patients' samples report expression of GLUT1. The results reveal that GLUT1 was positive in all 31 cases and was related to the grade of the tumor. | [173] |
| Pancreatic cancer | Reske *et al.* showed that overexpression of GLUT1 to increased FDG uptake in pancreatic carcinoma. | [174] |

**Table 1-7:** List of transporters and their substrates for cancer targeting [65].

| Transporter | Gene | Ligands/Substrates |
|---|---|---|
| SMVT [175] | SLC5A6 | Biotin |
| ASBT [176, 177] | SLC10A2 | Deoxycholic acid, TetraDOCA and Taurocholic acid |
| OCTN2 [178] | SLC22A5 | L-carnitine |
| GLUT1 | SLC2A1 | 2-Deoxy-D-glucose and glucose |
| GLUT4 | SLC2A4 | Glucose |
| $ATB^{0,+}$ | SLC6A14 | Lysine, Aspartate |
| LAT1 | SLC7A5 | Glutamate, phenylalanine |
| MCT1 | SLC16A1 | β-hydroxybutyrate |

**Table 1-8:** Active targeting strategies employing substrates of transporters. Modified and adopted from [65].

| Transporter | Gene | Substrate | Nanomedicine | Drug | Purpose |
|---|---|---|---|---|---|
| GLUT1 | SLC2A1 | 2-Deoxy-D-glucose and glucose | DMSA-DG-NPs and nanoparticles | NA | For increased site-specific absorption at the tumor site and brain |
| GLUT4 | SLC2A4 | Glucose | Quantum dots | NA | Increasing absorption in muscle |
| LAT1 | SLC7A5 | Glutamate | Nanoparticles | Paclitaxel | Breast cancer |
| MCT1 | SLC16A1 | β-hydroxybutyrate | Solid-lipid nanoparticles | Docetaxel | Increase site-specific absorption in brain |
| GLUT1 | SLC2A1 | 2-Deoxy-D-glucose<br>D-Glucosamine | Nanoparticles<br>Nanoparticles | Paclitaxel<br>Paclitaxel | To enhance blood-brain barrier permeation and increased glioma targeting |
| LAT1 | SLC7A5 | Glutamate | Liposomes | Docetaxel | |
| OCTN2 | SLC22A5 | L-carnitine | Nanoparticles | Paclitaxel | For enhanced oral absorption |
| ASBT | SLC10A2 | Deoxycholic acid and Taurocholic acid | Conjugates and micelles | Insulin and Docetaxel | |

*NA- Not applicable

### *1.7.2. Strategies to Target GLUT1 in Cancer*

Current research efforts are focused on developing novel drug delivery systems that structurally resemble the endogenous substrates (glucose and amino acids) and thereby enable them to reach the target sites, minimizing the amount reaching the non-target tissues. For this purpose, a major approach, known as carrier-mediated transport, is utilized to target and make use of endogenously expressed transport substrates for the development of drug delivery systems. The most recent strategies include nanoscale drug delivery systems, prodrug design and conjugating of drugs with the nutrients (glucose, amino acids), etc. In brief, the strategies involve: (i) modification of an existing drug or polymer to give a *'pseudo nutrient'* structure that could be recognized and transported by the endogenous transporter (ii) conjugation of drug or polymer with a nutrient that is able to be transported by the endogenous transporter (Figure 1-3). Various endogenous ligands for transporters are available for cancer drug targeting (Table 1-7). By using these ligands on the surface of a nanoparticulate vehicle, chemotherapeutic agents have been targeted to various cancer tissues (Table 1-8) [65], [144, 179-182].

Of all the nutritional transporters, GLUT1 has been extensively studied for cancer targeting due to its consistent over-expression in cancer patients (Section 1.7.1.2 and Table 1-6). The Table 1-9 below provides a collection of strategies that target high levels of GLUT1 in cancers for therapeutic purposes: to inhibit the function of GLUT1 or to deliver drugs using a prodrug strategy (Table 1-9) [180, 183, 184].

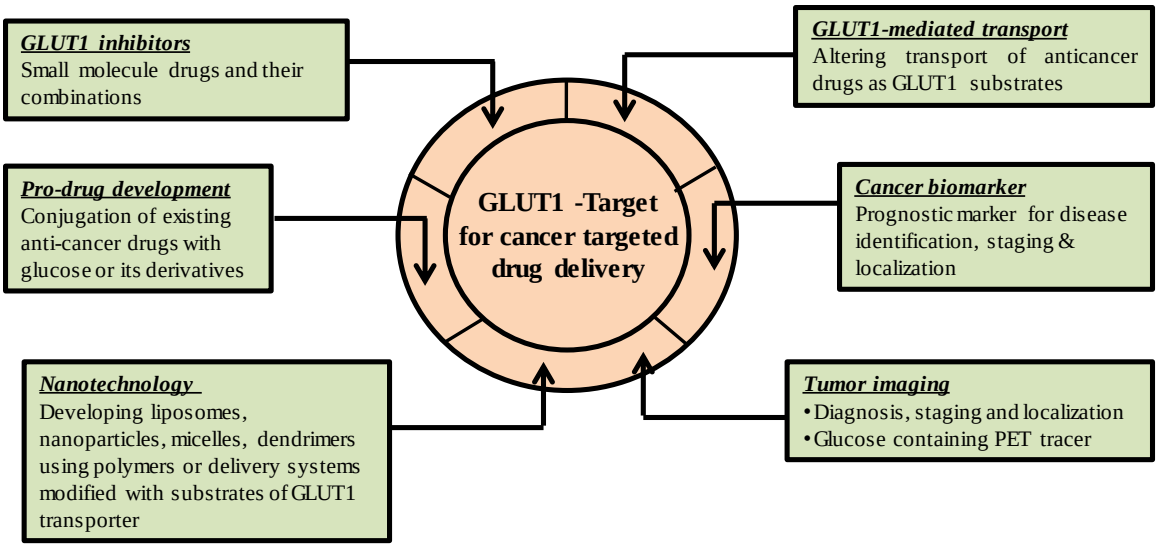


**Figure 1-3:** Potential Strategies to Target GLUT1 Transporters.

**Table 1-9:** Comprehensive list of various strategies using GLUT1 transporter in cancer.

| Drug | Polymer employed | Strategy and Therapeutic application | Major conclusions |
|---|---|---|---|
| Cisplatin [161] | NA | Novel platinum-glucose drug conjugates | Patra *et al.* in their work have synthesized three novel glucose-platinum conjugates (Glc-Pts 1-3). The conjugate (Glc-Pt 1) demonstrated preferential accumulation in cancer cells as opposed to the normal cells by utilization of the glucose and |

| | | | |
|---|---|---|---|
| | | | organic cation transporters that are overexpressed in cancers. |
| Oxaliplatin [182] | NA | Selective tumor targeting with fluorine-containing platinum (II) glycoconjugates | Liu *et al.* have reported fluorine substituted series of glucose, mannose, and galactose-conjugated (trans-R, R-cyclohexane-1, 2-diamine)-2-flouromalonato-platinum (II) complexes for their selective tumor targeting via the GLUT1 transporter. The conjugates demonstrate high aqueous solubility, improved cytotoxicity and enhanced cellular uptake on GLUT1 overexpressing cells. The glucose conjugated compound (5a) demonstrates enhanced *in-vivo* efficacy in an HT29 xenograft model and leukemia-bearing DBA/2 mice model as compared to oxaliplatin. |
| Oxaliplatin [185] | NA | Platinum complexes | The author reports two mannose conjugated platinum complexes. |

| | | | |
|---|---|---|---|
| | | conjugated to mannose for effective tumor targeting by GLUT1 transporter | Both these compounds show enhancement in water solubility and enhanced cytotoxicity in six different human cancer cell lines. *In-vivo* these compounds demonstrate efficacy and safety than oxaliplatin. |
| NA [179] | Glucose coated iron oxide NPs | Glucose-coated superparamagnetic iron oxide NPs via GLUT1 transporter in pancreatic adenocarcinoma cells | The NPs were effectively internalized in tumor cell lines overexpressing GLUT1. |
| NA [181] | P-aminophenyl-α-D-mannopyranoside | Modified liposomes of mannopyranoside within mice brain. | The mannose modified liposomes demonstrated higher cellular uptake in GLUT1 overexpressing cell lines. Transcytosis by GLUT1 and GLUT3 was responsible for the uptake of mannose modified liposomes into the brain. |

| | | | |
|---|---|---|---|
| NA [186] | $\gamma$-$Fe_2O_3$ NPs coated with DMSA, modified with 2-DG | Targeting GLUT1 overexpressing MDA-MB-231 cells with 2-DG modified SPIOs. | A novel 2-deoxy glucose-based contrast agent for magnetic resonance molecular imaging was developed. This agent demonstrated enhanced cellular uptake of SPIOs in GLUT1 overexpressing cells. This study reports the potential of SPIOs as promising candidates for tumor detection probe with potential use in MR imaging. |
| Doxorubicin [187] | mPEG-*p*Lys-*p*Phe | GLUT1 targeted nano-micelles for hepatocellular carcinoma cellular therapy | Guo *et al.* through their results show the development of nano-micelles targeted towards GLUT1. Cellular and *in-vivo* imaging studies demonstrate targeting property of micelles for hepatocarcinoma cancer. The micelles were found to show enhanced efficacy both *in-vitro* and *in-vivo*. |

*NA- not applicable.

### 1.8. Scope and Objectives

Recent advancements in nanotechnology have unfolded novel opportunities in medicine, especially in targeted therapeutics and medical imaging. However, the majority of the existing technologies for nanotechnology suffer from two major shortcomings in drug accumulation in cancer tissues: (i) rapid elimination from the systemic circulation before reaching the cancer tissue. (ii) poor tumor accumulation and penetration due to inadequate vasculature and extensive extracellular matrix in the tumor.

Delivering NPs through a systemic route poses a major challenge due to the recognition of the circulating NPs by the reticuloendothelial system (RES). The conventional approach to improve the circulation of nanocarriers has been surface modification either by coating or conjugating with polyethylene-glycol (PEG) (PEGylation). However, recent studies point toward an anomalous behavior of PEGylated nanocarriers such as the ABC phenomenon, where they are cleared much faster than expected. One reason might be that repeated injections of PEGylated nanocarriers result in the generation of anti-PEG IgM antibodies.

Recently, transporters have become emerging targets for the development of targeted-drug delivery systems. Nutritional transporters are a group of influx transporters that transport hydrophilic nutrients such as sugars or amino acids across the membrane. SLC transporters have been explored as alternatives to deliver drugs, diagnostic markers or nano-drug delivery systems across cancer cells for active drug targeting. GLUT1 is the most ubiquitous and extensively studied glucose transporter. Its properties have been extensively studied in RBCs. GLUT1 is highly expressed in the majority of cancer types. Current research efforts are focused on developing novel drug delivery systems that

structurally resemble the endogenous substrates (glucose and amino acids) and thereby enable them to reach the target sites, minimizing the amount reaching the non-target tissues. The overall goal is to demonstrate the feasibility of employing nutritional transporters (GLUT1) as novel approaches for cancer-targeted drug delivery.

To achieve this goal, the following were the specific aims of this dissertation:

**Objective 1:** Nano-Bio interactions to enhance the systemic circulation time, pharmacokinetics and tumor accumulation of nanomedicine in cancer by conjugating glucose on their surface (GLU-NPs) to ride on the RBCs through NPs-glucose interaction with glucose transporter-1 (GLUT1) that are abundantly expressed on the membrane of RBCs (chapter II).

**Objective 2:** Demonstrate the utility/feasibility of nutritional transporters (GLUT1) as an approach for cancer-targeted drug delivery (chapter III).

# CHAPTER II

## NANO-BIO INTERACTIONS TO ENHANCE THE SYSTEMIC CIRCULATION TIME AND TUMOR ACCUMULATION OF NANOMEDICINE IN CANCER

## 2.1. Introduction

Recent advancements in nanotechnology have unfolded novel opportunities in medicine, especially in targeted therapeutics and medical imaging [3, 4, 14, 188-190]. Nanotechnology-based delivery systems such as liposomes, micelles, nanoparticles, dendrimers, etc. have been studied extensively over the past decade for the delivery of drugs and/or imaging agents [3, 4, 14, 77, 188-192]. Nanomedicine holds several advantages over their free drug counterparts such as the sustained release of the encapsulated drug, protection from degradation in circulation, and active or passive targeting to target tissues like brain, lungs or cancer [79, 103, 112, 188, 193, 194]. Most of the nanomedicine work has been targeted towards cancer therapy. A critical need for reducing the toxicity of anti-cancer drugs along with the unique anatomical and physiological differences of cancer tissues have contributed to major developments in nanomedicine for targeted-drug delivery [14, 188, 190, 191]. However, still the delivery of nanoparticles (NPs) by the parenteral route, especially through intravenous administration, poses a major challenge mainly due to their recognition by the immune system as foreign particles, which leads to their rapid clearance from the circulation. Circulating NPs are mainly recognized by the reticuloendothelial system (RES) or mononuclear phagocyte system (MPS) following opsonization and are rapidly removed from the circulation [78, 112, 195]. The rate of clearance from circulation is determined by various properties of the particles such as size, surface chemistry, shape and charge of the NPs on their surface [82, 196-198]. Particles greater than 200 nm can be trapped in the fenestrations of other organs such as spleen [199, 200], whereas particles less than 50 nm are cleared through glomerular filtration in the kidney [82, 201]. Many particles are cleared within a matter of minutes

from the circulation before even reaching the target site, as a result, their applicability is heavily dependent upon their ability to remain in the circulation for a reasonable period of time [90, 91, 197, 202].

Existing state-of-the-art technology to prolong the circulation of the NPs utilizes surface modification of the particles by chemical or physical attachment of hydrophilic polymers or proteins [77-79]. The surface modification provides a repulsive and/or steric barrier, mainly to decrease the adsorption of biological components, thereby decreasing the opsonization and clearance [78]. The polymer of choice for such applications has been polyethylene glycol (PEG). Coating NPs with PEG (a process called PEGylation), results in increasing the circulation time of various nanocarriers including polymeric/inorganic NPs, liposomes, micelles and macromolecules [85, 89, 90, 199, 203]. However, recent studies point toward an anomalous behavior of PEGylated nanocarriers. Repeated administration of PEGylated nanocarriers to animals (mice [91, 99], rats [94, 99], beagles [99] and rhesus monkey [97]) resulted in an unexpected "Accelerated Blood Clearance" (ABC). ABC is a phenomenon where the clearance rates of the carriers from the bloodstream are raised upon repeated injections [91, 94, 97]. Furthermore, PEGylation may potentially interfere with the interaction of the nanocarriers to the target cells thereby reducing the efficiency of the therapy [93]. Moreover, toxicological studies have shown that PEG could lead to an increased tendency to cause blood clotting and clumping of cells [93, 203]. Thus, there is a strong need for an innovative, yet simple strategy applicable to a wide array of nanocarriers to enhance the nanocarriers' circulation time to replace the current state-of-the-art technology [86, 105, 112].

The solution to this problem is sought in nature. Several mammalian pathogens such as *Mycoplasma haemofelis* and *Mycoplasma suis* have been known to remain in the circulation for up to several weeks by attaching themselves to the red blood cells (RBCs) [204-206]. These pathogens, varying in diameter from 200 nm to 2000 nm, attach themselves to the outer membranes of RBCs, evade recognition by the RES system, and remain in circulation for prolonged periods of time. Recently, we and others in the field have utilized a similar strategy to enhance the circulation time of polymeric nanocarriers by enabling them to bind to the surface of RBCs and travel along with RBCs in the circulation, an approach known as *RBC-hitchhiking* [76, 80, 103-111, 114-116, 118, 207].

RBCs represent the most abundant cellular constituent of the blood (> 99%) with approximately 5 million RBCs found in one microliter of human blood. They have a long circulation time (~120 ± 20 days). The RBCs possess a highly flexible structure which allows them to pass through narrow capillary fenestrations without being leaked into various organs and tissues [110, 113]. Furthermore, RBCs possess abundant surface-markers such as glycan's, sialic acid derivatives and proteins on their membrane which play a critical role in suppressing immune activation/recognition [76]. The above characteristics of RBCs along with their high biocompatibility makes them an attractive target for carrying NPs for increased circulation time [116]. For a successful translation of RBC-hitchhiking strategy for enhancing circulation time, ideally, the interaction between the NPs and RBC-surface molecules should happen in-situ and the interaction should be reversible to allow the particles to escape the vasculature and reach the target site [80, 103, 107-109, 111, 113, 115, 118].

To address the above-mentioned goals, we have designed a unique strategy based on the physiological interaction between the nutritional transporters (glucose transporters-GLUT1) present on the RBCs membrane with their ligands [208]. The glucose transporter-1 (GLUT1) is abundantly expressed on the RBCs membrane. GLUT1 corresponds to ~10% of the total integral membrane protein [209, 210]. We hypothesize that by conjugating glucose on the surface of NPs enables them to bind to GLUT1 on the surface of RBCs to travel along for enhanced circulation time [208, 211]. Since the particles used are larger than the pore size of the GLUT1, the particles will not be transported into the cells but will be attached on the surface.

In this proof-of-concept study, we demonstrate that NPs conjugated with glucose (GLU-NPs) are capable of binding to human RBCs, *in-vitro* even in the presence of plasma, and to mouse RBCs in-situ after intravenous administration. Glucose conjugation significantly enhanced the blood circulation time of NPs compared to PEGylated NPs and bound to RBCs *in-vivo*. In addition, the interaction is reversed with a magnitude of shear that is usually experienced by RBCs in the blood capillaries. This unique in-situ strategy has tremendous applications, especially in targeted drug delivery to leaky vasculature of cancer tissues. Indeed, GLU-NPs were highly targeted to mouse breast tumors (4T1) that overexpresses the GLUT1 transporter. In addition, the concept is also applicable for tumor imaging, sustained drug delivery, and targeting to other organs such as liver or lungs, etc. Furthermore, this versatile approach is applicable for a wide spectrum of the nano-delivery system including liposomes, dendrimers, and micelles [208].

## 2.2. Materials

### 2.2.1 *Reagents and Chemicals*

Fluorescent polystyrene particles (Ex/Em 580/605) with surface carboxyl groups (100, 200 and 500 nm) were purchased from Life Technologies Inc. (Portland, OR, USA). Tetrahydrofuran, hydroxylamine (HA), 1-ethyl-3-(3-dimethyl aminopropyl) carbodiimide (EDC), 2-amino-2-deoxy-D-glucose (GLU), genistein, human and mouse plasma were purchased from Sigma Aldrich (St. Louis, MO, USA). $^{3}$H-labeled oleic and palmitic acids were purchased from Moravek, Inc. (Brea, CA, USA). Regional Blood Bank, (Sioux Falls, SD, USA) provided the human RBCs. GLUT1 rabbit monoclonal antibody (12939S) was obtained from Cell Signaling Technology (Danvers, MA, USA). The $DiRC_{18}$ (D12731) dye, snakeskin dialysis membrane (10 kDa cutoff), MES hydrate and polyethylene glycol of M. Wt. 2000 ($PEG_{2000}$) and all other biochemical reagents, cell culture media, solvents, and supplies were purchased from Fisher Scientific (Pittsburgh, PA, USA).

### 2.2.2 *Cell Lines and Cell Culture*

Mouse (4T1) origin breast cancer cells were purchased from the American Type Culture Collection (ATCC) (Manassas, VA, USA). The 4T1 cells were cultured in Roswell Park Memorial Institute (RPMI-1640) medium in a humidified atmosphere of 5% $CO_2$ at 37ºC. The medium was supplemented with penicillin/streptomycin and 10% fetal bovine serum (FBS).

### 2.2.3 *Animals*

BALB/cJ mice (6-weeks old) were purchased from Jackson Laboratories (Bar Harbor, ME, USA) or Charles River Laboratories (Wilmington, MA, USA). All animal experimentation was performed in compliance with the regulations of the Institutional Animal Care and Use Committee (IACUC) of the South Dakota State University, Brookings, SD, USA.

## 2.3. Methods

### 2.3.1 *Surface Modification of NPs*

The polystyrene NPs with carboxyl surface groups were conjugated with GLU, HA, and $PEG_{2000}$ by using EDC-chemistry [212, 213]. The NPs conjugated to GLU, HA or $PEG_{2000}$ are denoted as GLU-NPs, HA-NPs, and PEG-NPs hereafter. Unless specified, GLU-NPs stands for NPs with around 200 nm in diameter (GLU-NPs-200 nm). The GLU-NPs-100 and GLU-NPs-500 indicate glucose conjugated NPs with a diameter of around 100 nm and 500 nm, respectively. Briefly, 50 µl of polystyrene NPs from a 2% w/v suspension was washed with 50 mM MES buffer (pH 6.0) three times and resuspended in 400 µl of the MES buffer. The carboxylic groups were activated by adding EDC (7.5 mg) in the above suspension and incubating for 10 min at room temperature. Subsequently, 25 mg of GLU/HA/$PEG_{2000}$ in MES buffer was added to the suspension and the reaction was carried out for 4 h at room temperature covered in dark. After 4 h, the NPs were collected by centrifugation at 20,000g for 30 min and washed thrice with 50 mM phosphate-buffered saline, pH 7.0 (PBS). The NPs were stored at 4°C in presence of 20 mM sodium azide and 0.001 % Triton X-100 until further analysis.

### 2.3.2 *Characterization of Particles: Size and Surface Charge*

***2.3.2.1 Dynamic Light Scattering (DLS)***: The average size, polydispersity index and surface charge (ς-potential) of NPs were determined using the DLS technique. Initially, the NPs were dispersed in phosphate buffer (pH 7.4) 10 mM, sonicated using bath sonicator and then further diluted (1:10) using filter-sterilized deionized water before recording particle size and ς-potential using Malvern Zeta-Sizer, Malvern Ltd, MA, USA [214-217].

### 2.3.3 *Scanning Electron Microscopy*

A FEI XL40 SEM at 3-5 kV with a 5 mm working distance was used for imaging both the cells and the surface conjugated NPs. The cells and the NPs attached to RBCs were imaged in a dehydrated state and prepared using a standard cell surface fixation technique. The samples were incubated with a 2.5% glutaraldehyde solution for the cross-linking of surface proteins. Images were acquired after 2 min of palladium coating via a Hummer sputtering system [103].

### 2.3.4. *In-vitro Binding of NPs to RBCs*

The *in-vitro* binding of GLU, HA, $PEG_{2000}$ conjugated NPs with human RBCs was determined by incubating an increasing number of NPs with $1 \times 10^5$ RBCs in sterile PBS for 4 h at 37°C at 100 RPM. The RBCs were separated from unbound NPs by centrifugation at 800g for 10 min and washing three times with sterile PBS. The number of NPs bound to RBCs was determined by measuring fluorescence at Ex/Em 580/605 nm using fluorimeter (Molecular Devices SpectraMax Plus Microplate Reader). Precautions were taken to minimize light exposure to NPs.

The binding of GLU-NPs ($1 \times 10^9$) to $1 \times 10^5$ RBCs was also tested in the presence of various proportions of human plasma (0-100%) in PBS as mentioned above.

The involvement of GLUT1 transporter on the surface of RBCs in the binding of GLU-NPs was evaluated by utilizing genistein, a competitive inhibitor of GLUT1. Briefly, increasing concentrations of GLU-NPs were incubated with RBCs ($1 \times 10^5$) in the presence of genistein (100 μM) for 4 h at 37°C and 100 RPM. The number of NPs bound to RBCs in the presence or absence of genistein was determined as described above.

### 2.3.5 *Determination of RBC Lysis by GLU-NPs (In-vitro hematotoxicity)*

To determine the effect of binding of NPs on the integrity of human RBCs, an increasing number of NPs were incubated with $1 \times 10^5$ RBCs for 4 h at 37°C. The unbroken RBCs were separated by centrifuging at 800g for 10 min. The NPs in the supernatant were cleared by further centrifugation at 10,000g for 30 min. The lysis of the RBCs was quantified by determining the absorbance of hemoglobin in the supernatant at 548 nm using a UV-visible spectrophotometer (Molecular Devices SpectraMax Plus Microplate Reader). The percent lysis was calculated by considering RBC lysis with 1 % Triton X-100 as 100 % and PBS as 0 %.

### 2.3.6 *Effect of Shear Stress on the Binding of NPs to RBCs*

GLU-NPs were attached to the RBCs as mentioned under the *in-vitro* binding of NPs to RBCs [103]. The NP labeled RBCs were sheared in a 25-mm plate and the plate rheometer with a 0.1 mm gap (Paar Physica MCR300; Anton Paar, Ashland, VA). A solvent trap was employed to prevent water evaporation. Cells were sheared at a constant shear stress of 2,

5, 7 or 10 Pa for 30 min. The number of NPs attached on RBCs before and after the application of the shear was determined using a fluorimeter (Molecular Devices SpectraMax Plus Microplate Reader). In another experiment, after detachment using 5 Pa for 30 min, the NPs were allowed to reattach for 4 h and the number of NPs attached were determined as above [103].

### 2.3.7. *In-vitro Binding of Protein to NPs using Immunoblotting*

The *in-vitro* binding of proteins to NPs was studied by incubating NPs with 100 µl mouse plasma for a period of 4 h at 37°C at 100 RPM. At the end of the incubation, NPs were washed three times with PBS. The NPs were resuspended in sample buffer and the proteins were separated by 10% sodium dodecyl sulfate-polyacrylamide gel electrophoresis (SDS-PAGE). Proteins were then transferred onto a nitrocellulose membrane, and the blot was blocked with 5% nonfat milk. The protein levels were detected and immunoblotted with rabbit-anti-mouse Immunoglobulin (Ig) G antibody. The specific protein complexes were identified using chemiluminescence detection kit and the intensities of the bands were quantified [218, 219].

### 2.3.8. *Incorporation of Fluorescence and Radioactive Markers in NPs*

The conjugated NPs were radiolabeled as previously reported with modifications [80, 103, 107, 108]. Briefly, a 50 µl of 2% (w/v) GLU, HA and PEG conjugated NPs were swollen in a mixture of 60 µl tetrahydrofuran (THF) containing 50 µl of 1 mCi/ml $^{3}$H-oleic acid (for circulation time and biodistribution) or palmitic acid (for *in-vivo* binding of NPs to RBCs) and 500 µl water. NPs were incubated for 30 mins at room temperature, washed with water (~10 times) until no further radioactivity was detected in the supernatant. For

*in-vivo* tumor targeting studies, the NPs were loaded with a near IR dye $DiRC_{18}$ following similar swelling method. The incorporation the dye was confirmed by spectroscopic analysis at the excitation and emission wavelengths of 750 nm and 780 nm respectively. The dye was incorporated to a similar extent in all the NPs [80, 103, 107, 108].

### 2.3.9. *In-vivo Circulation Time and Biodistribution using Radiolabeled NPs*

Female BALB/c mice (7 mice per group) were injected with 5 x $10^9$ radiolabeled ($^3$H-oleic acid) NPs (GLU, HA, PEG conjugated) through the tail vein. Blood (50 µl) was collected after pre-determined time-points post-injection (5, 20, 90, 240, 480 and 720 min) in heparin-coated tubes, and plasma was separated by centrifugation. After 12 h of injection, the mice were sacrificed by cervical dislocation, the blood was perfused with normal saline and various organs were collected. The organs were homogenized in PBS at 1 g of tissue per ml. Subsequently, the plasma and the tissues were digested using tissue solubilizer (Biosol). The samples were mixed with 5 ml of Bioscint for plasma and 10 ml for tissues. The percentage of initial dose still remaining in the blood and in various organs were determined using the liquid scintillation counter (Beckman Coulter LS6500) [103].

### 2.3.10. *In-vivo RBC Binding using Radiolabeled NPs*

Female BALB/c mice (7 mice per group) were injected with 5 x $10^9$ radiolabeled ($^3$H-palmitic acid) NPs (GLU, HA, PEG conjugated) through the tail vein. Blood (50 µl) was collected after pre-determined time-points post-injection (at 2, 4, 8 and 12 h) in heparin-coated tubes, centrifuged to separate blood cells. Blood cells were subsequently digested using tissue solubilizer (Biosol). The samples were then mixed with 5 ml of Bioscint. The

number of NPs bound to RBCs was determined using the liquid scintillation counter (Beckman Coulter LS6500).

### 2.3.11. *In-vivo Tumor Accumulation of Surface Modified NPs*

Female BALB/c mice were used to study the tumor accumulation of surface-modified NPs *in-vivo*. Allograft tumors were developed by injecting ($1.5 \times 10^6$) 4T1 mouse breast cancer cells in 200 µL PBS under the skin through subcutaneous injection on the left or the right flank. All subcutaneous injections were given using a 25G needle and the hair was removed with clippers prior to injecting the tumor cells. The animals were divided into three groups and the NPs were administered. The mice were administered $4.54 \times 10^8$ particles/mouse equivalent surface-modified GLU, HA and PEG conjugated NPs containing near-infrared (IR) dye carbocyanine $DiRC_{18}$ (Ex/Em 750/780 nm) through the tail vein [217, 220]. HA-NPs and PEG-NPs were utilized as control. The mice were imaged using Bruker-Xtreme *in-vivo* imager before injection, 12 and 24 h post 1$^{st}$ injection. Another intravenous injection of NPs was administered, and the mice were imaged again at 12, 24 and 48 h after the 2$^{nd}$ injection. The intensity of the fluorescent signal was normalized and quantified using Xtreme *in-vivo* imager software. The perimeter of the tumor is marked by using a reflectance image.

### 2.3.12. *Data Analysis & Statistics*

All the experiments were performed in triplicate unless specified, and the results are expressed as mean ± standard deviation unless specified. The variance between groups was compared using *Student's t-test*, one-way or two-way ANOVA as required followed by

Bonferroni's or Dunnett's post-hoc multiple comparison tests (Instat, Graph Pad Software, CA).

## 2.4. Results

### 2.4.1. *Physicochemical Characterization of Polystyrene NPs*

To investigate the possibility of using glucose for attaching the NPs on to RBCs, polystyrene NPs conjugated with GLU on their surface were employed as a model. The ligands GLU, HA, and PEG were conjugated to NPs with surface carboxylate groups using EDC chemistry as represented in the Scheme 2-1. Polystyrene NPs with precise particles size and shape, surface modified with HA and PEG, were carefully selected as controls to rule out the role of particle size, shape, surface functional groups (-OH), charge, and hydrophilicity on the functionality of GLU-NPs (Table 2-1). The average particle diameter of the unconjugated NPs as recorded by DLS technique were 116.93 ± 0.76, 216.63 ± 2.10 and 542.13 ± 19.62 nm for NPs from commercial source labeled as 100, 200, and 500 nm, respectively. The surface zeta potential of the unconjugated NPs was from -30 to -40 mV, which is attributed to the presence of multiple surface carboxyl groups. The size of NPs after conjugating to ligands was increased (Table 2-1). The average diameter of NPs was altered to 246.73 ± 3.84 nm, 219.47 ± 2.66 nm and 288.33 ± 6.65 nm, for GLU-NPs, HA-NPs, and PEG-NPs, respectively. A similar pattern was observed with NPs of other sizes (Table 2-1). The increase in hydrodynamic radii of the ligand conjugated NPs along with the neutralization of surface charge of carboxyl groups is an indication of the successful conjugation of the ligands. The NPs were found to be monodisperse as can be seen from the polydispersity index values (Table 2-1).

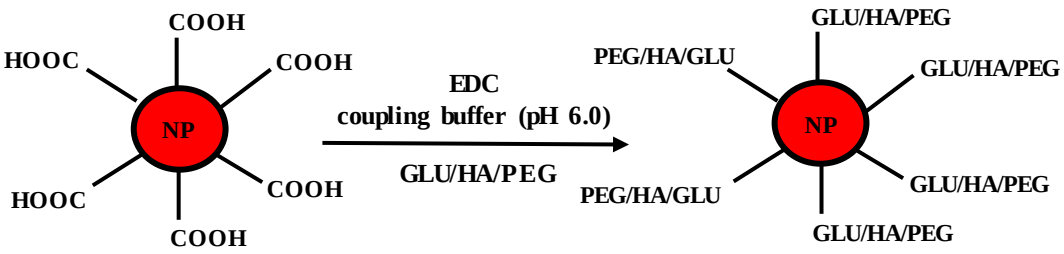


**Scheme 2-1:** Synthesis of surface-modified NPs using EDC chemistry.

**Table 2-1: Physicochemical characterization of surface-modified NPs.** The table represents the diameter (nm), polydispersity index (PDI) and zeta potential (mV) of polystyrene NPs. Data represent the mean ± standard deviation (n=3-4).

| Groups | Diameter (nm) | PDI | ZP (mV) |
|---|---|---|---|
| Unconjugated 100 nm NPs | 116.93 ± 0.76 | 0.02 ± 0.01 | -29.15 ± 3.24 |
| Unconjugated 200 nm NPs | 216.63 ± 2.10 | 0.03 ± 0.009 | -43.40 ± 0.30 |
| Unconjugated 500 nm NPs | 542.13 ± 19.62 | 0.19 ± 0.02 | -38.87 ± 0.83 |
| GLU-100 nm NPs | 157.50 ± 36.81 | 0.30 ± 0.14 | 3.71 ± 1.34 |
| GLU-200 nm NPs | 246.73 ± 3.84 | 0.10 ± 0.01 | 9.61 ± 0.26 |
| GLU-500 nm NPs | 602.40 ± 163.0 | 0.63 ± 0.02 | 1.47 ± 1.22 |
| HA-200 nm NPs | 219.47 ± 2.66 | 0.07 ± 0.02 | 8.30 ± 4.85 |
| PEG-200 nm NPs | 288.33 ± 6.65 | 0.18 ± 0.01 | 9.19 ± 2.37 |

### 2.4.2. *GLU-NPs Bind to human RBCs In-vitro in a Concentration-dependent Manner*

Human RBCs were incubated with surface modified fluorescent polystyrene NPs for 4 h at 37°C. The number of NPs bound per RBC were quantified using fluorimeter. HA-NPs or PEG-NPs were not able to bind in significant numbers to the isolated human RBCs (Figure 2-1A). In contrast, GLU on the surface of NPs enabled them to bind to RBCs in a concentration-dependent manner (Figure 2-1A) as shown using fluorimeter. The binding of GLU-NPs of ~ 100, 200 and 500 nm in diameter to RBCs also demonstrated a concentration-dependent binding (Figure 2-1C-E). The GLU-NPs bound to RBCs in concentrated domains, as GLUT1 segregates in lipid-rich domains (Figure 2D insert) [221-223]. The SEM images (Figure 2B(b)), further confirmed that GLU-NPs were bound to the RBCs in clusters as compared to HA-NPs (Figure 2B(c)) and PEG-NPs (Figure 2B(d)), which did not show any binding to the RBCs. Importantly, the ability of GLU-NPs to bind to the RBCs in the presence of plasma represents the in-situ scenario post-injection in the blood stream, which will make the strategy clinically feasible and relevant. When GLU-NPs were incubated with RBCs in the presence of different proportions of plasma, the GLU-NPs clearly demonstrated the ability to bind to the RBCs even at 100% plasma concentration (Figure 2-2). The effect of the binding of GLU-NPs on the integrity and the toxicity to human RBCs was evaluated using an increasing number of GLU-NPs in the presence of a fixed number of human RBCs. The lysis of the RBCs was estimated by determining hemoglobin released in the supernatant. Normal saline, RBCs treated with saline and 1% Triton-X100 were utilized as controls. GLU-NPs did not cause any detectable hemolysis up to $1\times10^9$ particles/million RBCs (Figure 2-3).

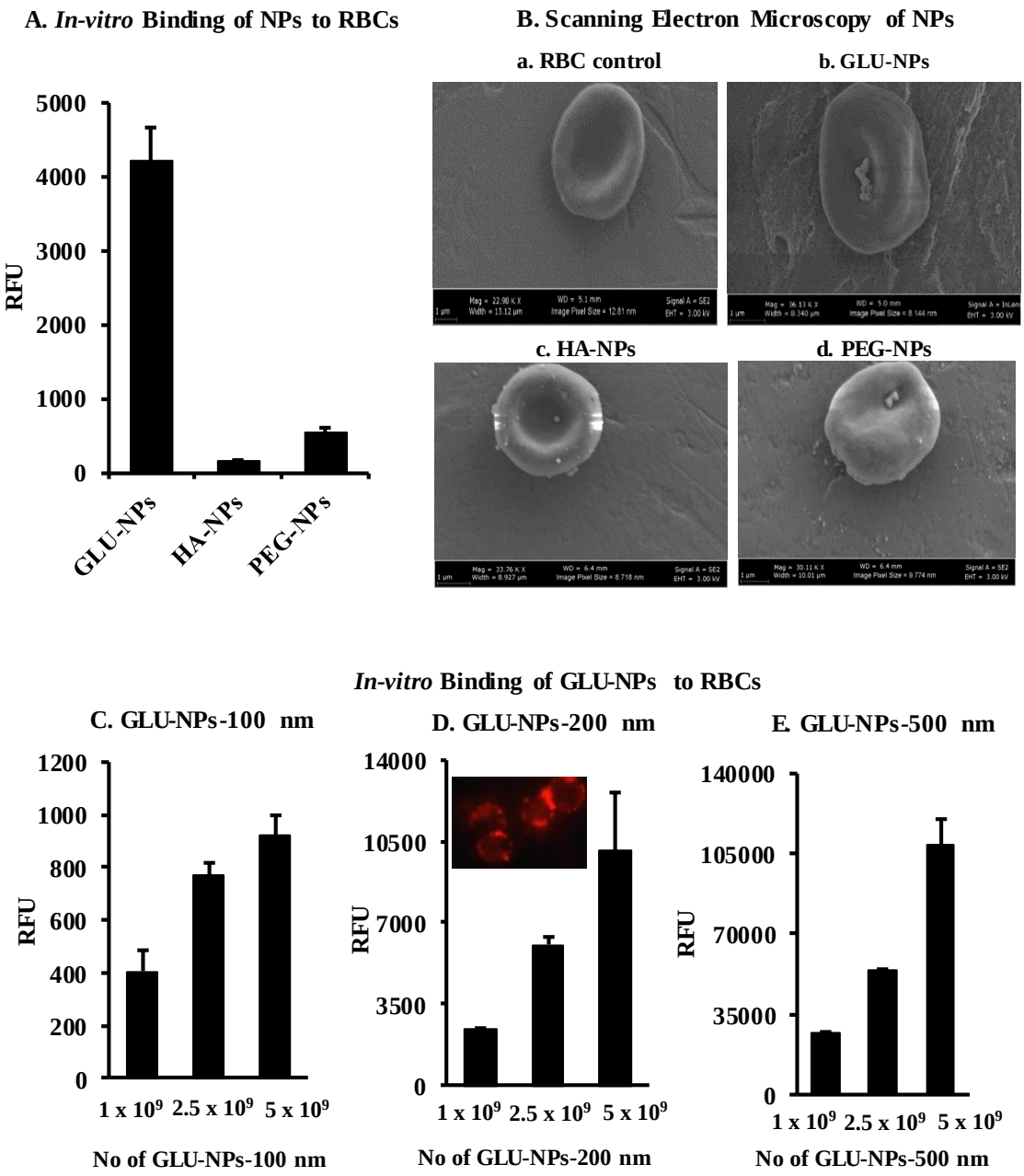


**Figure 2-1: *In-vitro* binding of NPs to RBCs.** (A) $2.5\times10^9$ GLU, HA, and PEG-NPs were incubated with $1\times10^5$ RBCs for a period of 4 h followed by washing and centrifugation at 800g to separate the RBCs bound with the NPs. The fluorescence of the RBCs was measured in a 96 well black bottom plate at 580/605 nm. (B) Scanning electron microscopy of NPs bound to RBC. *In-vitro* binding of GLU-NPs to RBCs. GLU-NPs-100 nm (C),

GLU-NPs-200 nm (D) and GLU-NPs-500 nm (E). $1\times10^9$ -$5\times10^9$ GLU-NPs were incubated with $1\times10^5$ RBCs for a period of 4 h followed by washing and centrifugation at 800g to separate the RBCs bound with the NPs. The fluorescence of the RBCs was measured in a 96 well black bottom plate at 580/605 nm using fluorimeter. Data represent the mean ± standard deviation (n=3-4). Relative fluorescence unit (RFU).

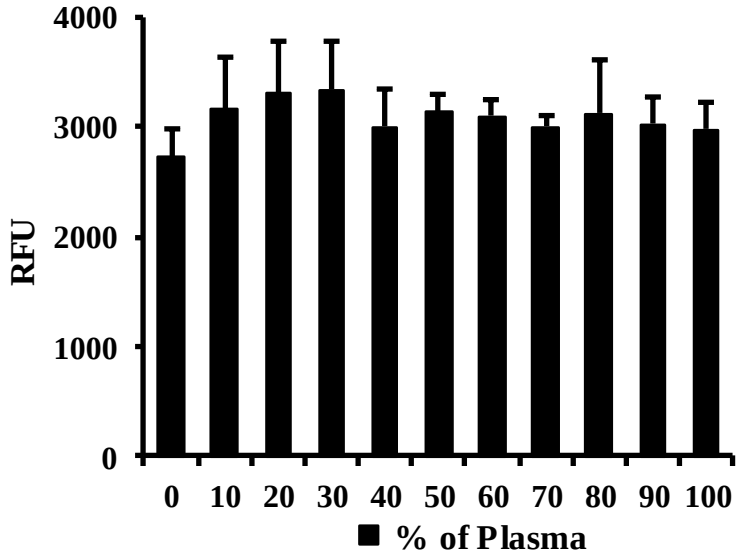


**Figure 2-2: Binding of GLU-NPs to RBCs in the presence of plasma.** $1\times10^9$ GLU-NPs-200 nm were incubated with $1\times10^5$ RBCs in presence of varying concentrations of plasma (0-100%) for a period of 4 h followed by washing and centrifugation at 800g to separate the RBCs bound with the NPs. The fluorescence of the RBCs was measured in a 96 well black bottom plate at 580/605 nm using fluorimeter. Data represent the mean ± standard deviation (n=3-4). Relative fluorescence unit (RFU).

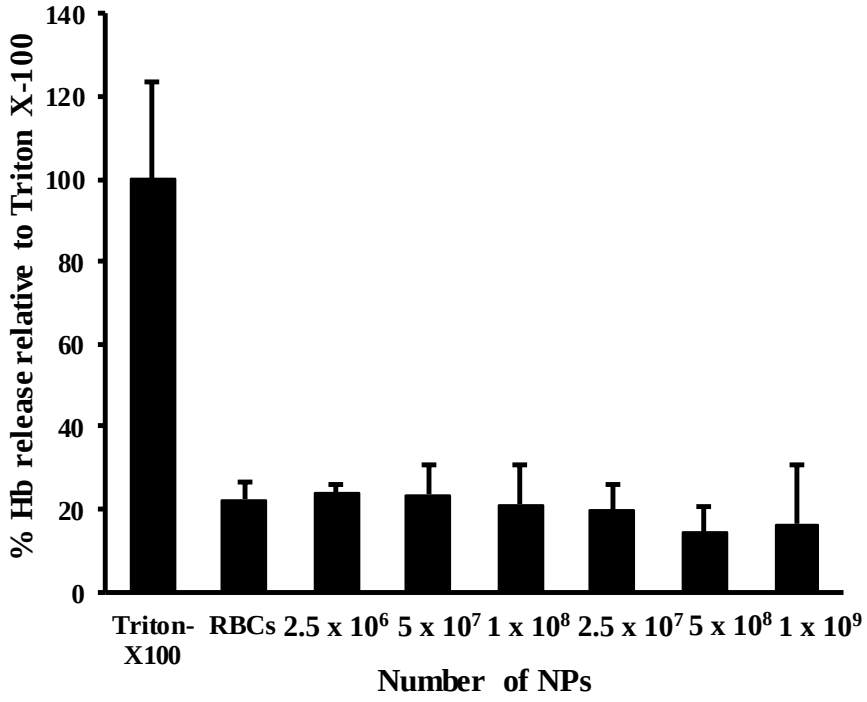


**Figure 2-3: The *in-vitro* hematotoxicity of NPs to RBCs.** An increasing number of NPs were incubated with $1\times10^5$ RBCs for a period of 4 h at 37˚C and 100 RPM. Following the incubation, the whole RBCs were separated from the NPs by centrifuging at 800g. The NPs in the supernatant were cleared by further centrifugation at 10,000g for 30 min. The lysis of the RBCs was estimated by determining hemoglobin released in the supernatant by measuring the absorbance of the supernatant at 548 nm. 1% Triton-X100 and RBCs were used as controls. Data represent the mean ± standard deviation (n=3-4).

### 2.4.3. *The Binding of GLU-NPs to RBCs is GLUT1 Dependent*

Once established that the surface GLU promotes the binding of polystyrene NPs to RBCs, the role of GLUT1 on the membrane of RBCs in binding was investigated by quantifying the binding in the presence of genistein, a known competitive inhibitor of the glucose-

GLUT1 interaction [224, 225]. The RBCs were pre-incubated with 100 µM genistein before the addition of GLU-NPs. Genistein inhibited the binding of GLU-NPs to RBCs ~60-80% when incubated with GLU-NPs ($2.5 \times 10^6$ - $5 \times 10^8$) (Figure 2-4). The attachment of GLU-NPs with RBCs was inhibited significantly by genistein, indicating that glucose-GLUT1 interaction may contribute to the surface attachment of GLU-NPs.

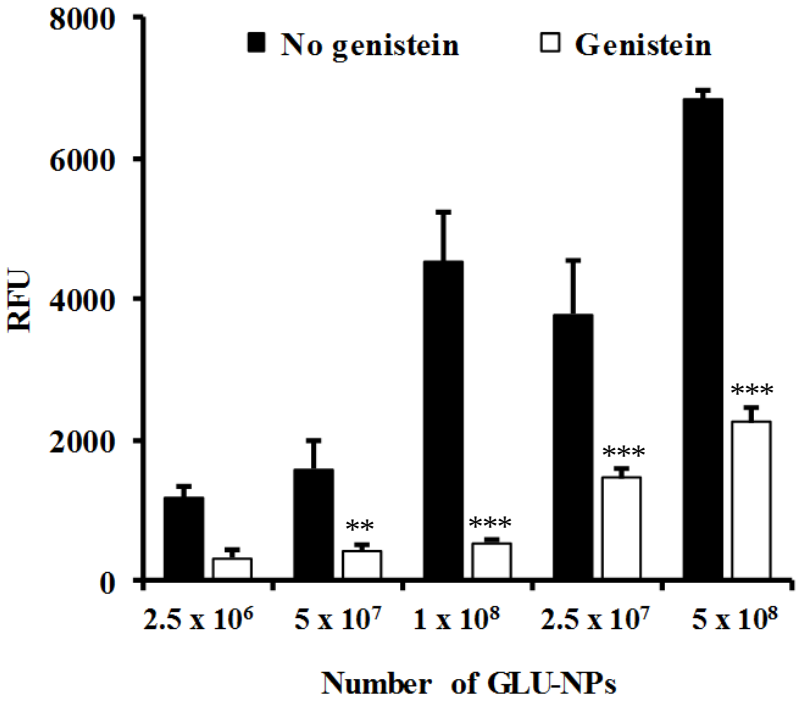


**Figure 2-4: Binding of GLU-NPs to RBCs in the presence or absence of genistein.** An increasing number of GLU-NPs-200 nm were incubated with $1 \times 10^5$ RBCs in the presence or absence of genistein (100 µM) for a period of 4 h followed by washing and centrifugation at 800g to separate the RBCs bound with the NPs. The fluorescence was measured in a 96 well black bottom plate at 580/605 nm using a fluorimeter. Data represent the mean ± standard deviation (n=3-4). Relative fluorescence unit (RFU). ** and *** indicates that the results are statistically significant at $p \leq 0.01$ and $p \leq 0.001$ as compared

to no genistein group calculated using two way-ANOVA followed by Bonferroni's multiple comparison test.

### 2.4.4. *The Binding of GLU-NPs to RBCs is Non-covalent and Reversible*

The practicality of this approach rests heavily on the ability of the attached GLU-NPs to have a reversible interaction with RBCs, which would allow them to reach the target tissue for pharmacological action. RBCs usually experience shear stress of the magnitude ranging between 0.01 to 14 Pa when squeezed through finer capillaries in the circulation [226]. Such shear has been shown to detach the surface-bound NPs. To simulate the conditions *in-vitro*, we utilized a plate and plate viscometer to impart measurable stress to the NPs bound RBCs. The stress of 2, 5, 7 or 10 Pa was applied over a time period of 30 min to the NPs bound RBCs in plasma. The particles that remained attached to the RBCs were subsequently quantified. The percent of particles detached at various shear stress (Pa) ranged from 20 % at 2 Pa to 60 % at 10 Pa. The implementation of stress dislodged the NPs from the surface of RBCs (Figure 2-5A). The GLU-NPs, which were dislodged from the RBCs, were able to reattach after 4 h of incubation in absence of shear (Figure 2-5B). The ability of the GLU-NPs to reversibly attach to RBCs could be critical in utilizing the strategy for drug delivery.

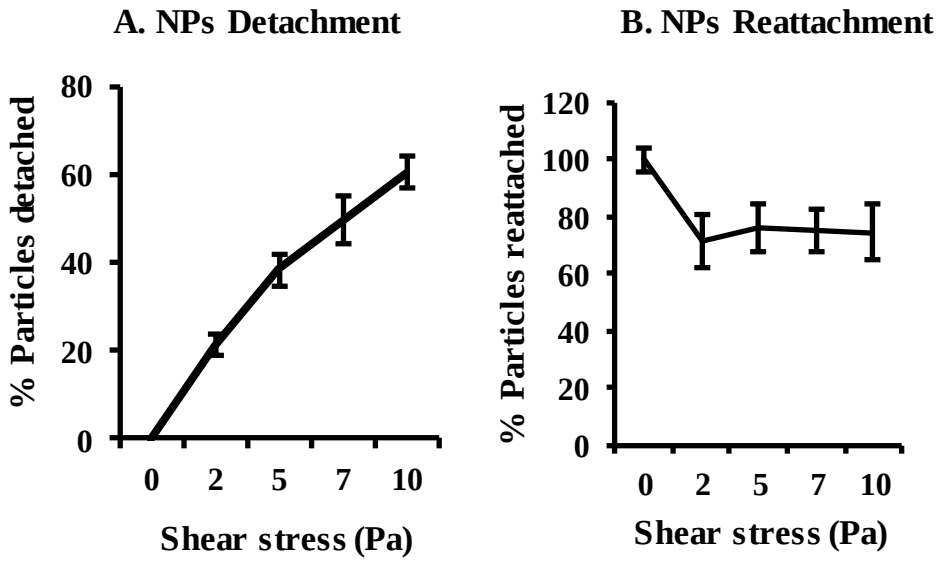


**Figure 2-5: Reversibility of Binding**. (A) **Shear stress-induced particle detachment**. $2\times10^5$ NPs were bound per $1\times10^5$ RBCs. The particle labeled RBCs were subjected to stress in a plate and plate viscometer for a period of 30 min. (B) **Reattachment of NPs after removal of stress**. $2\times10^5$ NPs were bound per $1\times0^5$ RBCs. The particle labeled RBCs were subjected to shear stress in a plate and plate viscometer for a period of 30 min. Following which they were allowed to rebind to the RBCs for 4 h. In both instances, the percentage of particles detached and reattached was determined by measuring the fluorescence of the RBCs at 580/605 nm using a fluorimeter. Data represent the mean ± standard deviation (n=3-4). *This experiment was performed, and the data was generated by Pratik Muley.

### 2.4.5. *GLU-NPs do not cause any Major Opsonization of Proteins*

The *in-vivo* behavior and biodistribution of intravenous administered NPs are influenced by the interaction of the particles with the blood proteins [227]. One factor that influences the NPs-protein corona is the number of proteins that interact with the NP surface. Immunoglobulin (Ig) G is by far one of the dominant proteins of the adsorption patterns,

representing over 70% of the total detected protein amounts. IgG plays a very important role in the opsonization related clearance of the intravenously injected particles [227-230]. We determined the amount of IgG bound to NPs using immunoblotting by incubating equal amounts of NPs with mouse plasma for 4 h. GLU-NPs demonstrated significantly weak protein adsorption, more specifically IgG as compared to HA-NPs and PEG-NPs. GLU-NPs with ~100 nm diameter have shown higher IgG opsonization compared to GLU-NPs with ~ 200 nm or 500 nm diameter (Figure 2-6). This may be due to the presence of a greater number of NPs and larger surface energy per microgram of the NPs for 100 nm as opposed to 200 nm/500 nm NPs. Relative to PEG-NPs, the GLU-NPs with ~100 nm diameter showed ~65 % IgG opsonization, whereas GLU-NPs of 200 nm and 500 nm diameter demonstrated ~48 % and 53% IgG opsonization (Figure 2-6).

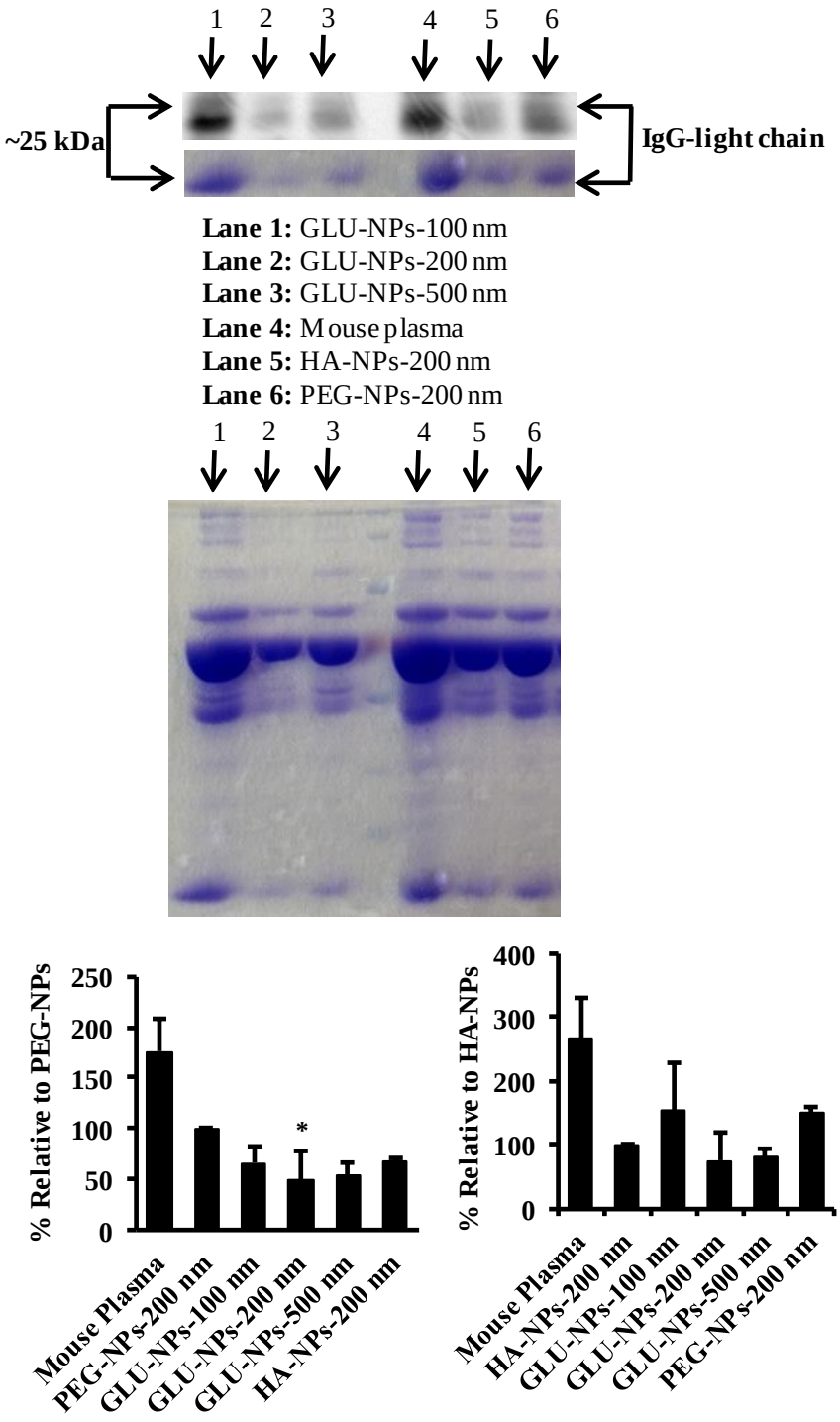


**Figure 2-6: Protein adsorption patterns on surface-modified NPs.** *In-vitro* binding/adsorption of proteins (IgG-light chain) to surface-modified NPs in the presence

of mouse plasma for a period of 4 h and the percentage protein adsorbed on surface-modified NPs relative to PEG-NPs and HA-NPs. Data represent the mean ± standard deviation (n=3-4). * indicates that the results are statistically significant at $p \leq 0.05$ as compared to PEG-NPs-200 nm, calculated using two way-ANOVA followed by Dunnett's multiple comparison test.

### 2.4.6. *GLU-NPs Bound to Mouse RBCs In-vivo*

Once the binding of GLU-NPs to RBCs is established *in-vitro*, the concept was advanced *in-vivo* using GLU-NPs loaded with radiolabeled palmitic acid (section 2.3.8). The surface adsorbed palmitic acid was washed before injecting the particles. GLU, HA and PEG NPs ($5\times10^9$ particles/mouse) radiolabeled with ($^3$H-palmitic acid) were injected by tail vein in BALB/cJ mice. Blood was collected after pre-determined time points (at 2, 4, 8 and 12 h) post-injection in heparin-coated tubes, centrifuged to separate the blood cells. Subsequently, the blood cells were digested using a tissue solubilizer (Biosol) and mixed with 5 ml of Bioscint. The number of NPs bound to RBCs was determined using the liquid scintillation counter. The results demonstrate that GLU-NPs bound to RBCs in-*vivo* in significant numbers as opposed to the HA-NPs and PEG-NPs at 4, 8 and 12 h post-injection (Figure 2-7). Specifically, at 4 h and 8 h post-injection, ~1 (at $p \leq 0.001$) and 0.45 (at $p \leq 0.05$) GLU-NPs were bound per RBC as compared to HA-NPs and PEG-NPs (Figure 2-7). On an average 0.3-1 GLU-NPs per RBC were bound 2-12 h post-injection. HA-NPs and PEG-NPs showed considerably less binding than GLU-NPs. PEG-NPs demonstrate non-specific binding at 2 h as can been seen from (Figure 2-7). GLU-NPs demonstrated significantly higher efficiency of binding to RBCs because of the glucose-GLUT1

interaction from the GLUT1 present on the RBC surface. The *in-vivo* binding of GLU-NPs to GLUT1 on RBCs could potentially play a critical role in enhancing the circulation time of NPs.

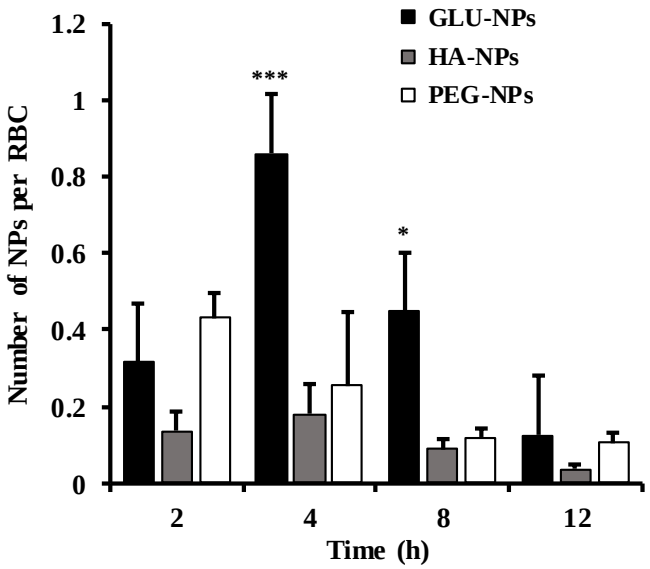


**Figure 2- 7: *In-vivo* binding of surface-modified NPs to RBCs.** Surface modified NPs ($5\times10^9$ particles/mouse) radiolabeled with ($^3$H-palmitic acid) were injected by tail vein in BALB/cJ mice. Blood was collected after pre-determined time points (at 2, 4, 8 and 12 h) post-injection and digested using tissue solubilizer (Biosol) and mixed with Bioscint. The number of NPs bound to RBCs was determined using the liquid scintillation counter. Data represent mean ± standard error of the mean (n=7 mice). *** and * indicates that the results are statistically significant at $p \leq 0.001$ and $p \leq 0.05$ as compared to both HA-NPs and PEG-NPs, respectively using two way-ANOVA followed by Bonferroni's multiple comparison test.

### 2.4.7. *GLU-NPs Demonstrate Enhanced Systemic Circulation Time without Altering the Biodistribution*

One of the main goals of the study is to enhance the circulation time of NPs by hitchhiking on to the RBCs using glucose-GLUT1 interaction. Therefore, the ability of conjugating GLU on the surface of NPs in enhancing blood circulation time was assessed in mice using GLU-NPs that are encapsulated with the radiolabeled oleic acid (section 2.3.8). Blood samples were collected at pre-determined time intervals (at 5, 20, 90, 240, 480 and 720 min) and the radioactivity was measured using liquid scintillation counter. Various pharmacokinetic parameters were calculated for GLU, HA, and PEG-NPs. The circulation half-life ($t_{50\%}$) and the time required to clear 90% of the particles from the circulation ($t_{90\%}$) of GLU-NPs was significantly higher than the HA, and PEG NPs (Figure 2-8A and C). The $T_{90\%}$ was ~7 h for GLU-NPs as compared to 4 h and 1 h for PEG-NPs and HA-NPs, respectively (Figure 2-8C). The GLU-NPs demonstrated at least 2-fold (at $p \leq 0.001$) longer circulation half-life as compared to the HA-NPs and PEG-NPs. The elimination rate constant was much lower, and the volume of distribution was higher for GLU-NPs compared to HA-NPs and PEG-NPs (Table 2-2). Thus, the presence of surface glucose reduced the systemic clearance of NPs in mice.

The concentration of NPs in various organs was determined by isolating the organs 12 h post-injection and calculating the NPs remaining as % of injected dose (Figure 2-8B). At the end of 12 h, all groups of NPs demonstrated a similar biodistribution in various tissues including liver, kidney, lungs, spleen, and brain. This indicates that the general pharmacokinetic distribution pattern of NPs did not alter by conjugating glucose on their surface, however, glucose significantly improved circulation time.

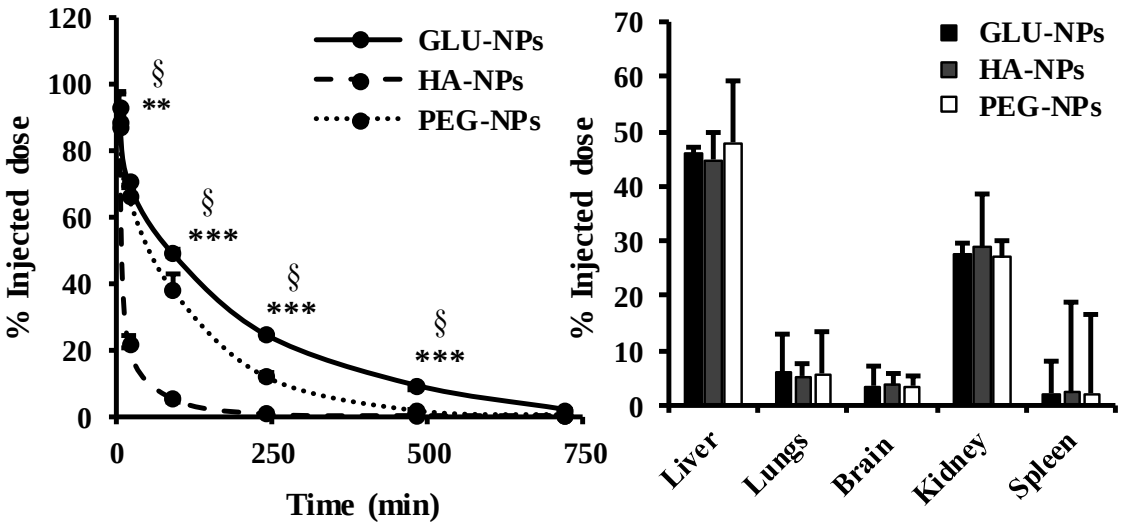


**C. Pharmacokinetic Parameters**

| Parameters | GLU-NPs | HA-NPs | PEG-NPs |
|---|---|---|---|
| $t_{50}$ circulation (min) | 126 ± 12.56 | 7.96 ± 1.52 | 75.80 ± 1.52 |
| $t_{90}$ circulation (min) | 452 ± 10.56 | 62.35 ± 7.52 | 253.26 ± 6.56 |
| Kel (Elimination rate constant) ($hr^{-1}$) | 0.00551 ± 0.00054 | 0.0871 ± 0.004 | 0.00914 ± 0.00074 |
| $V_d$ (Volume of distribution) (L) | 1.16 ± 0.065 | 0.763 ± 0.084 | 1.01 ± 0.097 |

**Figure 2-8: *In-vivo* circulation time and biodistribution of surface-modified NPs.** (A) Radiolabeled nanoparticles ($^3$H-oleic acid) were injected by tail vein in BALB/cJ mice and the percent of injected dose remaining was calculated and plotted against time. (B) Biodistribution of surface-modified NPs. After 12 h of injection, the mice were sacrificed by cervical dislocation, the blood was perfused with normal saline and various organs were

collected. The percentage of initial dose still remaining in various organs was determined using the liquid scintillation counter. (C) The pharmacokinetic parameters calculated considering IV bolus dose and one compartment open model of the NPs. Data represent the mean ± standard deviation (n=7 mice). *** and § indicates that the results are statistically significant at $p \leq 0.001$ as compared to HA-NPs and PEG-NPs respectively using two way-ANOVA followed by Bonferroni's multiple comparison test. *This experiment was performed, and the data was generated by Pratik Muley.

### 2.4.8. *GLU-NPs Demonstrate Increased Tumor Accumulation*

Once the concept of enhancement of circulation time and binding of GLU-NPs to RBCs was established *in-vivo*, we have studied the tumor accumulation of GLU-NPs by live mouse imaging. The mice were divided into three groups and ($4.54 \times 10^8$ particles/mouse) equivalent surface-modified GLU, HA and PEG NPs loaded with a near IR dye $DiRC_{18}$ were injected through the tail vein (Figure 2-9A). The incorporation of the dye was confirmed by spectroscopic analysis at the excitation and emission wavelengths of 750 nm and 780 nm respectively. The extent of GLU-NPs circulating in the body was significantly higher as seen from the imaging results than HA-NPs or PEG-NPs (Figure 2-9B) at 12 h, and 24 h post 1$^{st}$ injection (Figure 2-9B and C) and at 12 h, 24 h and 48 h post 2$^{nd}$ injection (Figure 2-10B and C). The quantification of the results further demonstrate that GLU-NPs has ~3 fold higher accumulation into tumors at 12 h and 24 h post 1$^{st}$ injection (at $p \leq 0.001$) and ~6 fold (at 12 h) and 3 fold (at 24 h) (at $p \leq 0.001$) higher accumulation into tumors as opposed to HA-NPs and PEG-NPs post 2$^{nd}$ injection respectively (Figure 2-10B and C). Thus, GLU-NPs demonstrate higher tumor accumulation than HA-NPs and PEG-NPs

(Figure 2-9B and C, Figure 2-10B and C). One of the possible reasons for the enhanced tumor accumulation is that 4T1 tumors are known to overexpress GLUT1 transporter and the GLU-NPs localized into the tumor utilizing a combination of passive, and active targeting. Moreover, RBCs are known to have significantly higher GLUT1 transporter and the results from the *in-vivo* pharmacokinetic study also demonstrate enhancement of circulation time (Figure 2-8) and binding of GLU-NPs to RBCs (Figure 2-7). GLU-NPs also showed considerably less opsonization of protein (IgG) than PEG-NPs (Figure 2-6). Thus, GLU-NPs demonstrate enhancement in tumor accumulation due to the combined passive, active targeting, reduced opsonization, and enhancement in circulation time.

**A. Scheme for *in-vivo* Tumor Accumulation**

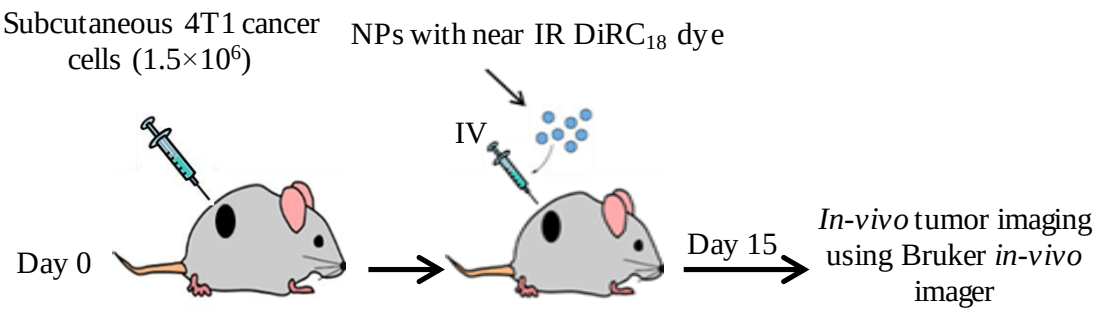


**B. *In-vivo* Tumor Accumulation**

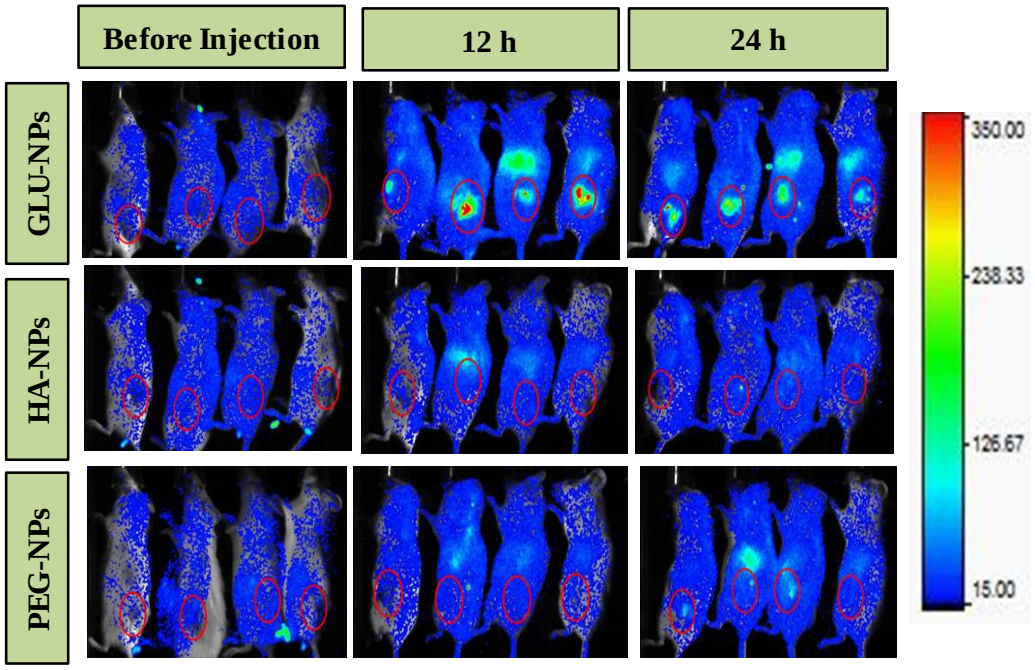


**C. Quantification of Tumor Accumulation**

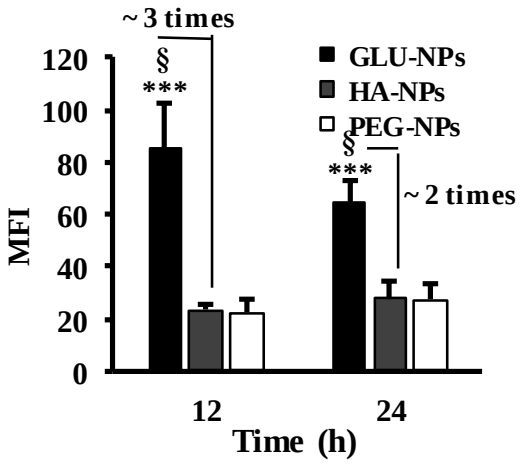

**Figure 2-9: *In-vivo* tumor accumulation of surface-modified NPs after 1st injection.** (A) Scheme for *in-vivo* administration of surface-modified NPs. The mice were inoculated with 4T1 ($1.5\times10^6$) breast cancer cells via subcutaneous injection. GLU, HA, and PEG NPs ($4.54\times10^8$ particles/mouse) were encapsulated with near IR dye $DiRC_{18}$ and administered IV to BALB/cJ mice. The mice were subjected to tumor imaging at various predetermined time points (before injection, at 12 and 24 h) using a Bruker *in-vivo* imager. (B) Representative *in-vivo* fluorescence images (before injection, 12 and 24 h) obtained after time-lapse imaging using a Bruker *in-vivo* imager. The mice were anesthetized using isoflurane before imaging. The scale represents normalized intensities. The red circle indicates the tumor site. (C) Quantification of tumor accumulation of surface-modified NPs. The amount of NPs in the tumor was quantified after normalizing the intensities using Bruker MI software. The data represents mean fluorescence intensities at various time points. Data represent the mean ± standard deviation. *** and § indicates that the results are statistically significant at $p \leq 0.001$ as compared to HA-NPs and PEG-NPs respectively using two way-ANOVA followed by Bonferroni's multiple comparison test.

**A. Scheme for *in-vivo* Tumor Accumulation**

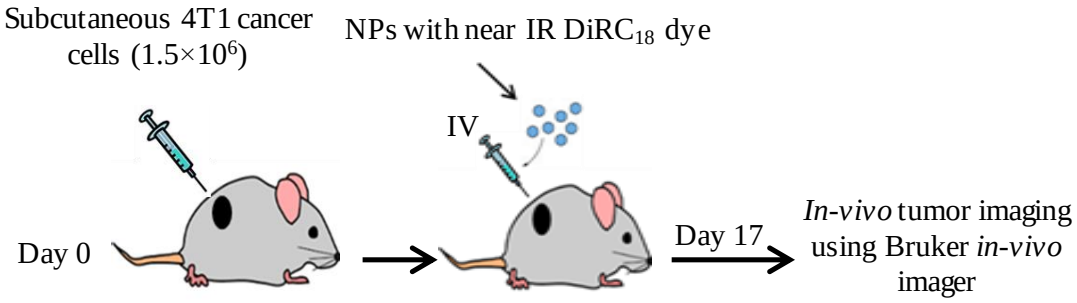


**B. *In-vivo* Tumor Accumulation**

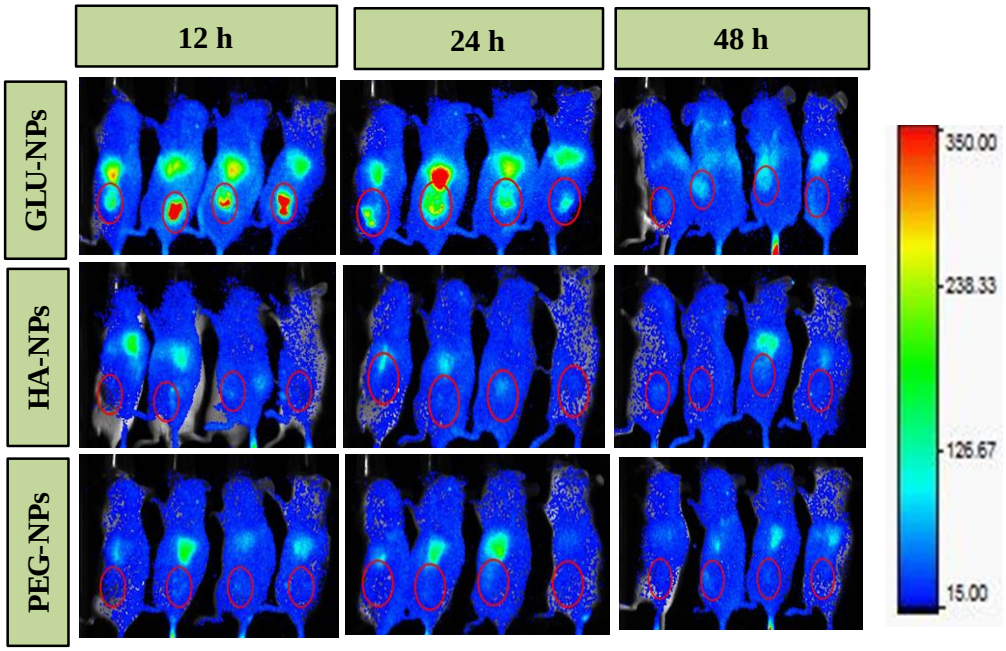


**C. Quantification of Tumor Accumulation**

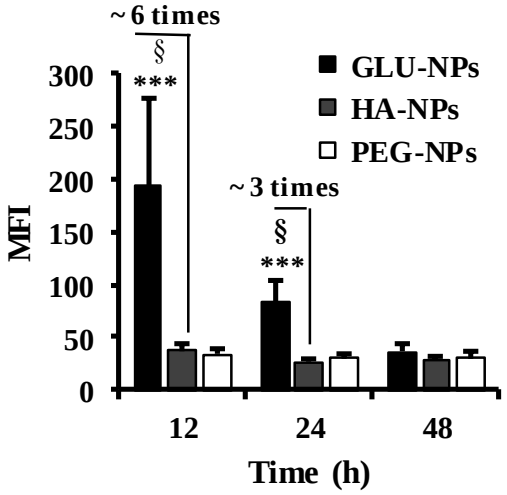

**Figure 2-10: *In-vivo* tumor accumulation of surface-modified NPs after the 2nd injection (day 17).** (A) Scheme for *in-vivo* administration of surface-modified NPs. The mice were inoculated with 4T1 ($1.5\times10^6$) breast cancer cells via subcutaneous injection. GLU, HA, and PEG NPs ($4.54\times10^8$ particles/mouse) were encapsulated with near IR dye $DiRC_{18}$ and administered IV to BALB/cJ mice. The mice were subjected to tumor imaging at various predetermined time points (at 12 h, 24 h, and 48 h) using a Bruker *in-vivo* imager. (B) Representative *in-vivo* fluorescence images (at 12 h, 24 h, and 48 h) obtained after time-lapse imaging using a Bruker *in-vivo* imager. The mice were anesthetized using isoflurane before imaging. The scale represents normalized intensities. The red circle indicates the tumor site. (C) Quantification of tumor accumulation of surface-modified NPs. The amount of NPs in the tumor was quantified after normalizing the intensities using Bruker MI software. The data represents mean fluorescence intensities at various time points. Data represent the mean ± standard deviation. *** and § indicates that the results are statistically significant at $p \leq 0.001$ as compared to HA-NPs and PEG-NPs respectively using two way-ANOVA followed by Bonferroni's multiple comparison test.

## 2.5. Discussion

The short half-life of nanoparticles in the systemic circulation is a major roadblock in advancing the intravenously injected nanomedicine for both imaging and/or drug delivery [80, 103, 107, 108, 189, 196, 197]. Particulate delivery systems are foreign in nature and therefore, are quickly recognized and eliminated by MPS of the immune system such as circulating monocytes and macrophages of the liver, spleen, lung, and bone marrow [231, 232]. This study provides a unique strategy of trapping NPs on the surface of RBCs with natural, reversible, non-covalent interaction to evade rapid clearance and making them available at capillaries for efficient accumulation and targeting for cancer therapeutics and/or imaging [75]. In this study, polystyrene NPs were surface modified with glucose (GLU-NPs) to interact with GLUT1 transporter on the membrane of RBCs, thereby enhancing systemic circulation time and tumor accumulation [208].

Three major physiological mechanisms are involved in the clearance of particulate matter form the circulation; opsonization by plasma proteins (opsonin's), phagocytosis by cells of the MPS, and renal filtration. Opsonization enhances recognition by phagocytic cells and accelerates clearance [75, 112, 233-237]. Together, they constitute a potent mechanism to clear pathogens and particles from the circulation, as early as 10 minutes [231, 233, 234, 238]. Numerous strategies have been designed to target specific/multiple mechanisms of clearance mentioned above. For example, increasing the size of NPs more than 10 nm has generally been shown to reduce the renal clearance [239, 240]. In this study, we have selected spherical polystyrene NPs of around 200 nm diameter to represent the majority of the nano-drug delivery systems currently being investigated, which is expected to reduce renal filtration.

The existing state-of-the-art technology to prolong the circulation of NPs targets opsonization and utilizes surface modification with hydrophilic polymers or proteins [77-79]. Since opsonin's preferentially bind to hydrophobic surfaces, modification with a hydrophilic polymer provides a repulsive and/or steric barrier to reduce the opsonization [78]. The polymer of choice for such applications has been PEG [79, 86, 87, 89, 90]. PEGylation increases the circulation time of various nanocarriers including polymeric/inorganic NPs, liposomes, micelles and macromolecules [85, 89, 90, 203]. However, recent studies point toward an anomalous behavior of PEGylated nanocarriers. Repeated administration of PEGylated nanocarriers to animals (mice [91], rats [94], beagles [99] and rhesus monkey[97]) resulted in an unexpected *"Accelerated Blood Clearance" (ABC)* mainly due to the generation of anti-PEG-IgM antibodies from splenic B-cells [95, 98, 241-243]. ABC is a phenomenon where the clearance rates of the carriers from the bloodstream are raised upon repeated injections [91, 94, 97]. Furthermore, PEGylation potentially interferes with the interaction of the nanocarriers to the target cells, thereby reducing the efficiency of the intended therapy [93]. More importantly, the cost of the technology also plays a significant role to translate the potential of nanomedicine from laboratory to patient. Mono and bi-functional PEGs commonly used in PEGylation are very expensive and add significantly to the cost of the final product. Moreover, toxicological studies have shown that PEG could lead to an increased tendency to cause blood clotting and clumping of cells [93, 203].

In this study we have addressed the drawbacks with PEGylation by surface modification of NPs using glucose with the following evidence/rationale(s): (i) being a smaller endogenous ligand, glucose is not expected to evoke antibody response or undergo

ABC-mediated removal from circulation; (ii) glucose is safer than synthetic macromolecules (iii) glucose conjugation reduced opsonization much better than PEGylation (Figure 2-6); (iv) as glucose is a ligand for active targeting for cancer cells [145, 163, 174, 182, 244], it improves the interaction and accumulation of NPs in the cancer tissue, thereby demonstrating increased tumor accumulation (Figure 2-9 and 2-10) (v) modifying NPs with glucose imparts an ability to hitchhike on RBCs (Figure 2-8), which has been recently discovered as an efficient strategy for enhanced circulation time [80, 86, 103-105, 107, 108, 113]. GLU-NPs enhanced the circulation half-life of NPs by ~2 fold compared to PEG-NPs without the drawback associated with PEGylation.

The circulation time of the particulate delivery system depends on multiple physicochemical properties of NPs such as size, shape, surface functionality (a charge, functional groups), and mechanical properties [46, 198, 245-248]. In addition, NPs could also bind to the membrane of RBCs non-specifically depending on their physicochemical properties [103]. The role of the above parameters in the binding of GLU-NPs to RBCs and improved clearance time were ruled out by using control NPs that are surface conjugated with hydroxylamine (Table- 2-1). GLU-NPs showed a significant increase in binding to human RBCs *in-vitro* even in the presence of plasma (Figure 2-1 and 2-2) and to mouse RBCs *in-vivo* (Figure 2-7) indicating the specific role of glucose in the interaction with the RBCs. The involvement of GLUT1 in the binding of GLU-NPs to RBCs was further confirmed by the inhibition of binding in the presence of genistein, a competitive inhibitor of glucose-GLUT1 interaction (Figure 2-4). GLU-NPs bound to RBCs in clusters (Figure 2-1), which may be due to the localization of GLUT1 in microdomains of lipid rafts [221-223].

For a strategy based on hitchhiking on RBCs to improve circulation time, it is essential for particles to detach from RBCs before reaching the target tissue unless the target tissue is the blood. Since the physiological interaction of glucose with GLUT1 is non-covalent and transient [249], the majority of GLU-NPs bound to GLUT1 of RBCs were detached when a shear of 10 Pa was applied. The shear stress employed is similar to the stress experienced by RBCs during their passage through circulation (0.01 to 14 Pa). The ability of the GLU-NPs to detach from the RBCs under shear stress and then reattach when stress is removed might be a key factor in the accumulation of GLU-NPs in target cancer tissue (Figure 2-5A and B) [103]. Such detachment also supports the data that GLU-NPs were almost cleared from the circulation after 12 h (Figure 2-8) despite having an improved circulation half-life compared to PEGylated NPs (Figure 2-8C)

RBCs are one of the highly studied endogenous cells used as drug delivery vehicles because of their biocompatibility, abundance, ease of manipulation and long-circulating half-life [86, 113]. Indeed, several pathogens such as hemobartonella *(Mycoplasma haemofelis)*, eperythrozoonosis and *Plasmodium falciparum* utilize RBCs as carriers to evade immune-clearance. These pathogens remain in circulation for weeks to months by attaching themselves onto the surface of RBCs [204-206]. Such strategy from nature has been explored previously by us and other groups to create stealth nanoparticles and targeting to specific organs [110, 111, 115, 118, 250-252]. The work reported here will provide practical feasibility to the approach by using physiological interactions between glucose and GLUT1 on RBCs.

In addition, GLUT1 is uniquely positioned for enhanced circulation time as well as tumor accumulation for cancer therapeutics since it is over-expressed in multiple cancer

types [145, 151, 153, 179, 187, 253-255]. In addition, to serve the needs of the rapidly growing cancerous tissues, through the release of vascular endothelial growth factor (VEGF) and other factors by the cancer cells, rapid vascularization is promoted. Such rapid vascularization often leads to a leaky and defective vascular architecture devoid of the basement membrane and impaired lymphatic drainage. The abnormal fenestrations in the cancer vasculature allow the nanocarriers to leak into cancerous tissues, sparing the normal tissues [41, 42, 256]. Since the cancer tissues lack a well-developed lymphatic drainage capability, NPs that enter are retained within the tissues for prolonged periods of time. This phenomenon is called the enhanced permeability and retention (EPR) effect [42]. We hypothesize that the GLU-NPs that are attached to the RBCs, eventually detach from it at fine capillaries because of shear forces and cellular interactions (Figure 2-11).

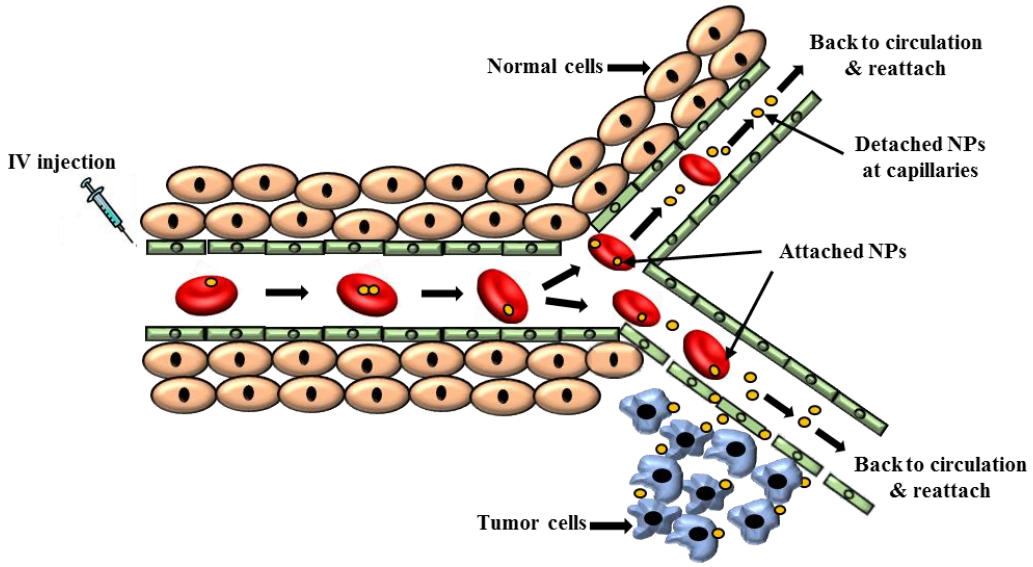


**Figure 2-11:** Schematic diagram representing an enhancement of circulation time and tumor accumulation by GLU-NPs through an attachment on to RBCs.

Upon detachment, the NPs may enter the cancer tissues through EPR effect and will be retained for prolonged periods of time for better tumor accumulation (Figure 2-8). Similar

results were obtained through *in-vivo* tumor accumulation which depicts that GLU-NPs demonstrates higher tumor accumulation (~3-6 folds) post 1$^{st}$ and 2$^{nd}$ injection in mice bearing 4T1 breast cancer tumors (Figure 2-9 and 2-10). Several factors may have contributed for enhanced accumulation of GLU-NPs in the tumor tissue: a) longer circulation time; b) passive targeting through EPR effect; and c) since 4T1 cells overexpress GLUT1, the penetrated GLU-NPs may have been retained through active targeting.

## 2.6. Conclusions

In conclusion, we have developed a novel and unique strategy to enhance the systemic circulation time and tumor accumulation of polymeric NPs through an attachment on to the surface of RBCs through GLUT1 transporters. As the interaction of glucose to GLUT1 is physiological, GLU-NPs interaction with GLUT1 is non-covalent, reversible, occurs even in the presence of plasma and importantly, extended to *in-vivo* conditions. In addition, natural nutrient glucose is not expected to develop antibodies or toxicity. Moreover, since several cancers overexpress GLUT1, the same interaction also benefits to preferentially accumulate NPs in the tumors as shown from the *in-vivo* tumor accumulation studies. In addition to cancer, the concept is also applicable for various other applications such as tumor imaging, sustained drug delivery, and targeting to other tissues. Furthermore, the versatility of this approach could be applicable to potentially any nanoparticulate delivery system to enhance their circulation and potentially impact a wide variety of research in diverse fields.

# CHAPTER III

## INDUCED TRANSPORTER-MEDIATED ENDOCYTOSIS (TME): IMPLICATIONS IN CANCER-TARGETED DRUG DELIVERY

### 3.1. Introduction

Cancer, one of the leading causes of mortality in the United States (US), is a heterogeneous group of diseases involving complex molecular alterations at the cellular level. The clinical therapy of cancer using the traditional chemotherapeutic drugs is not satisfactory due to serious adverse effects and the higher risk of developing drug resistance [1, 2, 5] [3, 4, 6-10]. One of the primary goals of the current research in cancer therapeutics is to either identify cancer-specific targets for new drug discovery *(targeted therapies)* or to deliver the existing chemotherapeutic drugs specifically to the cancer cells *(targeted drug delivery)*. Targeted drug delivery is an economical and quicker approach than targeted therapies to address the urgent unmet need for safe cancer therapeutics [13, 14, 257]. The current approaches for targeted drug delivery primarily focuses on two principles: delivering large drug cargo through particle-based drug delivery systems instead of small molecular drugs and modifying the delivery system to interact specifically with the receptors that are overexpressed in cancer cells compared to normal cells [14, 23, 34, 43, 44, 59, 66, 69]. Despite having tremendous success in preclinical studies, the progress of this (receptor-based active targeting) strategy has been challenging for clinical translation. Some critical challenges include rapid clearance of particulate delivery systems, variability in receptor expression patterns and complexity with the ligand structures [127, 258-261]. Therefore, the recent focus has been to identify alternate molecular targets, having small and stable ligands, that are differentially expressed in cancer cells [65, 127].

Rapid proliferation, poor vasculature, and hypoxia have been the key hallmarks of cancer cells. Rapid cell proliferation increases the demand for nutrients (glucose, amino acids, vitamins, and fatty acids), which serves as the carbon source for the synthesis of

DNA, RNA and as a source of metabolic energy. Switching the metabolic pathways from mitochondrial oxidative phosphorylation to glycolysis under hypoxic conditions is an important adaptive mechanism for cancer cells, which requires excess amounts of intracellular glucose [129]. This increased demand for glucose often leads to high levels of expression and activity of cell surface glucose transport proteins (GLUTs) [143].

GLUT1 is the most ubiquitous and extensively studied glucose transporter among the 14 members of the GLUT family. GLUT1 is a key rate-limiting factor in the transport and metabolism of glucose in cancer cells [129, 142, 145, 151, 160, 179]. Importantly, GLUT1 is overexpressed in a number of cancer types including breast, brain, ovarian, hepatic, pancreatic, esophageal, renal, lung, cutaneous, colorectal, endometrial, bladder, cervical, hepatocellular, head and neck and gastric cancers [138, 145, 151]. Its expression is also positively correlated with increased malignant potential, metastasis, differentiation, and invasiveness of the tumor along with poor prognosis and poor overall survival of the patient [139, 141, 144, 145, 151, 153, 155, 158, 167, 187, 262]. For example, breast cancer has demonstrated increased expression of GLUT1, with as high as 91% positive staining of the invasive ductal carcinomas as compared to the control [61, 153-157, 263]. Due to the above reasons, GLUT1 has been recognized as a prognostic marker and explored for *in-vivo* tumor diagnosis using $^{18}$F-fluoro-2-deoxy-D-glucose in positron emission tomography (PET) [167, 174].

In addition, glucose as a ligand on nanocarriers provides several advantages over ligands for receptors with respect to targeted drug delivery. Most of the ligands for receptors are macromolecules such as monoclonal antibodies. They require to maintain the structural conformation for effective binding to receptors, which might be challenging after

chemical conjugation to nanocarriers and/or after long storage. Furthermore, glucose is a stable ligand and does not evoke an immune response, unlike macromolecular ligands. It doesn't add to the bulkiness of the nanocarriers and therefore, it does not compromise the advantage(s) of passive targeting of nanocarriers through enhanced permeation and retention effect (EPR effect). Recently, we have developed a long-circulating nanocarrier system (stealth) by conjugating glucose onto their surface, which enables them to attach onto the outer membrane of red blood cells (RBCs) through surface-expressed GLUT1 [208]. The modification of nanocarriers with glucose on the surface significantly enhanced the blood circulation time of NPs in mice compared to PEGylated NPs, the current state-of-art technology (chapter II). The enhanced circulation of glucose conjugated nanocarrier is hypothesized to facilitate the accumulation of NPs in cancer tissues, which has leaky vasculature.

To further advance the technology for cancer management, in this study, we have demonstrated the feasibility of glucose-modified nanoparticles (GLU-NPs) as a smart drug delivery system to differentiate breast cancer cells from normal cells based on the expression levels of GLUT1. Glucose is conjugated onto the surface of nanoparticles (GLU-NPs) in a confirmation that retained the ability to bind to GLUT1. GLU-NPs delivered significantly higher cargo to breast cancer cells (MDA-MB-231 and 4T1) compared to the control NPs. The bound GLU-NPs were internalized into cancer cells, which was specifically dependent on the glucose-GLUT1 interaction and involves caveolae-mediated endocytosis for subsequent transport into the lysosomal compartment. To further demonstrate the translation of the technology to cancer therapeutics, we have synthesized poly(lactic-co-glycolic acid) conjugated to glucose (PLGA-GLU) as a novel

functional polymer. The NPs prepared with PLGA-GLU (PLGA-GLU-NPs) showed the ability to differentiate breast cancer cells (MDA-MB-231 and MCF7) versus non-cancer cells (MCF10a) based on the expression levels of GLUT1. The *in-vivo* tumor accumulation of GLU-NPs was evaluated in an allograft mouse model (4T1 breast cancer) using imaging techniques. Thus, through a proof-of-concept and mechanistic analysis, we demonstrate the feasibility of employing GLUT1 transporters as a novel approach for cancer-targeted delivery.

## 3.2. Materials

### 3.2.1. *Chemicals and Reagents*

Fluorescent polystyrene particles with surface carboxyl groups (100, 200 and 500 nm in diameter) and Alexa Fluor™ 488 Phalloidin (A12379) were purchased from Life Technologies Inc. (Portland, OR, USA). Tetrahydrofuran, 2-amino-2-deoxy-D-glucose (GLU), hydroxylamine (HA), genistein, 1-Ethyl-3-(3-dimethyl aminopropyl) carbodiimide (EDC), and poly(lactic-co-glycolic acid) (PLGA RG-653H) were purchased from Sigma Aldrich (St. Louis, MO, USA). Regional Blood Bank, (Sioux Falls, SD, USA) gifted human RBCs. $^{3}$H-labeled oleic acid was purchased from Moravek, Inc. (Brea, CA, USA). GLUT1 rabbit monoclonal antibody (12939S) was obtained from Cell Signaling Technology (Danvers, MA, USA). The $DiOC_{18}$ dye, snakeskin dialysis membrane (10 kDa cutoff), MES hydrate, N-Hydroxysuccinimide (NHS), Nile red, polyethylene glycol of M.Wt. 2000 ($PEG_{2000}$), and all other biochemical reagents, solvents, and supplies were purchased from Fisher Scientific (Pittsburgh, PA, USA).

### 3.2.2. *Cell Lines and Cell Culture*

4T1 (Mouse breast cancer), MDA-MB-231 (Human breast cancer), OVCAR3 (Human ovarian cancer), ID8 (Mouse ovarian cancer), HCT116 (Human colorectal carcinoma), PC3 (Human prostate cancer), MCF7 (Human breast cancer), MCF10a (Breast epithelial cells), NCI-H226 (human lung squamous carcinoma), LnCAP (Human prostate cancer) and SKMEL-2 (Human malignant melanoma) were purchased from the American Type Culture Collection (ATCC) (Manassas, VA, USA). The cells were cultured in Dulbecco's Modified Eagle Medium (DMEM) or Roswell Park Memorial Institute (RPMI-1640) medium based on the recommendations of ATCC in a humidified atmosphere of 5% $CO_2$ at 37ºC. The culture media also contained 10% fetal bovine serum (FBS) and penicillin/streptomycin.

### 3.2.3. *Animals*

All animal experimentation was performed in compliance with the regulations of the Institutional Animal Care and Use Committees (IACUC) of the South Dakota State University, Brookings, SD, USA.

## 3.3. Methods

### 3.3.1. *Surface Modification of NPs*

The polystyrene NPs with carboxyl surface groups were conjugated with GLU, HA, and $PEG_{2000}$ by using EDC chemistry [212, 213]. The NPs conjugated with glucose, HA, $PEG_{2000}$ are denoted as GLU-NPs, HA-NPs, and PEG-NPs from here after. Unless specified, GLU-NPs stands for NPs with around 200 nm in diameter. The GLU-NPs-100 and GLU-NPs-500 indicate glucose conjugated NPs with a diameter of around 100 nm and

500 nm, respectively. Briefly, a 50 µl of polystyrene NPs from a 2% w/v suspension was washed with 50 mM MES buffer (pH 6.0) three times and resuspended in 400 µl of the MES buffer. The carboxylic acid groups were activated by adding EDC (7.5 mg) and incubating for 10 min at room temperature. Subsequently, 25 mg of GLU/HA/$PEG_{2000}$ in MES buffer was added to the suspension and the reaction was carried out at room temperature in dark. After 4 h, the NPs were collected by centrifugation at 20,000g for 30 min and washed thrice with 50 mM phosphate-buffered saline, pH 7.0 (PBS). The NPs were stored at 4°C in the presence of 20 mM sodium azide and 0.001 % Triton X-100 until further analysis.

### 3.3.2. *Characterization of NPs: Size, Surface Charge, and Morphology*

***3.3.2.1. Dynamic Light Scattering (DLS)***: The average size, polydispersity index and the surface charge (ς-potential) of NPs were determined using the DLS technique. Initially, the NPs were dispersed by bath sonication in filter-sterilized 10 mM phosphate buffer (pH 7.4) and then further diluted (1:10) using deionized water before recording particle size and ς-potential using Malvern Zeta-Sizer, Malvern Ltd, MA, USA [214, 215, 217].

***3.3.2.2. Scanning Electron Microscopy (SEM)***: Scanning electron microscope (SEM, Model S-3400N, Hitachi, Japan) was used to investigate the shape and the morphology of GLU-NPs, HA-NPs, and PEG-NPs. For the preparation of samples, a smear of the NPs was created on a glass slide using a suspension of NPs in filter-sterilized water and a section of glass slide was mounted on the metal holder using conductive double-sided tape. The particles were sputter-coated with a 10-nm gold layer before analysis. The micrographs

were captured at an accelerating voltage of 20 kV, with a working distance of 10–15 mm and a spot size of three [214, 215, 217].

### 3.3.3. *In-vitro Binding of NPs to RBCs*

The *in-vitro* binding of GLU-NPs with human RBCs was determined by incubating an increasing number of NPs with $1 \times 10^5$ RBCs in sterile PBS for 4 h at 37°C and 100 RPM. The RBCs were separated from unbound NPs by centrifugation at 800g for 10 min and washing three times with sterile PBS. The number of NPs bound to RBCs was determined by measuring fluorescence at Ex/Em wavelengths of 580/605 nm using a fluorimeter (Molecular Devices SpectraMax Plus Microplate Reader). Precautions were taken to minimize light exposure to NPs [208].

### 3.3.4. *Microscopic Analysis of Internalization of GLU-NPs by Cancer Cells*

The internalization of GLU-NPs by various cancer cells (MDA-MB-231, NCI-H226, LnCAP, and SKMEL-2) was studied as described below. Briefly, $1\times10^5$ cells were seeded on glass coverslips in 6 well-plates and allowed to adhere for 24 h. Subsequently, the cells were incubated with medium, GLU-NPs or HA-NPs for 4 h at 37°C and 5 % $CO_2$. After incubation, the cells were washed thrice with PBS and fixed with freshly prepared 4 % w/v paraformaldehyde (PFA) for 10 min. The actin was stained with Alexa Fluor™ 488 Phalloidin and the nucleus with 4′,6-diamidino-2-phenylindole (DAPI). The coverslips were mounted using ProLong™ Gold Antifade mounting medium (P10144). The images were collected under a fluorescence or confocal microscope [215].

### 3.3.5. *In-vitro Quantitative Cell Uptake of GLU-NPs by Breast Cancer Cells*

*In-vitro* quantitative cell uptake of GLU-NPs by MDA-MB-231 cells was evaluated by flow cytometry. Untreated cells or cells treated with HA-NPs were employed as controls. Briefly, $1\times10^5$ cells/well were seeded in 24 well-plates. After 24 h, the cells were treated with medium, GLU-NPs or HA-NPs at $91.24 \times 10^9$ particles in 1 ml of cell culture medium at 37°C and 5 % $CO_2$. At different time points (0.5-4 h), cells were washed with PBS and, trypsinized. The cells were fixed using 4 % PFA and stored at 4°C in PBS until further analysis. Sample acquisition was performed using BD Biosciences FACS LSR Fortessa using the excitation laser of 561 nm and the red fluorescence channel. The data were analyzed using CellQuest Pro Software (BD) [214, 215, 217].

Similarly, GLU-NPs of various sizes (~100 nm, 200 nm, and 500 nm) were used to study the effect of the diameter of the NPs on the uptake. Untreated cells were employed as controls. The experiment was performed, and the cells were processed as mentioned in the above paragraph. An equal number of GLU-NP-100 nm, GLU-NPs-200 nm and GLU-NPs-500 nm NPs ($91.24 \times 10^9$ particles) was added to the cells during this experiment.

The specificity of internalization of GLU-NPs by MDA-MB-231 cells was studied using a mixture of NPs with a unique combination of surface modification (HA or GLU) and fluorescence markers (red and/or blue). Briefly, $1\times10^5$ cells in a 6-well plate were incubated with medium or the combination of HA-NPs and GLU-NPs containing different fluorescent markers at 37°C and 5 % $CO_2$. After 4 h, the cells were washed thrice with PBS, and fixed with 4 % w/v PFA for 10 min and observed under a confocal microscope

using the appropriate set of filters. The excitation/emission wavelengths for red and blue particles were 580/605 nm and 365/415 nm, respectively.

### 3.3.6. *Immunoblotting*

We evaluated the GLUT1 expression levels of various cancer cells using immunoblotting. The total cell protein content from the cells was extracted using 0.25 mL of cold fresh lysis buffer [1% Triton X-100, 150 mM NaCl, 0.5 mM $MgCl_2$, 200 mM EGTA, and 50 mM Tris-HCl (pH 7.4) with aprotinin (2 mg/mL), Dithiothreitol (DTT, 2 mM), and phenylmethylsulfonyl fluoride (PMSF, 1 mM)] by incubating on ice for 30 min [218, 219]. The soluble lysate was separated by centrifugation at 20,000g for 10 min. The protein content in the lysates was estimated using Bicinchoninic acid assay (BCA) (Pierce™ BCA Protein Assay Kit). Around 50 µg of proteins from lysates were separated on an 8-10% SDS-PAGE (sodium dodecyl sulfate-polyacrylamide gel electrophoresis) under reducing conditions. Proteins were then transferred onto a nitrocellulose membrane, and the blot was blocked with 5% nonfat milk [218, 219]. The protein levels were detected by immunodetection with GLUT1 specific antibody (1:1500 dilution). The specific protein complexes were identified using chemiluminescence detection kit.

We further elucidated the interaction of GLU-NPs with GLUT1 by an affinity-pulldown assay. In brief, MDA-MB-231 cells were incubated with GLU-NPs representing various sizes (100 nm, 200 nm, and 500 nm) and HA-NPs (200 nm). After 4 h of incubation, the cells were washed with PBS to remove unbound NPs. The cells were lysed using lysis buffer, centrifuged at 20,000g for 30 min to separate NPs from the lysate. The

NPs were washed thrice with PBS and the proteins associated with the NPs were separated using SDS-PAGE as described in the above paragraph.

### 3.3.7. *In-vitro Cell Uptake of GLU-NPs in the Presence or Absence of GLUT1 Inhibitors*

Briefly, $1\times10^5$ cells/well were seeded in 24 well-plates. After 24 h, the cells were treated with genistein (10 μM and 200 μM) or cytochalasin B (200 μM) for 30 min in the presence of serum-free low glucose DMEM medium. Subsequently, GLU-NPs ($91.24 \times 10^9$ particles) were added to the cells to further incubate for 3 h at 37°C and 5 % $CO_2$. The cells without pre-treatment with inhibitors were used as controls. The efficiency of internalization of NPs was quantified using flow cytometry as described in section 3.3.5. and qualitative images were collected as described in section 3.3.4.

### 3.3.8. *Studying the Endocytosis Pathway(s) involved in the Cell Uptake of GLU-NPs*

Pharmacological inhibitors were employed to determine the endocytic pathway(s) responsible for cell uptake and internalization of the surface-modified NPs. MDA-MB-231 cells were incubated with previously optimized doses (in terms of toxicity) of chloroquine diphosphate (100 μM), dynasore (100 μM), nystatin (100 μM), rottlerin (5 μM) and nocodazole (20 μM) for 30 min in the presence of serum-free low glucose DMEM medium [264, 265]. Subsequently, GLU-NPs ($91.24 \times 10^9$) were incubated with cells for 4 h at 37°C in the continuous presence of inhibitors. Cells treated with medium or only GLU-NPs without inhibitors were employed as controls. Internalization of NPs was studied using flow cytometry as mentioned in section 3.3.5.

To elucidate the destination of GLU-NPs after internalization, MDA-MB-231 cells were seeded onto 6-well plates ($5\times10^4$ cells/well). After 24 h, the cells were transfected with Lamp1 (lysosomal-associated membrane protein 1) tagged with a green fluorescent protein (GFP) using CellLight® Reagent BacMam 2.0 baculovirus vector for 16 h as per the instructions provided by the supplier (Life Technologies Inc.). Subsequently, GLU-NPs were added to the cells. After 4 h, cells were washed three times with PBS and the cells were imaged using fluorescence and/or confocal microscope with appropriate filters.

### 3.3.9. *Synthesis of Glucose Conjugated PLGA Polymer*

One gram of PLGA–carboxylate (PLGA RG-653H) was dissolved in 5 ml methylene chloride. To this, NHS (27 mg) and EDC (26 mg) dissolved in 2 ml methylene chloride were added. PLGA–NHS was precipitated with the addition of 10 ml of ethyl ether/methanol (1:1 ratio). The precipitated PLGA–NHS was washed with ethyl ether/methanol mixture thrice and collected by centrifugation at 4000g for 20 min. The PLGA–NHS pellet was dried under vacuum for 1-2 h to remove the residual solvents. Subsequently, PLGA–NHS was dissolved in methylene chloride (4 ml) followed by addition of GLU (100 mg) and triethylamine (17 μl). The resulting polymer was precipitated in and washed with deionized water. The pellet was dried under vacuum and used for the NP preparation [266]. The formation of PLGA-GLU was confirmed by Fourier transform infrared (FTIR), proton nuclear magnetic resonance spectroscopy (NMR), and powder X-ray diffraction (PXRD) analysis.

**3.3.10.** ***Characterization of the Polymer:***

***3.3.10.1. FTIR Spectroscopy:*** The conjugation of GLU to PLGA was confirmed by recording the FTIR spectrum. The FITR spectrum of GLU, PLGA RG-653H, and PLGA-GLU were recorded between 4000 $cm^{-1}$ and 400 $cm^{-1}$ at a resolution of 4 $cm^{-1}$ using Nicolet 380 ATR-FTIR spectrophotometer (Thermo Electron Corp., Madison, WI). The average of 50 scans of data is represented [214, 215, 217, 267].

***3.3.10.2. NMR Spectroscopy*:** To confirm the conjugation of GLU to PLGA, $^{1}$H-NMR spectra of GLU, PLGA RG-653H, and PLGA-GLU were recorded on a Bruker 600 MHz NMR spectrometer. Briefly, 30 mg of the compound was dissolved in DMSO-$d_6$ and the NMR spectra were recorded for all the solutions [214, 215, 267].

***3.3.10.3. PXRD Analysis:*** Powder X-ray diffraction measurements of the polymers: PLGA RG-653H and PLGA-GLU were recorded. All measurements were recorded using Rigaku powder x-ray diffractometer with copper (Cu) radiation, running at 40 kV and 44 mA. For this study, samples were mounted on double-sided silicone tape and measurements were performed from 2°C to 60°C at a scan speed of 4°C/min and increments of 0.02°C [215, 267].

**3.3.11.** ***Preparation of PLGA and PLGA-GLU-NPs:*** PLGA and PLGA-GLU-NPs encapsulated with Nile red (model hydrophobic dye) or $^{3}$H-labeled oleic acid were prepared by the solvent evaporation technique. The PLGA-GLU polymer (100 mg) and Nile red (10 mg) was dissolved in 5 ml of dichloromethane (DCM). The solution was then added dropwise into an aqueous phase containing 30 ml deionized water and 0.5% w/v PVA with continuous stirring for approximately 12-16 h. The precipitated particles were collected via centrifugation at 50,000 g for 30 min at 4°C. The collected particles were

washed and re-suspended in PBS pH 7.4, and subsequently lyophilized (VirTis, Gardiner, NY). The blank PLGA-GLU-NPs were prepared in the same manner without the dye. Nanoparticles were also prepared using PLGA as a polymer instead of PLGA-GLU by a similar method [214, 215, 267].

### 3.3.12. *Characterization of Particles: Size, Polydispersity Index and Surface Charge*

***3.3.12.1. Dynamic Light Scattering (DLS)***: The size, size distribution (polydispersity index) and surface charge (ς-potential) of PLGA and PLGA-GLU-NPs were analyzed by the procedure described in section 3.3.2.1 [214, 215, 217].

***3.3.12.2. Scanning Electron Microscopy (SEM):*** Scanning electron microscopy (SEM, Model S-3400N, Hitachi, Japan) was used to investigate the shape and the morphology of PLGA-GLU-NPs. The procedure for acquiring images is described in section 3.3.2.2 [214, 215, 267].

### 3.3.13. *In-vitro Quantitative Cell Uptake of PLGA-GLU-NPs*

*In-vitro* cell uptake of PLGA and PLGA-GLU-NPs encapsulated with Nile red by 4T1 and MDA-MB-231 cells were evaluated in the presence or absence of genistein (10 μM and 200 μM) by flow cytometry. The treatments and the analysis is similar to the method described in section 3.3.5. and section 3.3.7 [215, 217].

We further compared the ability of PLGA-GLU-NPs in differentiating and delivering the encapsulated cargo to various breast cancer cells (MDA-MB-231 and MCF7) versus non-cancer breast epithelial cells (MCF10a). PLGA-NPs and PLGA-GLU-NPs encapsulated with $^{3}$H-labeled oleic acid were employed for this purpose. Briefly, the cells were incubated with the medium, PLGA-NPs or PLGA-GLU-NPs loaded with $^{3}$H-labeled

oleic acid for 4 h in the presence and absence of 5% glucose at 37°C and 5% $CO_2$. The cell uptake was calculated by measuring radioactive counts using the liquid scintillation counter (Beckman Coulter LS6500).

### 3.3.14. *In-vivo Tumor Accumulation*

Female BALB/c mice were used to study the tumor accumulation of surface-modified NPs *in-vivo*. Allograft tumors were developed by orthotopically injecting ($1.5 \times 10^6$) 4T1 mouse breast cancer cells in 200 µL PBS under the skin through subcutaneous injection on the left or the right flank. All subcutaneous injections were given using a 25G needle and the hair was removed with clippers prior to injecting the tumor cells. The animals were divided into three groups and the NPs were administered. The mice were administered polystyrene NPs-surface modified with GLU, HA and PEG ($4.54 \times 10^8$ NPs) through the tail vein. The NPs contained near-infrared (IR) dye carbocyanine $DiRC_{18}$ (Ex/Em 750/780 nm) for detection. The procedure to encapsulate the IR dye into the NPs is described in section 2.3.8. The incorporation of the dye was confirmed by spectroscopic analysis at the excitation and emission wavelengths of 750 nm and 780 nm respectively. After injection, the mice were imaged using reflectance and fluorescence modules at various time points (before injection, at 4, 8, 12, 24 and 36 h) under isoflurane anesthesia. The mice were imaged using Bruker-Xtreme *in-vivo* imager at excitation/emission wavelengths of 730/790 nm. The intensity of the fluorescent signal was normalized and quantified using Xtreme *in-vivo* imager software. The perimeter of the tumor is marked by using a reflectance image.

### 3.3.15. *Data Analysis & Statistics*

All the experiments were performed in triplicate unless specified, and the results are expressed as mean ± SD. The variance between groups was compared using *Student's t-test*, one-way or two-way ANOVA as required followed by Bonferroni's or Dunnett's post-hoc multiple comparison tests (Instat, Graph Pad Software, CA).

## 3.4. Results

### 3.4.1. *Physicochemical Characterization of Polystyrene NPs*

To investigate the use of glucose for attaching the NPs to cancer cells using surface-expressed GLUT1, polystyrene NPs with surface carboxyl groups were conjugated with GLU, HA, and PEG using EDC chemistry as represented in the Figure 3-1A. Control polystyrene NPs with similar size range to GLU-NPs, which were conjugated with HA or PEG on the surface, were carefully selected to rule out the role of particle size, shape, surface functional groups (-OH), charge, and hydrophilicity on tumor accumulation. The results of particle size, polydispersity index and zeta potential analysis of unconjugated, GLU, HA and PEG surface-modified NPs are presented in Table 3-1 and Figure 3-1B and C. The average particle diameter of the unconjugated NPs as recorded by DLS technique was 113.23 ± 1.55, 224.03 ± 3.81 and 548.60 ± 25.93 nm for NPs from commercial source representing 100, 200, and 500 nm, respectively (Table 3-1). The surface zeta potential of the unconjugated NPs was ranging from -30 to -40 mv, attributed to the multiple surface carboxyl groups (Table 3-1). The size of NPs was increased after conjugating to ligands. The average diameter of NPs was altered to 247.90 ± 3.55, 243.93 ± 3.90 and 247.4 ± 77.11 nm for GLU-NPs, HA-NPs, and PEG-NPs respectively (Table 3-1). A similar pattern was observed with NPs of other sizes (Table 3-1). The increase in hydrodynamic radii of the

ligand conjugated NPs along with the neutralization of surface charge of carboxyl groups is an indication of the successful conjugation of the ligands. The NPs were found to be monodisperse as can be seen from the polydispersity index values. The results from the SEM experiment revealed a spherical shape of the NPs with a narrow size distribution (Figure 3-1B). Taken together, the results from the physicochemical characterization of NPs indicates that the ligand conjugated NPs were spherical in shape, with similar size range and surface charge (Figure 3-1 and Table 3-1).

**Table 3-1: Physicochemical characterization of surface-modified NPs.** The table represents the diameter (nm), polydispersity index (PDI) and zeta potential (mV) of polystyrene NPs. Data represent the mean ± standard deviation (n=3-4).

| Groups | Diameter (nm) | PDI | ZP (mV) |
|---|---|---|---|
| Unconjugated 100 nm NPs | 113.23 ± 1.55 | 0.02 ± 0.01 | -30.47 ± 1.91 |
| Unconjugated 200 nm NPs | 224.03 ± 3.81 | 0.03 ± 0.02 | -36.47 ± 1.25 |
| Unconjugated 500 nm NPs | 548.60 ± 25.93 | 0.20 ± 0.04 | -40.60 ± 0.36 |
| GLU-NPs-100 nm | 125.77 ± 3.78 | 0.47 ± 0.03 | 3.13 ± 2.24 |
| GLU-NPs-200 nm | 247.90 ± 3.55 | 0.09 ± 0.02 | 2.69 ± 0.87 |
| GLU-NPs-500 nm | 580.90 ± 78.37 | 0.56 ± 0.05 | 2.00 ± 0.85 |
| HA-NPs-200 nm | 243.93 ± 3.90 | 0.13 ± 0.03 | 3.75 ± 8.50 |
| PEG-NPs-200 nm | 247.4 ± 77.11 | 0.12 ± 0.01 | 7.46 ± 5.39 |

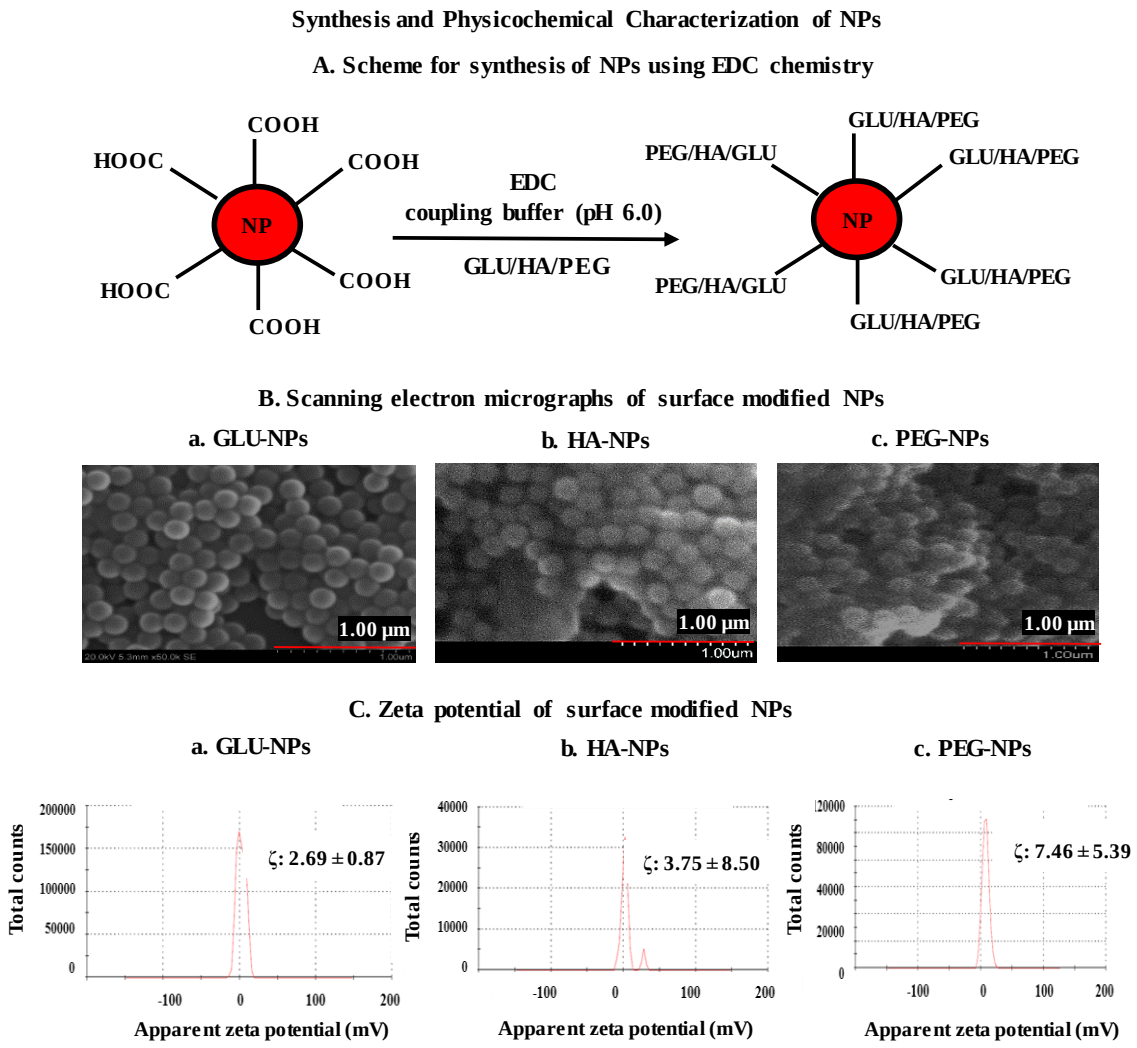


**Figure 3-1: Synthesis and physicochemical characterization of polystyrene NPs.** (A) Scheme for the synthesis of surface-modified (GLU/HA/PEG) NPs using EDC chemistry. (B). Scanning electron micrograph confirming the spherical morphology and size distribution of GLU-NPs (a), HA-NPs (b) and PEG-NPs (c) in the nanometer range. (C). Zeta potential (mV) of GLU-NPs (a), HA-NPs (b) and PEG-NPs (c). Data represent the mean ± standard deviation (n=3-4).

The functional competence of GLU-NPs to bind to GLUT1 was assessed using human RBCs. Human RBCs heavily express GLUT1 on their surface and are expected to bind to GLU-NPs (chapter II, section 2.4.2). NPs modified with HA or PEG did not bind to the human RBCs when incubated for a period of 4 h at 37°C and 100 RPM (Figure 2-1A, chapter II). However, GLU-NPs were able to bind to the surface of RBCs in a concentration-dependent manner (Figure 3-2).

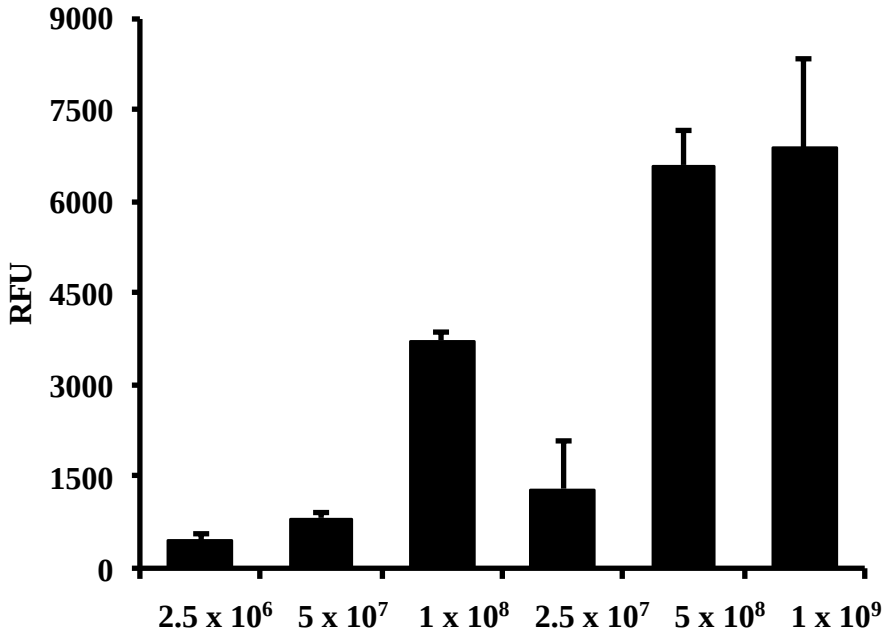


**Figure 3-2: *In-vitro* binding of GLU-NPs to RBCs.** Increasing amounts of fluorescent GLU-NPs ($2.5 \times 10^6$-$1 \times 10^9$) were incubated with $1 \times 10^5$ RBCs for a period of 4 h followed by centrifugation at 800g to separate the RBCs bound with the NPs. The RBCs were washed 4 times and the number of NPs bound to RBCs was quantified as relative fluorescence units (RFU) by measuring fluorescence at excitation/emission wavelengths of 580/605 nm using a fluorimeter. Data represent the mean ± standard deviation (n=3-4).

### 3.4.2. *GLU-NPs were Internalized into Vesicles by Various Cancer Cells*

We have studied the ability of GLU-NPs as a drug delivery vehicle to enter various cancer cells including MDA-MB-231, NCI-H226, LnCAP, and SKMEL-2 cells. Polystyrene NPs with neutral surface charge (HA-NPs) failed to enter the cells (Figure 3-3A). However, when the surface of the NPs was modified with glucose (GLU-NPs), breast cancer cells internalized a significantly higher number of NPs (Figure 3-3B). The GLU-NPs entered the cell as a distinct perinuclear vesicle (Figure 3-3C), which might be indicative of the involvement of endocytosis. Similar results were confirmed with cells representing multiple cancer types: lung cancer (Figure 3-3D), prostate cancer (Figure 3-3E) and melanoma (Figure 3-3F). The specificity of GLU-NPs entering cancer cells was confirmed by both flow cytometry in addition to fluorescence microscopy. GLU-NPs and HA-NPs loaded with similar physicochemical characteristics except for the surface ligand (Figure 3-1 and Table 3-1) were incubated with MDA-MB-231 cells. At different time periods, the amount of fluorescence detected inside cells was quantified. GLU-NPs (~200 nm) on average demonstrated ~ 25 (at 0.5 h), 17 (at 1 h), 15 (at 2 h) and 10 (at 4 h) folds higher cell uptake than HA-NPs (Figure 3-4A).

Not only the internalization of GLU-NPs was established with multiple cancer cells, but the phenomenon was also validated with GLU-NPs of various sizes (~100 nm, 200 nm, and 500 nm) as quantified by flow cytometry (Figure 3-4B). An equal number of particles were added to cells for comparison. The efficiency of internalization was determined as relative fluorescence intensity (RFI) using flow cytometry (Figure 3-4B). The GLU-NPs with around 500 nm in diameter showed the delivery of larger fluorescent cargo into cancer cells compared to the smaller NPs (Figure 3-4B). This may be due to the observation that

the fluorescent intensity of GLU-NPs with 500 nm diameter was higher compared to 200 nm and 100 nm. After normalizing the relative fluorescence intensity of NPs, the data were plotted as a relative number of particles entered per cell (Figure 3-4C). The NPs with around 100 nm in diameter were more efficient in entering the cancer cell in numbers compared to larger particles. The number of NPs entering the cell increased with increasing the incubation time from 0.5-4 h (Figure 3-4C).

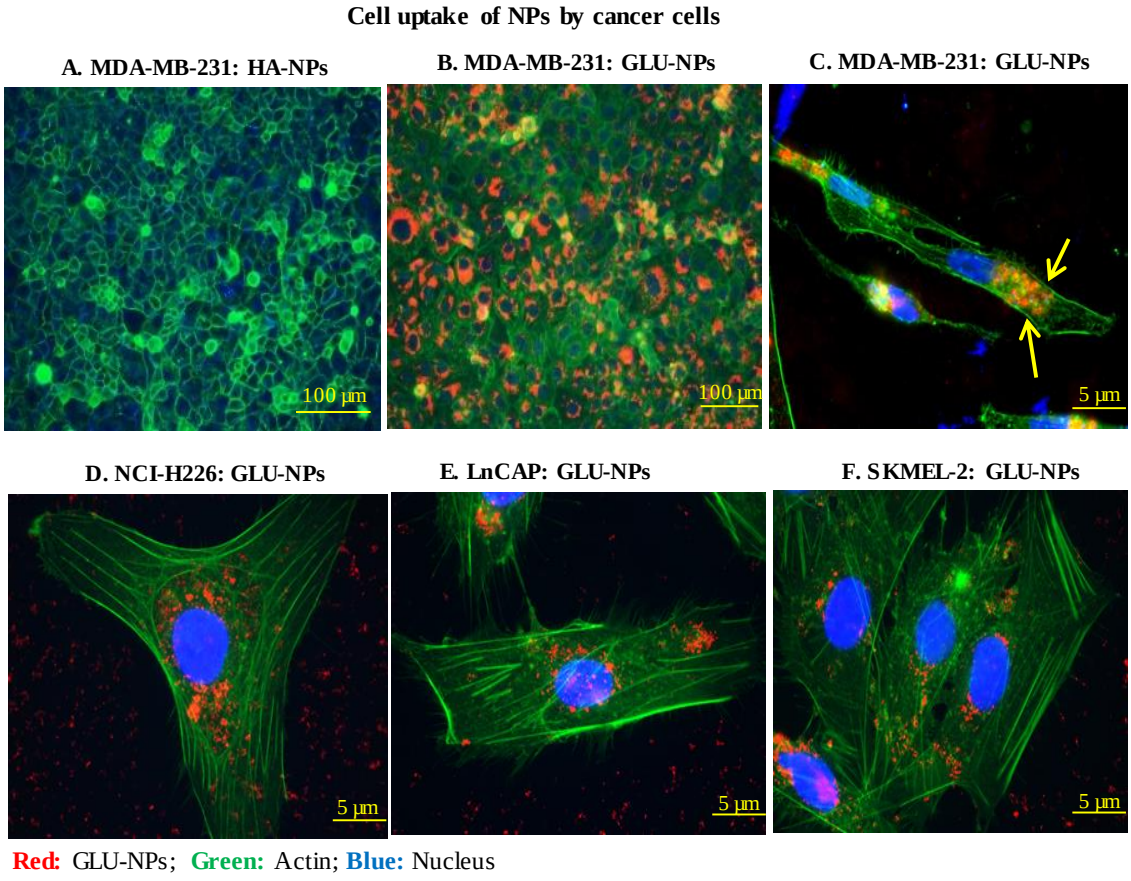


**Figure 3-3: *In-vitro* internalization of GLU-NPs by cancer cells.** MDA-MB-231 cells were incubated with HA-NPs (A) and GLU-NPs (B) for 4 h at 37°C. (C) Internalization of GLU-NPs by MDA-MB-231 cells at higher magnification. The internalization of GLU-NPs by NCI-H226 (D), LnCAP (E) and SKMEL-2 (F), After incubation (A-F), cells were

extensively washed with PBS, fixed in 4% (w/v) paraformaldehyde, and observed under a fluorescence or confocal microscope. The nucleus was stained with DAPI. *This experiment was performed, and the data was generated by Pratik Muley.

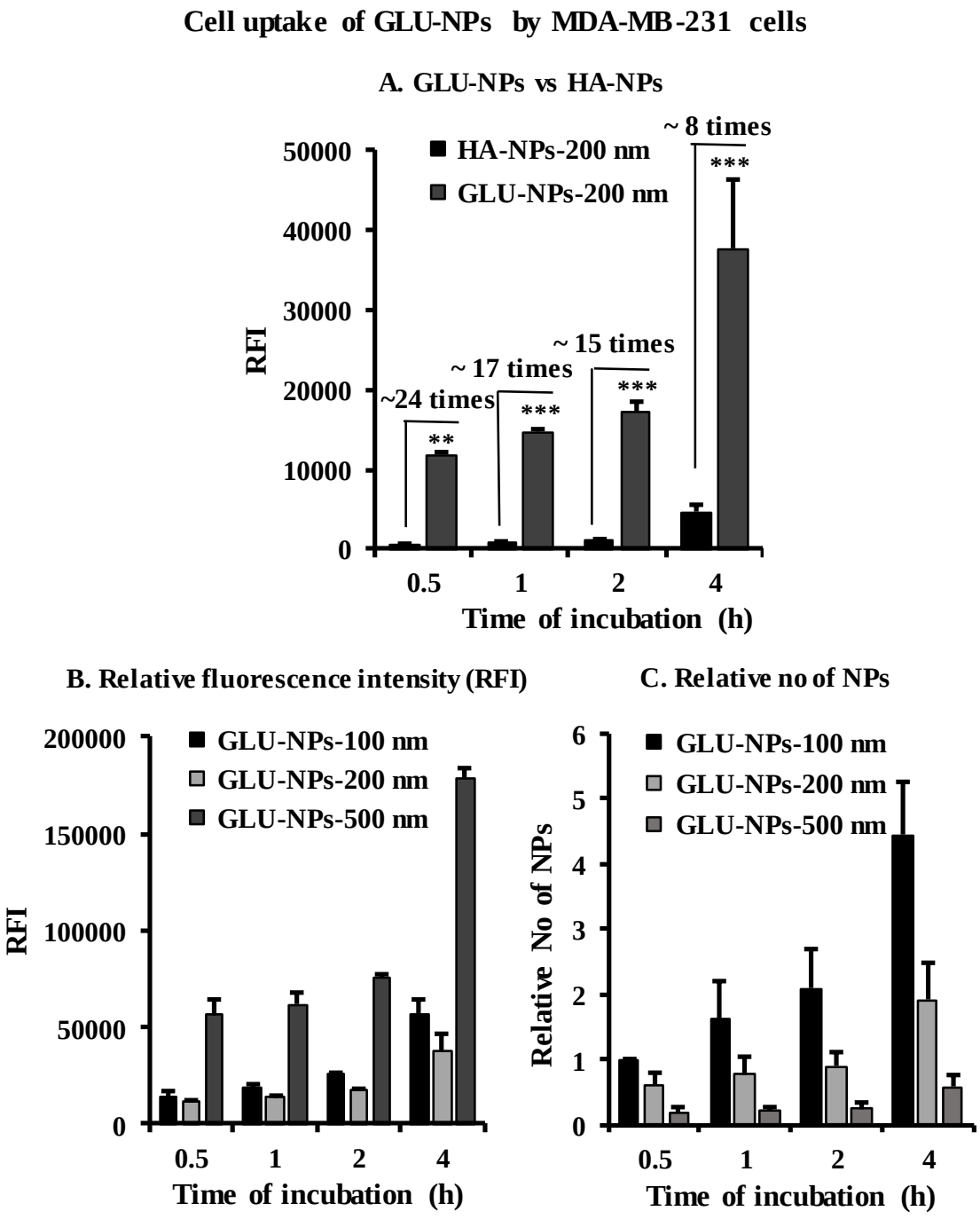

**Figure 3-4: Cell uptake of surface-modified NPs by MDA-MB-231 cells.** (A) MDA-MD-231 cells were incubated with the GLU or HA NPs for 0.5-4 h. The uptake of surface-modified NPs was quantified by flow cytometer by measuring the relative fluorescence intensity (RFI) of each cell. (B) MDA-MD-231 cells were incubated with the equal number of GLU-NPs (~ 100, 200 and 500 nm in diameter) for 0.5-4 h. The uptake of surface-modified NPs was quantified by flow cytometer. (C) The relative number of NPs entered the cell with respect to the time of incubation. Data represent the mean ± standard deviation (n=3-4). *** indicates that the results are statistically significant at $p \leq 0.001$ as compared to HA-NPs using two way-ANOVA followed by Bonferroni's multiple comparison test.

The specificity of uptake was further confirmed by using unique internal controls within the treatment. The cells (MDA-MB-231) were incubated with a mixture of blue and red fluorescent NPs that are specifically labeled with HA or GLU (Figure 3-5). When cells were incubated with a mixture of red NPs labeled with HA and blue NPs labeled with GLU, only GLU-NPs entered the cell as shown by only blue signal inside cells. When both blue and red NPs were labeled with GLU, the vesicles represented both red and blue NPs (Figure 3-5).

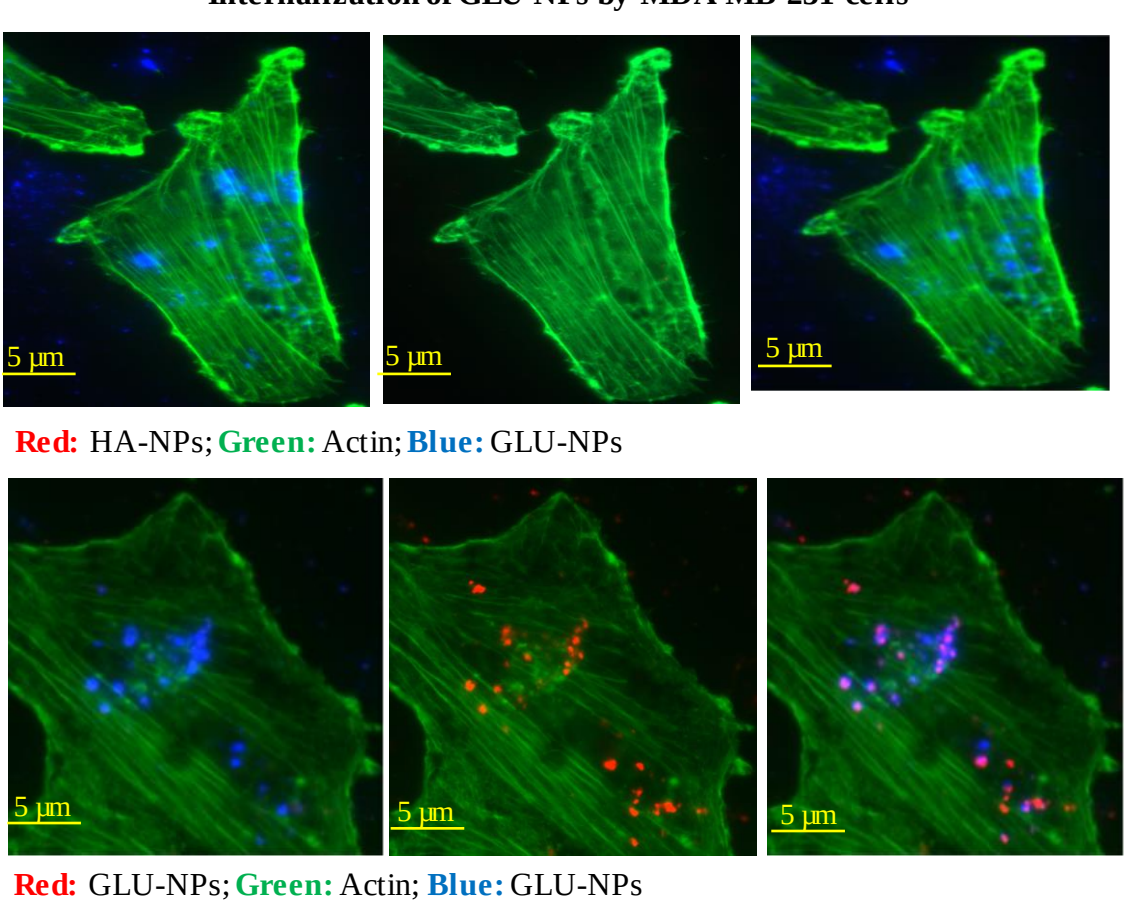


**Figure 3-5: Internalization of GLU-NPs by MDA-MB-231 cells.** MDA-MD-231 cells were incubated with a mixture of blue and red fluorescent dyes that are specifically labeled with HA or GLU. After incubation, cells were extensively washed with PBS, fixed in 4% (w/v) PFA, and observed under a confocal microscope. *This experiment was performed, and the data was generated by Pratik Muley.

### 3.4.3. *The Internalization of GLU-NPs is Through Glucose-GLU1 Interaction*

Accumulating evidence clearly demonstrates the over-expression of GLUT1 in various cancers [145, 149-151, 153, 154, 156, 157, 163, 166, 179, 182, 186, 187, 262, 263]. The

protein levels of GLUT1 in various cancer cells such as MDA-MB-231, OVCAR3, ID8, HCT116, PC3, 4T1, and MCF7 indicates variable expression levels of GLUT1 depending on the cell type with relatively lowest level observed in prostate cancer cell line (PC3) and the highest levels observed with human colorectal cells (HCT116) among the cell lines tested (Figure 3-6A). We further compared the protein levels of GLUT1 in breast cancer cells (MDA-MB-231 and MCF7) with non-cancer cells (MCF10a), which reveals a significantly higher expression levels in MDA-MB-231, followed by MCF7 as opposed to MCF10a (Figure 3-6A). This differential expression of GLUT1 in cancer cells esp., in MDA-MB-231 further provides evidence of GLUT1 as a target for cancer-specific drug delivery.

We evaluated the involvement of GLUT1 transporters in the internalization of GLU-NPs by multiple strategies. After incubation with the cancer cells for 4 h, the cells were washed, and cell lysates were prepared. The cellular proteins that were bound to GLU-NPs were pulled down by centrifuging the cell lysates. Western blot analysis of the proteins bound to GLU-NPs identified GLUT1 as an interacting molecule. Control NPs (HA-NPs), with similar surface functional groups (-OH) and size, which did not enter the cancer cells further failed to interact with GLUT1 on the surface of cancer cells (Figure 3-6B and 3-6D(a)). Furthermore, the role of glucose-GLUT1 interaction in the internalization of GLU-NPs was investigated by quantifying the internalization of GLU-NPs using flow cytometry in the presence or absence of inhibitors of glucose-GLUT1 interaction. The cellular uptake of GLU-NPs was reduced by 30-40 % in the presence of genistein (10 μM and 200 μM). Moreover, cytochalasin B (200 μM) demonstrated ~50 % reduction in the cell uptake of GLU-NPs (Figure 3-6C). The qualitative results from fluorescence microscopy confirm a

significant reduction in the internalization of GLU-NPs in presence of genistein (Figure 3-6D(c)). Taken together, the data clearly indicates that the interaction of glucose from GLU-NPs with the GLUT1 on cancer cells plays a role in the internalization of GLU-NPs.

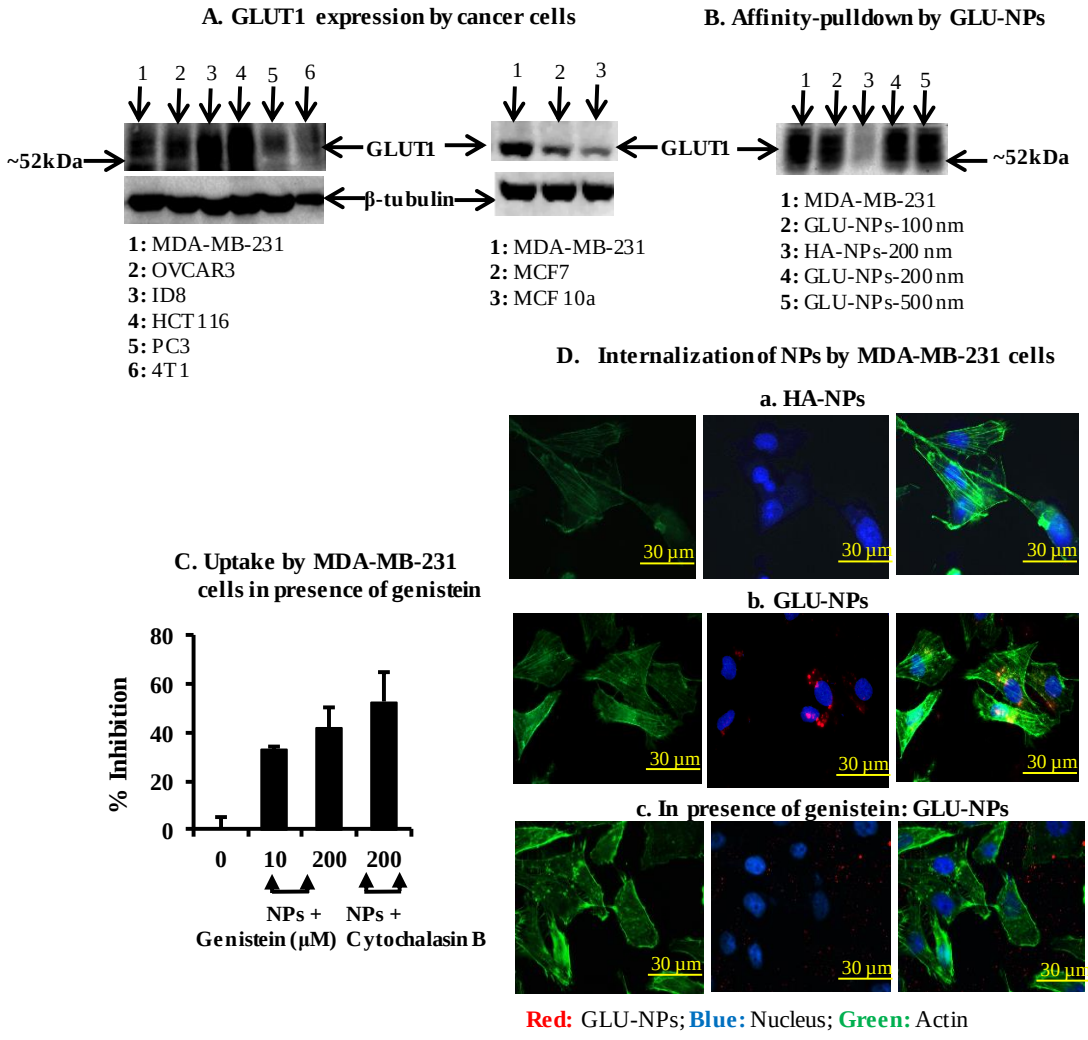


**Figure 3-6: GLU-NPs interact with GLUT1 transporter.** A. GLUT1 expression in various cells (cancer and non-cancer cells) examined by immunoblotting. B. Affinity-pulldown of proteins by GLU-NPs (MDA-MB-231 cells). Blots were reprobed with β-tubulin as a loading control. C. MDA-MB-231 cells were pre-incubated with the genistein (10 μM and 200 μM) or cytochalasin B (200 μM). After 30 min of incubation, cells were

incubated with the medium or GLU-NPs for additional 4 h. The uptake of GLU-NPs was quantified by flow cytometer and the percent inhibition was calculated relative to GLU-NPs uptake. The data is represented as % inhibition of the uptake with respect to GLU-NPs without inhibitors. Data represent the mean ± standard deviation (n=3-4). D. Internalization of NPs by MDA-MB-231 cells HA-NPs (a), and GLU-NPs (b) in the presence of genistein (GLU-NPs) (c). *The data in the figure 3-6D was generated by Pratik Muley.

### 3.4.4. *GLU-NPs Utilize Caveolae-mediated Endocytosis for Internalization*

Once it was established that GLU-NPs are internalized by induced GLUT1-mediated endocytosis, specific pathways involved in the process of endocytosis were identified using a panel of pharmacological inhibitors. The concentrations (μM) used were selected from the literature and optimized to avoid cytotoxicity with the cell line tested [105, 265, 268, 269]. The internalization of fluorescent GLU-NPs by MDA-MB-231 cells was quantified using flow cytometry in the presence or absence of the inhibitors. The data is represented as percent inhibition of internalization (calculated from the MFI) of GLU-NPs by the inhibitors (Figure 3-7A). Dynasore, an inhibitor of both clathrin and caveolae-mediated endocytosis prevented the uptake of GLU-NPs by ~63 %. In contrast, rottlerin, a macropinocytosis inhibitor showed only very minimal (20%) inhibition on the uptake of GLU-NPs (Figure 3-7A). Nocodazole depicted ~40-45% inhibition of the uptake and subsequent internalization (Figure 3-7A). Nocodazole is an inhibitor of polymerization of actin and microtubule cytoskeleton, which is necessary for endocytosis. More specifically, inhibitors of caveolae-mediated endocytosis such as genistein, cytochalasin B (Figure 3-6C) and nystatin (Figure 3-7A) inhibited the uptake of GLU-NPs, which is further

confirmed by visual inspection using fluorescence microscopy (Figure 3-6D). In addition to caveolae-mediated endocytosis inhibitor, chloroquine an inhibitor of clathrin-mediated endocytosis also showed around ~45% reduction in the uptake of GLU-NPs. These results demonstrate that caveolae-mediated endocytosis could play a predominant role in the internalization of GLU-NPs, with a minor contribution by clathrin-mediated endocytosis. After internalization through endocytosis, GLU-NPs were localized in the lysosomes as shown by co-localization studies using a lysosomal marker (Lamp-1-GFP) (Figure 3-7B). The images were collected by confocal microscopy.

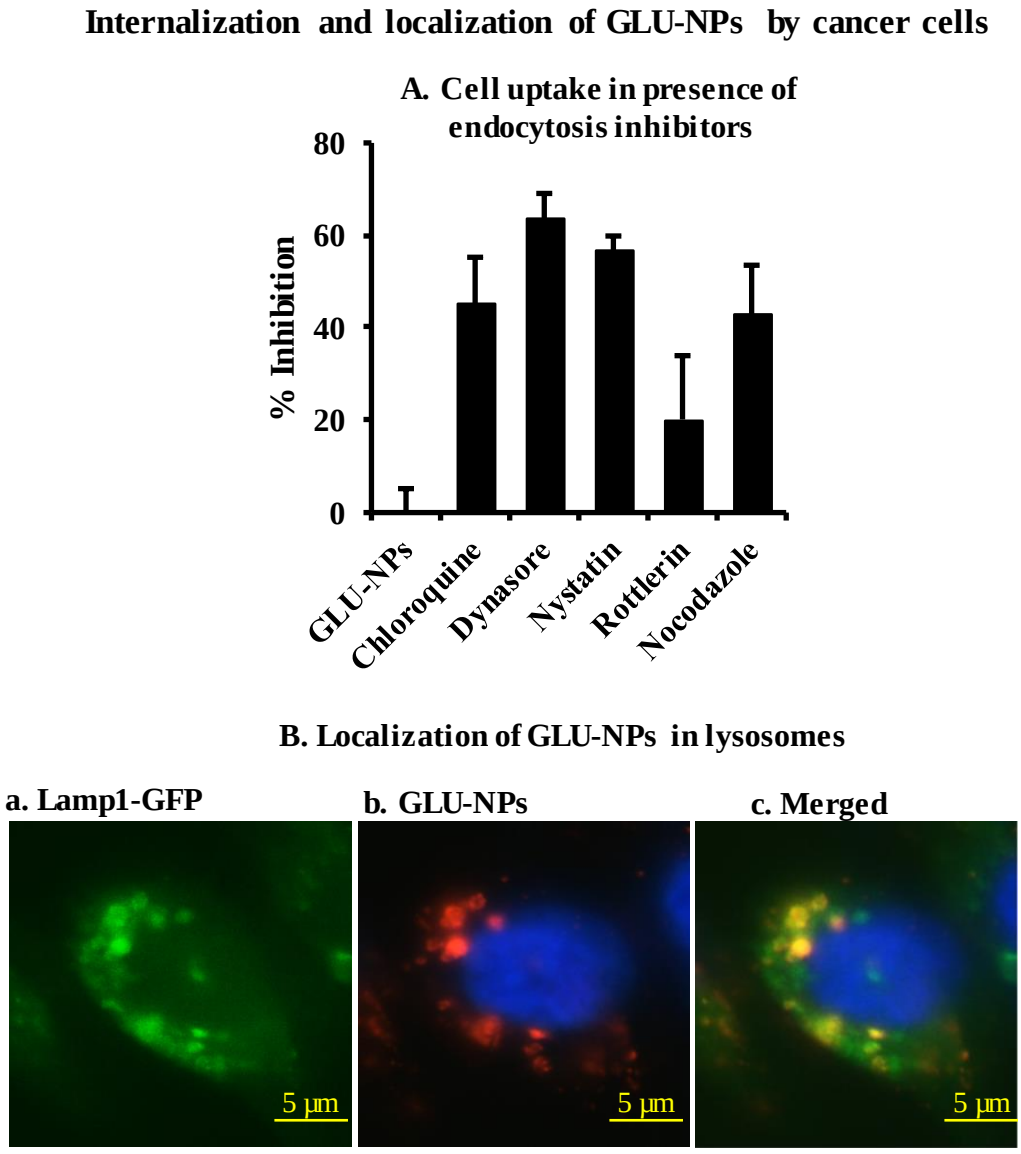


**Figure 3-7: Internalization and localization of GLU-NPs by MDA-MB-231 cells.** (A) MDA-MB-231 cells were pre-incubated with various pharmacological inhibitors of major endocytosis pathway(s). After 30 min of incubation with or without inhibitors, cells were incubated with medium or GLU-NPs for additional 4 h in presence or absence of inhibitors. The uptake of GLU-NPs was quantified using flow cytometer by measuring the mean

fluorescence intensity (MFI) of each cell and the percent inhibition was calculated relative to GLU-NPs uptake without inhibitors. Data represent the mean ± standard deviation (n=3-4). (C) Localization of GLU-NPs in the lysosomal compartments using Lamp1 (lysosomal-associated membrane protein 1) tagged with a green fluorescent protein (GFP). *The data in the figure 3-7B was generated by Pratik Muley.

### 3.4.5. *Preparation and Characterization of PLGA-GLU Polymer and PLGA-GLU-NPs*

After establishing the proof-of-concept using polystyrene NPs that over-expressed GLUT1 on cancer cells could be targeted for the delivery of NPs by induced-endocytosis, the concept was further confirmed using the most popular nanoparticle-based drug delivery system PLGA-NPs. For this purpose, we have conjugated GLU at the carboxyl-terminal of the PLGA-RG-653H polymer using the EDC/NHS chemistry. The conjugation of GLU to PLGA was confirmed by FTIR, and NMR spectroscopy. The FTIR spectrum of GLU at about 3300 $cm^{-1}$ region was characteristic of O-H stretching vibration. The peaks at 1000–1100 $cm^{-1}$ were characteristic of -C-O and -C-N stretching vibrations, whereas the FTIR spectrum of PLGA shows a bimodal peak of aliphatic $CH_2$ group at 2900-2800 $cm^{-1}$. The FTIR spectrum of synthesized PLGA-GLU, shows a characteristic peak at ~3300 $cm^{-1}$, ~1700 $cm^{-1}$ (-C=O), and bimodal peaks at 2900-2800 $cm^{-1}$ characteristic of C-$H_2$ stretch vibration (Figure 3-8A). The NMR spectrum of GLU displayed characteristic peaks of GLU at 8.09 ppm (-OH), 7.16 ppm (anomeric -OH), 5.07 ppm (-$NH_2$), 3.57 ppm ( -CH and -$CH_2$), 3.14 ppm (anomeric -CH) and 2.83 ppm (-CH). The NMR spectrum of PLGA-RG653H showed characteristic peaks at 5.2 ppm (-CH), 4.91 ppm (-$CH_2$) and 1.43 ppm (-$CH_3$). The NMR of PLGA-GLU polymer shows the chemical shift at 8.1 ppm which

confirms the presence of the amine NH proton. The consistency of synthesized PLGA-GLU from batch to batch was assessed by FTIR and proton NMR analysis. The polymers were further characterized by PXRD analysis. The XRD spectrum indicates that both polymers were predominantly amorphous in nature (Figure 3-8C) with no distinct peaks of crystallinity observed. This indicates that the synthetic modification did not alter the polymer characteristics.

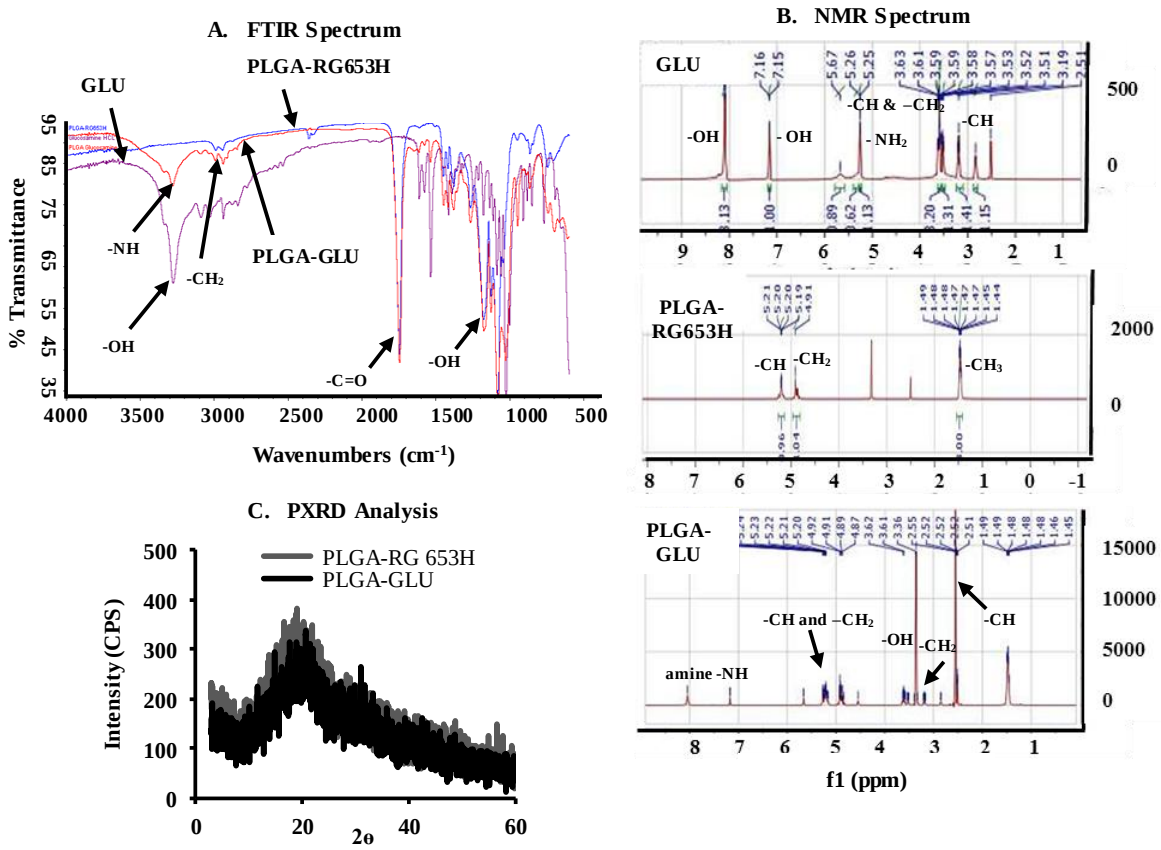


**Figure 3-8: Synthesis and characterization of PLGA-GLU.** (A) FTIR spectrum of GLU, PLGA-RG653H, and PLGA-GLU. (B). The $^{1}$H-NMR spectrum of GLU, PLGA-RG653H, and PLGA-GLU in DMSO-$d_6$ (C) X-ray diffraction spectrum of PLGA-RG653H and PLGA-GLU suggesting the amorphous nature of the polymers.

PLGA-GLU-NPs were prepared encapsulated with Nile red or $^{3}$H-labeled oleic acid. PLGA-GLU particles were spherical in shape with an average diameter of 397.30 ± 52.47 nm (Figure 3-9B) as shown by DLS-technique. The charge on PLGA-NPs was slightly negative ($\zeta$= -5.23) (Figure 3-9A), whereas NPs prepared with PLGA-GLU were slightly positive ($\zeta$= 6.45), indirectly indicating the availability of glucose at the surface (Figure 3-9B). PLGA-GLU particles were spherical in shape as shown by the SEM image (Figure 3-9C). PLGA and PLGA-GLU particles prepared without the dye were utilized as control/blank particles.

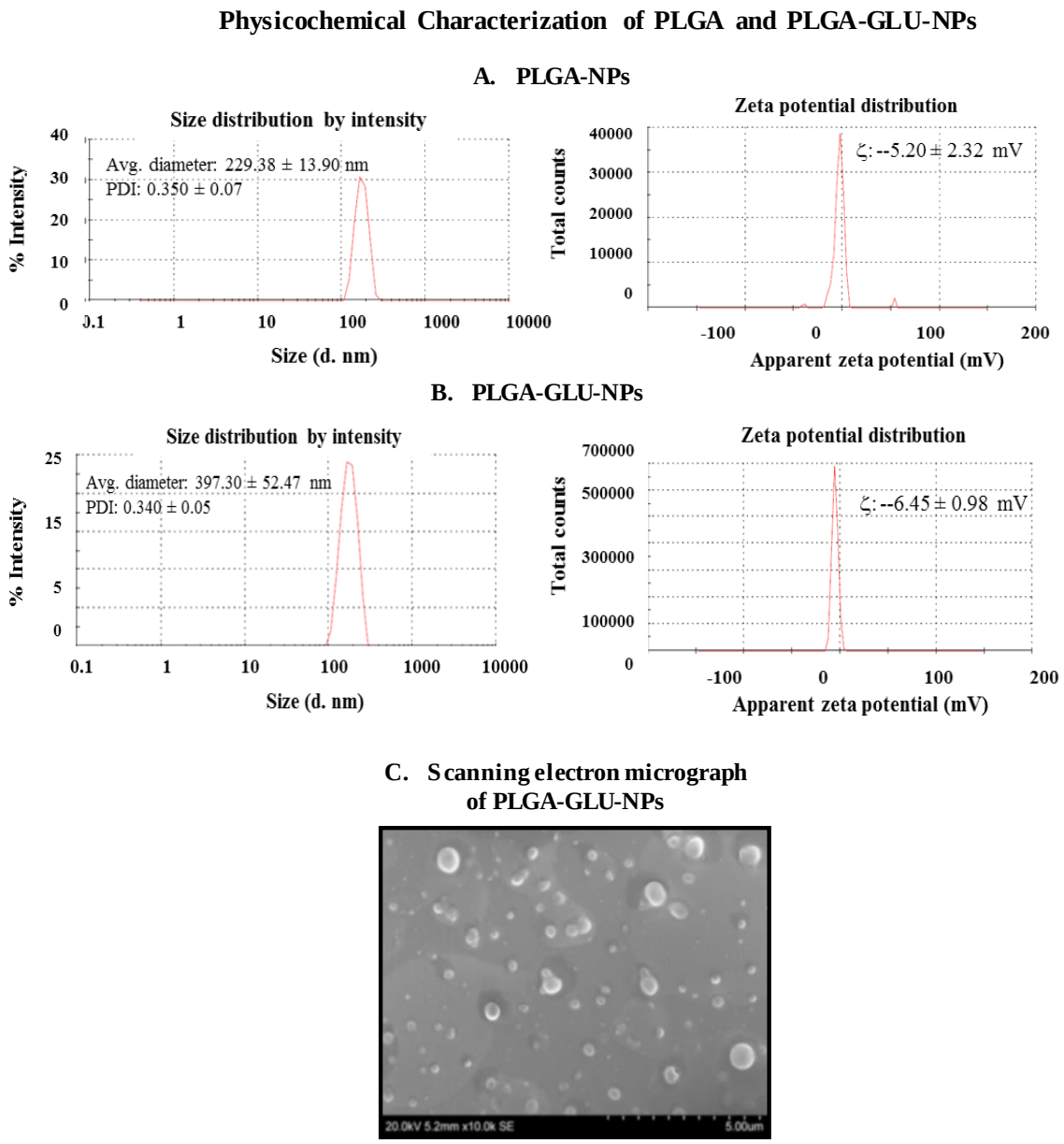


**Figure 3-9: Physicochemical characterization of NPs.** Particle size (nanometers) represented as % intensity and surface zeta potential (ζ-potential) represented as total counts of PLGA-NPs (A) and PLGA-GLU-NPs (B). (C) Scanning electron micrograph of PLGA-GLU-NPs.

### 3.4.6. *PLGA-GLU-NPs are Highly Efficient Cancer-targeted Drug Delivery System*

NPs loaded with Nile red (lipophilic dye) were incubated with 4T1 (mouse) and MDA-MB-231 (human) breast cancer cells. The amount of Nile red delivered per cell was quantified using a flow cytometer. As a delivery system, PLGA-GLU-NPs were able to deliver 3.5-4-fold higher cargo (Nile red) to 4T1 cells compared to PLGA-NPs (Figure 3-10A(a). Similarly, around 3-fold enhanced delivery of the encapsulated dye was observed after GLU conjugation on PLGA in case of MDA-MB-231 cells (Figure 3-10B(a). Consistent with the previous results (Figure 3-6C), incubating 4T1 cells, with genistein reduced the uptake of PLGA-GLU-NPs by ~50 % and ~70% at concentrations of at 10 µM and 200 µM, respectively (Figure 3-10A(b)). In the case of MDA-MB-231 cells, 10 µM and 200 µM of genistein reduced the cellular uptake of PLGA-GLU-NPs by ~30 % and 60 %, respectively (Figure 3-10B(b)). The above results clearly demonstrate that PLGA-GLU-NPs are highly efficient in delivering the cargo to cancer cells, possibly through their interaction with GLUT1 transporter protein.

The specificity of PLGA-GLU-NPs in delivering the cargo to cancer cells versus non-cancer cells was evaluated by loading the NPs with $^{3}$H-labeled oleic acid. The internalized cargo was quantified using a liquid scintillation counter. Three cell lines with variable expression levels of GLUT1 were selected: MDA-MB-231 cells with the highest expression, followed by MCF7 cells and MCF10a cells. MCF10a cells are non-cancerous human breast epithelial cells with low expression of GLUT1. As shown in Figure 3-10C, PLGA-NPs failed to differentiate cancer versus non-cancer cells. Similar to the previous experiment with Nile red (Figure 3-10A(a) and 3-10B(a)), PLGA-GLU-NPs were highly efficient in delivering the cargo to cancer cells; ~3 folds higher compared to PLGA-NPs

with MDA-MB-231 cells. More importantly, glucose conjugation to the polymer enabled the particles to differentiate cancer versus non-cancer cells (MCF10a) based on the level of expression of GLUT1 transporter (Figure 3-10C). This becomes essential while targeting the NPs specifically to cancer cells and thereby avoiding toxicity to normal cells. The binding and uptake of PLGA-GLU-NPs were competed out with very high glucose in the incubation buffer (50 mM PB with 5% glucose). The presence of a very high concentration of glucose not only compromised their ability for the intracellular delivery of large quantities of the cargo but also disabled the NPs to differential cancer vs noncancer cells (Figure 3-10D).

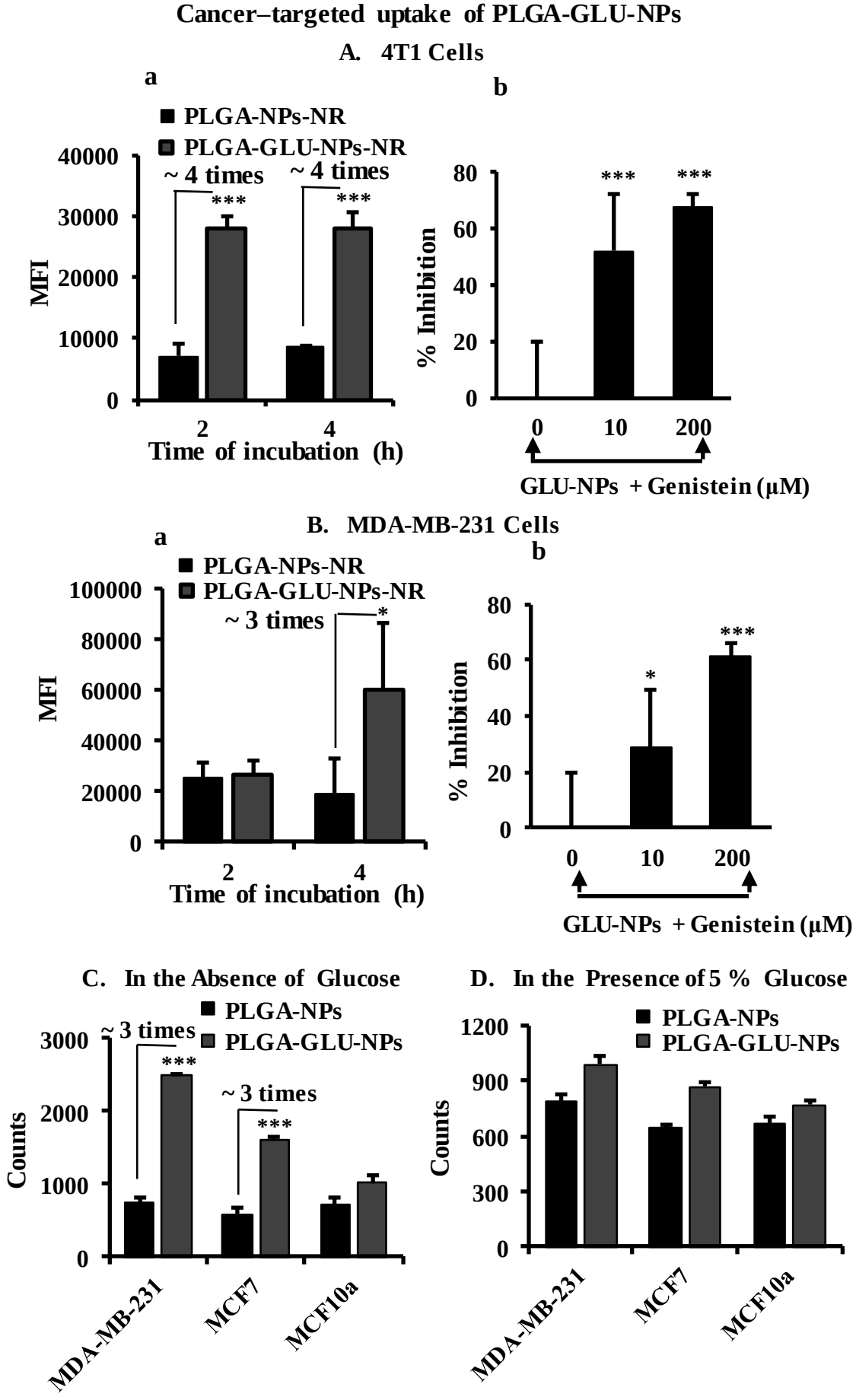
Cancer–targeted uptake of PLGA-GLU-NPs
A. 4T1 Cells
a
PLGA-NPs-NR
PLGA-GLU-NPs-NR
~ 4 times
~ 4 times
***
***
MFI
40000
30000
20000
10000
0
2
4
Time of incubation (h)
b
% Inhibition
80
60
40
20
0
***
***
0
10
200
GLU-NPs + Genistein (µM)
B. MDA-MB-231 Cells
a
PLGA-NPs-NR
PLGA-GLU-NPs-NR
~ 3 times
*
MFI
100000
80000
60000
40000
20000
0
2
4
Time of incubation (h)
b
% Inhibition
80
60
40
20
0
*
***
0
10
200
GLU-NPs + Genistein (µM)
C. In the Absence of Glucose
PLGA-NPs
PLGA-GLU-NPs
~ 3 times
~ 3 times
***
***
Counts
3000
2000
1000
0
MDA-MB-231
MCF7
MCF10a
D. In the Presence of 5 % Glucose
PLGA-NPs
PLGA-GLU-NPs
Counts
1200
900
600
300
0
MDA-MB-231
MCF7
MCF10a

**Figure 3-10: Cancer-targeted uptake of PLGA-GLU-NPs.** 4T1 (A) and MDA-MB-231 (B) cells were incubated with the following groups (i) PLGA-NPs-NR (iii) PLGA-GLU-NPs-NR for 2 and 4 h in the presence or absence of genistein (10 μM and 200 μM). The extent intracellular NPs was quantified by flow cytometer by measuring the mean fluorescence intensity (MFI) of each cell and the percent inhibition was calculated relative to PLGA-GLU-NPs-NR uptake without genistein. NR stands for Nile red. (C) MDA-MB-231, MCF7, and MCF10a cells were incubated with PLGA-NPs and PLGA-GLU-NPs loaded with $^{3}$H-labeled oleic acid in the presence or absence of 5 % glucose. The internalized cargo was quantified using a liquid scintillation counter. Data represent the mean ± standard deviation (n=3-4). * and *** represents that the values are statistically significant at $p \leq 0.05$ and $p \leq 0.001$, respectively calculated using two-way ANOVA followed by Bonferroni's multiple comparison test. *The data in the figure 3-10C and D was generated by Pratik Muley.

### 3.4.7. *GLU-NPs Demonstrate Increased Tumor Accumulation*

Once the concept of cancer-specific delivery of GLU-NPs was established *in-vitro*, we studied the tumor accumulation of GLU-NPs by live mouse imaging. In order to detect and quantify the NPs for *in-vivo* studies, the polystyrene NPs (~200 nm in diameter) were loaded with near IR dye $DiRC_{18}$ (section 2.3.8). Both the polymer and entrapped dye are highly hydrophobic, as there was no leakage of the dye from the particles and the combination has been used before for *in-vivo* analysis [217, 220]. The incorporation of the dye was confirmed by spectroscopic analysis at the excitation and emission wavelengths of 750 nm and 780 nm, respectively.

The mice with subcutaneous tumors developed using allogenic 4T1 cells were divided into three groups and GLU, HA and PEG-modified polystyrene NPs containing carbocyanine $DiRC_{18}$ ($4.54 \times 10^8$ particles/mouse) were injected through the tail vein. The HA and PEG NPs were employed as control (Figure 3-11B). The extent of GLU-NPs circulating in the body and targeted to the tumor was significantly higher as seen from the imaging results (qualitative) than HA-NPs or PEG-NPs (Figure 3-11B) at 4, 8, 12, 24 and 36 h post-injection. Quantitative results from *in-vivo* imaging depict GLU-NPs accumulated in higher amounts (~2-4 fold) (at $p \leq 0.05$ and $p \leq 0.001$) in the tumor as opposed to the HA-NPs or PEG-NPs at various time periods post-injection (8, 12, 24 and 36 h injection (Figure 3-12).

**A. Scheme for *in-vivo* Tumor Accumulation**

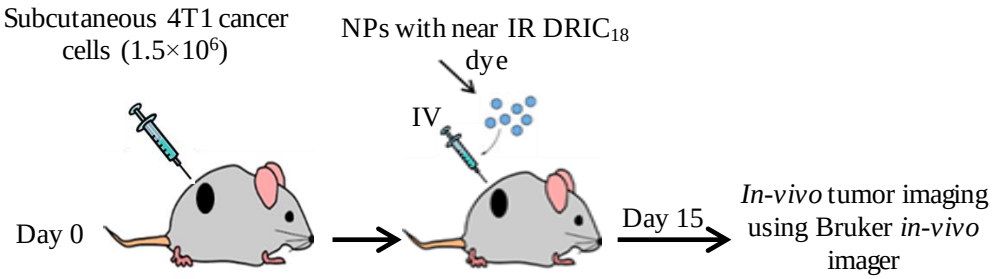


**B. *In-vivo* Tumor Imaging**

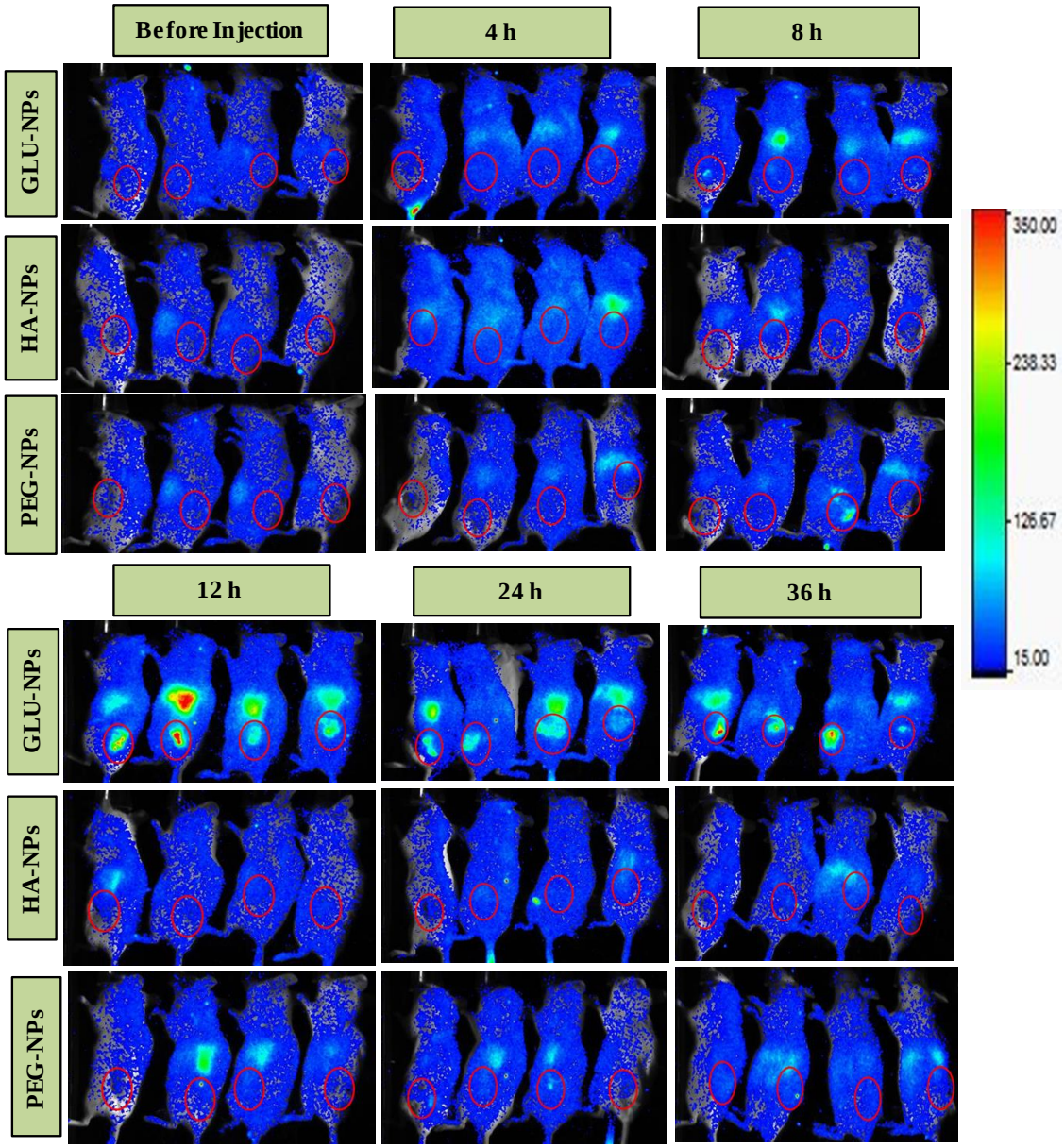

**Figure 3-11: *In-vivo* tumor accumulation of surface-modified NPs.** (A) Scheme for *in-vivo* tumor accumulation of NPs. The mice were inoculated with 4T1 ($1.5\times10^6$) breast cancer cells via subcutaneous injection. GLU, HA and PEG NPs containing $DiRC_{18}$ ($4.54\times10^8$ particles/mouse) were injected through tail-vein on day 15 post tumor cell inoculation. The mice were anesthetized using isoflurane before imaging at various predetermined time points using Bruker *in-vivo* imager (B). The scale represents normalized intensities. The red circle indicates the tumor site identified by the reflectance image. In the figure, the fluorescent images were overlapped on reflectance images of the mice.

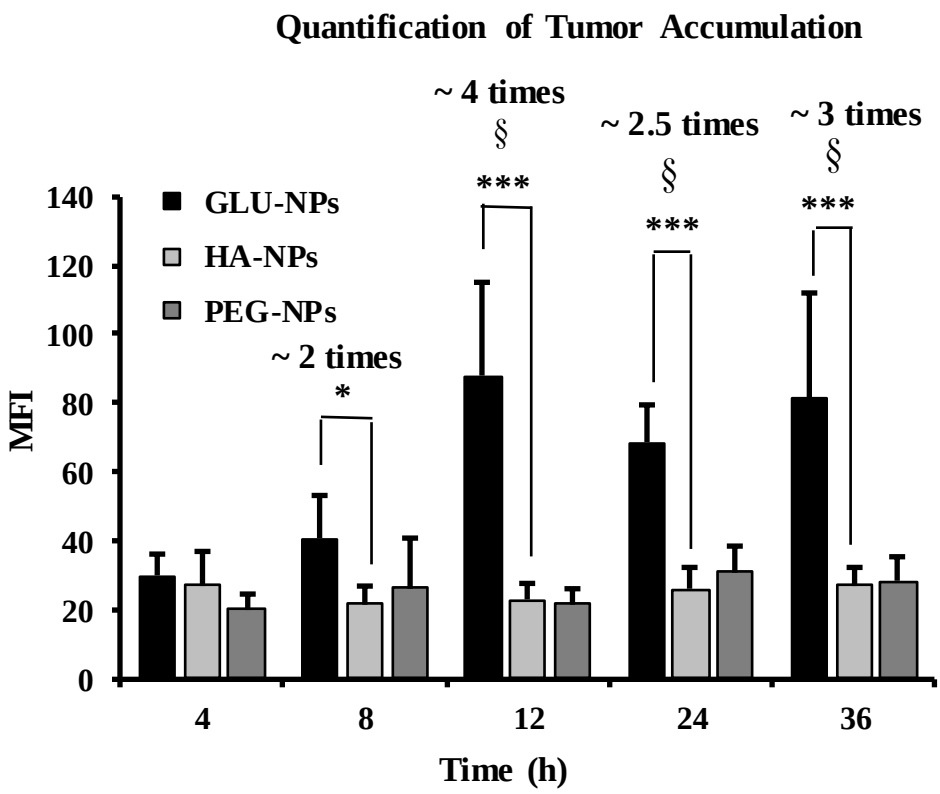

**Figure 3-12: Quantification of tumor accumulation of surface-modified NPs.** BALB/cJ mice (n=4) inoculated with 4T1 tumors, were intravenously injected (100 μl) through tail vein GLU, HA, and PEG-NPs at $4.54\times10^8$ particles/mouse. The mice were anesthetized using isoflurane and imaged at 4, 8, 12, 24 and 36 h post-injection. The accumulation of NPs in the tumor was quantified after normalizing the mean fluorescence intensities (MFI) from the images using the Bruker-MI software. The data are plotted as mean ± standard deviation (n=4 mice). *, *** indicates that the results are statistically significant at $p \leq 0.05$ and $p \leq 0.001$, respectively as compared to HA-NPs, whereas § indicates significant differences at $p \leq 0.001$ as compared to PEG-NPs calculated using two way-ANOVA followed by Bonferroni's multiple comparison test.

### 3.5. Discussion

The current approaches for cancer-targeted drug delivery primarily focus on utilizing receptors that are over-expressed in cancer tissue as targets to deliver a large cargo of drugs using nanocarriers [65, 127]. Some of the challenges in this strategy have been the variability in receptor expression levels between patients and the complexity of the ligands utilized for the receptors. The key parameters for the design of a successful cancer-targeted drug delivery system include: (i) the availability of molecular targets that are differentially expressed on cancer cells, (ii) the accessibility of the receptor for anchoring the delivery system, (iii) initiation of appropriate signaling for the internalization of nanocarriers, and (iv) the feasibility of the approach for *in-vivo* system [270-272]. In this study, we have investigated the feasibility of glucose transporter (GLUT1), which is over-expressed in

multiple cancer types, as a target for delivering nanocarriers (GLU-NPs) with respect to the above key parameters.

Recently, nutritional transporters, which are over-expressed in multiple cancer types (e.g.; GLUT1 and LAT1) are emerging as targets for new drug development and drug delivery systems [273-275] [145, 182, 186, 276]. The recent interest is based on the following reasons: (i) Transporters are consistently over-expressed in multiple cancers with a strong positive correlation between the expression levels and the invasiveness of cancer along with poor prognosis for patients [277, 278]. (ii) The expression levels of transporters between patients and within the same patient during various stages of cancer are less variable as compared to the receptors [260]. (iii) Most of the ligands for receptors are macromolecules, whereas in case of transporters they are small molecules, which are structurally stable and easy for chemical modification(s) and conjugation to nanocarriers. (iv) Being hydrophilic small molecules, the nutrient ligands do not induce immune recognition/response unlike larger complex ligands for receptors.

Due to the consistency in over-expression of GLUT1 in number of cancer types along with its proven clinical utility as a target for cancer imaging using $^{18}$F-fluoro-2-deoxy-D-glucose ($^{18}$-FDG) [139, 167, 174, 279], in this study, GLUT1 was selected as an active target for the delivery of NPs using glucose as a ligand (GLU-NPs). GLUT1 is the most ubiquitous, extensively studied glucose transporter among the 14 members of the GLUT family and critical for the uptake of glucose in cancer cells. GLUT1 is over-expressed in a number of cancer types and its expression is also associated with increased malignant potential, tumor differentiation, poor prognosis, poor overall survival, and invasiveness. This overexpression of GLUT1 in various cancers is utilized for cancer

management. Specifically, GLUT1 is expressed in 42% of breast tumors with increased expression in cancers of higher grade and proliferative activity as compared to non-cancerous tissues. This suggests that GLUT1 is a prognostic indicator and a potential therapeutic target in tumors

The conjugation of glucose on the surface of NPs (GLU-NPs) was designed carefully to allow the necessary hydroxyl groups available for binding to GLUT1 protein. To retain high affinity towards GLUT1, glucose requires the presence of free hydroxyl groups at the carbon 1, 4 and 6 to form hydrogen bonds with the transmembrane alpha-helices of GLUT1 [141, 276]. The amino group of 2-amino-2-deoxy-D-glucose (GLU) was employed to conjugate to the NPs and binding was confirmed using human RBCs as a model, which expresses as high as 10 % of their surface proteins as GLUT1 (Figure 3-2) [143].

When incubated with MDA-MB-231 breast cancer cells, GLU-NPs were internalized into vesicular compartments in larger numbers (Figure 3-3B-F) compared to NPs conjugated with hydroxylamine (HA-NPs) (Figure 3-3A). The cellular internalization of NPs mostly depends on the size, shape, surface charge and surface functional groups [46, 245, 246] of the particles. We have employed hydroxylamine modified NPs (HA-NPs) with similar size, shape, and surface hydroxyl groups as a control to rule out the role of above physicochemical characteristics in the internalization of GLU-NPs (Figure 3-1 and Table 3-1). GLU-NPs demonstrated ~25 and 15 folds higher cell uptake at 0.5 h and 1 h of incubation time, respectively and ~10 folds after 2 and 4 h of incubation compared to HA-NPs (Figure 3-4A). Similarly, the time-dependent uptake of glucose conjugated iron oxide nanoparticles was demonstrated previously in breast cancer cells (MDA-MB-231) [179].

The internalization and localization in the intracellular vesicles were consistent among multiple cancer types: lung cancer, human prostate cancer and human malignant melanoma cells (Figure 3-3D-F). The role of glucose on NPs and its interaction with GLUT1 on cancer cells for the internalization of GLU-NPs was confirmed using affinity pulldown assays and competitive inhibitors of GLUT1 (Figure 3-6B and C). Affinity pulldown assay with GLU-NPs identified GLUT1 as a protein that interacts with GLU-NPs. HA-NPs with similar surface functional group and size that did not enter the cancer cells (Figure 3-6B) failed to interact with GLUT1. Furthermore, GLUT1 inhibitors such as genistein and cytochalasin B reduced the uptake of GLU-NPs into MDA-MB-231 cells by 40-50 % (Figure 3-6C). Taken together, the data from the above *in-vitro* experiments indicate that GLU-NPs represent efficient nanocarriers for the delivery of cargo (drugs/imaging agents) to cancer cells and are internalized through their interaction with GLUT1 on cancer cells.

Polystyrene particles were selected for their precise physicochemical properties to establish proof-of-concept and preliminary mechanistic studies. However, the feasibility of this approach for drug delivery for cancer was further evaluated using PLGA NPs, which are the most commonly used polymeric particles for drug delivery. For this purpose, the polymer PLGA was modified by conjugating with glucose (PLGA-GLU) (Figure 3-8 and 3-9). PLGA polymers are excellent carriers for drug delivery with several advantages: approved by FDA for human use, biodegradable, biocompatible, possess the ease of surface modifications, proven to a delivery variety of molecules such as small and macro-molecules and demonstrate the sustained release of the cargo [280, 281]. Similar to polystyrene NPs, internalization studies with PLGA-GLU-NPs showed increased delivery (~3-4 folds) of cargo (Nile red) or ($^{3}$H-labeled oleic acid) to cancer cells compared to

PLGA-NPs without glucose (Figure 3-10). Importantly, PLGA-GLU-NPs differentiated cancer (MDA-MB-231, MCF7) and non-cancer (MCF10a) cells based on their GLUT1 expression levels (Figure 3-10C and D). In contrast, PLGA-NPs without glucose failed to differentiate the above cells (Figure 3-10C and D). The ability to deliver the encapsulated cargo more specifically to cancer cells is essential in avoiding the toxicity to normal cells when loaded with chemotherapeutic drugs. Consistent with the previous results with polystyrene NPs (Figure 3-6C and D), competitive inhibitors of glucose-GLUT1 interaction, such as genistein and 5 % glucose (Figure 3-10C and D), disabled the PLGA-GLU-NPs to specifically target cancer cells that are expressing high GLUT1 protein.

The ability of the cell surface receptors to undergo endocytosis after ligand binding has been the key element for ligand-based active targeting strategies for drug delivery. In contrast to receptors, transporters, including GLUT1, deliver their ligands across the membrane using transmembrane protein channels. In this study, we have established that nutrient transporters such as GLUT1 could be induced to signal for endocytosis when the bound ligand cannot be passed through the channel. This phenomenon is also recently been observed by other groups [274]. We have demonstrated that GLU-NPs, when interacted with GLUT1, were internalized predominantly by caveolae-mediated endocytosis with minor contribution by clathrin-mediated mechanisms as a minor pathway (Figure 3-7). Most of the materials internalized by endocytosis are sorted to either hydrolytic lysosomal compartments [65, 178, 265, 268, 269, 282] or enter Golgi apparatus for recycling. GLU-NPs were distributed into lysosomal compartment systems after 4 h of incubation as shown by their co-localization to lysosomal marker protein Lamp1. The cargo carried by these

NPs is expected to be released in the lysosomes and then potentially enter cytosol (Figure 3-7B) as shown with many other nanocarriers entering the lysosomes [283-286].

To advance the *in-vitro* potential of GLU-NPs as a drug delivery vehicle for cancer, the final challenge is to prove its feasibility in an *in-vivo* system. The two key parameters for the success of intravenously injected cancer-targeted nano-drug delivery are their ability to remain in circulation to leak through tumor vasculature, accumulation and retention in the tumor through their interaction with the target receptor/transporter. In chapter II, we have clearly demonstrated that GLU-NPs have longer circulation time in mice than PEGylation, which is the current state-of-art technology for enhanced circulation of NPs. This was demonstrated through multiple mechanisms; reduced opsonization (Figure 2-6) and hitchhiking on RBCs (Figure 2-7). The increased circulation time of GLU-NPs was achieved without altering the biodistribution pattern of NPs in various organs as compared to PEG-NPs (Figure 2-8B). We have also demonstrated that GLU-NPs could interact with GLUT1 on RBCs in-situ during circulation. The reduced clearance of GLU-NPs could potential provide an opportunity to leak through tumor vasculature due to their unique anatomical anomalies of larger fenestrations.

The accumulation of GLU-NPs in the tumor was assessed using a syngeneic mouse breast cancer model using 4T1 cells. NPs with around 200 nm in diameter were selected for the study based on the observation that 100–200 nm demonstrated enhanced tumor accumulation as compared to the size of NPs < 100 and >200 nm [68] [287]. GLU-NPs clearly demonstrated significantly enhanced tumor accumulation as compared to the HA and PEG-NPs (Figure 3-11B and 3-12). The enhanced accumulation in the tumor observed could be due to multiple factors: (i) increased circulation time; (ii) passive targeting using

EPR effect, and (iii) active targeting through GLUT1 transporters. Additionally, the enhancement of tumor targeting and circulation could be due to the neutral to ±10 mV surface charge of GLU-NPs, in contrast to charged particles that are cleared quickly by the immune system [67, 288]. A similar strategy has been demonstrated by Shan *et al*. using γ-$Fe_2O_3$ nanoparticles coated with dimercaptosuccinic acid and modified with 2-deoxy-D-glucose (γ-$Fe_2O_3$@DMSA-DG NPs) for *in-vivo* tumor diagnosis using $^{18}$F-fluoro-2-deoxy-D-glucose (FDG) in positron emission tomography [186, 289]. Another study using 2-deoxy-D-glucose-modified nano-drug delivery system demonstrated efficient glioma treatment and simultaneous targeting to the blood-brain barrier and glioma cells [181]. The results from this study demonstrate the ability of GLU-NPs not only for drug delivery but also for tumor imaging and diagnosis.

### 3.6. Conclusions

In conclusion, through a proof-of-concept study, the feasibility of GLUT1 transporters as a novel target for cancer-targeted delivery has been demonstrated. GLU-NPs provide an exciting option for cancer-targeted drug delivery or imaging through multiple advantages: (i) GLUT1 is differentially over-expressed in multiple cancer types, (ii) GLUT1 is expressed on the surface and is accessible for binding to glucose without large linkers, (iii) binding of GLU-NPs to GLUT1 initiates necessary signals for the internalization of GLU-NPs through endocytosis, (iv) by increasing the *in-vivo* circulation time, GLU-NPs provide additional benefits as a nanocarrier, and (v) glucose as a ligand is safer and is not expected to induce major physiological or immune responses.

## 4. SUMMARY AND FUTURE STUDIES

The work in this dissertation addresses two major aspects of cancer-targeted drug delivery using nanocarriers: (i) enhancing the systemic circulation time of nanocarriers. (ii) investigating nutritional transporter GLUT1 as an alternate to receptors as a target for active targeting of nanocarriers.

In **chapter I**, we have compiled the literature and discussed the current status of cancer-targeted drug delivery and the role of nanomedicine. The advantages and the limitations of the nanomedicine for cancer-targeted drug delivery are addressed.

In **chapter II**, a recently reported concept of enhancing the circulation time of nanocarriers by hitchhiking on RBCs was extrapolated to a clinically relevant strategy by utilizing the natural interactions between glucose and GLUT1 transporter on the surface of RBCs. By covalently conjugating glucose on the surface of nanoparticles (GLU-NPs), GLU-NPs were able to bind to human RBCs *in-vitro* and mouse RBCs *in-vivo*. The presence of plasma did not hinder the binding of GLU-NPs to human RBCs, as the strategy is based on physiological interaction. Results from the *in-vivo* pharmacokinetics clearly showed that the glucose conjugation significantly increased the circulation time of NPs in mice. The $t_{1/2}$ of GLU-NPs was ~2 folds more (~126 ± 12.56 mins) as compared to PEG-NPs (75.80 ± 1.52 mins). PEG-NPs are the current state-of-the-art technology in the field for enhancing circulation time. In addition, GLU-NPs demonstrated enhanced accumulation (~3-6 folds) in orthotopically developed breast tumor using 4T1 cells at 12 and 24 h post $1^{st}$ and $2^{nd}$ injection compared to PEG-NPs. Since the interaction of glucose with GLUT1 is physiological and occurs in-situ, the approach could be easily extended to clinical application. Thus, this study demonstrates a practical approach of altering the

pharmacokinetics of nanoparticles for improved circulation and tumor accumulation by functionalizing the NPs with glucose.

The next logical steps for this study is to test the proof-of-concept study from polystyrene particles to more clinically relevant drug delivery systems such as liposomes, micelles, and dendrimers. Additional studies are needed to utilize the unique property of the interaction of GLU-NPs with RBCs, to advance them in other therapeutic applications such as liver targeting or targeting to the brain.

In **chapter III**, through a proof-of-concept study, we demonstrate the ability of GLU-NPs as an efficient nanoparticulate delivery system to differentiate between cancer versus non-cancer cells based on their GLUT1 expression levels. The specific uptake and subsequent internalization of GLU-NPs by cancer cells were dependent on the glucose-GLUT1 interaction as studied through competitive inhibitors of GLUT1, and affinity pulldown assays. Unlike RBCs, the bound GLU-NPs were internalized into intracellular vesicles in cancer cells. Mechanistic studies indicated the involvement of caveolae-mediated endocytosis for the internalization. The results from *in-vivo* tumor accumulation depict that the GLU-NPs localized into tumors (4T1 mouse breast cancer) in significantly higher amounts (~2-4 folds) possibly through a combination of passive, and active targeting. Thus, the results from this study provide the evidence on the feasibility of employing GLUT1 as a target for active targeting of nanocarriers for cancer, which will have implications both in drug delivery and cancer imaging.

Despite significant developments and promising application(s) of transporter-targeted nano-drug delivery systems, several questions need to be studied in future research in the field. For instance, in the case of tumor-targeted delivery, although transporters have

shown over-expression on tumor cells, they are of importance to normal cells as well. Thus, addressing the off-target distribution of transporter-based nano-drug delivery systems in normal cells needs to be studied in full detail. Some reports have shown the brain distribution of glucose conjugated nanocarriers. However, in our study, we did not find significant levels/accumulation in the brain. More studies are needed to address the effect of the rigidity of the particles, linker size and the availability of specific -OH groups on the glucose on the biodistribution of GLU-NPs.

In summary, this dissertation provides considerable evidence on the ability of GLU-NPs as smart nano-drug delivery systems for the *in-vivo* enhancement of systemic circulation time, and tumor-targeted accumulation.

## 5. REFERENCES

[1] R.A. Smith, K.S. Andrews, D. Brooks, S.A. Fedewa, D. Manassaram-Baptiste, D. Saslow, O.W. Brawley, R.C. Wender, Cancer screening in the United States, 2018: a review of current American Cancer Society guidelines and current issues in cancer screening, CA: a cancer journal for clinicians, 68 (2018) 297-316.

[2] R.L. Siegel, K.D. Miller, S.A. Fedewa, D.J. Ahnen, R.G. Meester, A. Barzi, A. Jemal, Colorectal cancer statistics, 2017, CA: a cancer journal for clinicians, 67 (2017) 177-193.

[3] S.S. Kesharwani, S. Kaur, H. Tummala, A.T. Sangamwar, Overcoming multiple drug resistance in cancer using polymeric micelles, Expert opinion on drug delivery, 15 (2018) 1127-1142.

[4] S.S. Kesharwani, S. Kaur, H. Tummala, A.T. Sangamwar, Multifunctional approaches utilizing polymeric micelles to circumvent multidrug resistant tumors, Colloids and Surfaces B: Biointerfaces, (2018) 581-590.

[5] R.L. Siegel, K.D. Miller, A. Jemal, Cancer statistics, 2019, CA: a cancer journal for clinicians, (2019) 7-34.

[6] S.A. Kaliberov, D.J. Buchsbaum, Cancer treatment with gene therapy and radiation therapy, in: Advances in cancer research, Elsevier, 2012, pp. 221-263.

[7] M. Arruebo, N. Vilaboa, B. Saez-Gutierrez, J. Lambea, A. Tres, M. Valladares, A. Gonzalez-Fernandez, Assessment of the evolution of cancer treatment therapies, Cancers, 3 (2011) 3279-3330.

[8] M.S. Ricci, W. X. Zong, Chemotherapeutic approaches for targeting cell death pathways, The oncologist, 11 (2006) 342-357.

[9] K.O. Alfarouk, C.-M. Stock, S. Taylor, M. Walsh, A.K. Muddathir, D. Verduzco, A.H. Bashir, O.Y. Mohammed, G.O. Elhassan, S. Harguindey, Resistance to cancer chemotherapy: failure in drug response from ADME to P-gp, Cancer cell international, 15 (2015) 1-13.

[10] X. Dong, R.J. Mumper, Nanomedicinal strategies to treat multidrug-resistant tumors: current progress, Nanomedicine, 5 (2010) 597-615.

[11] H. Maeda, M. Khatami, Analyses of repeated failures in cancer therapy for solid tumors: poor tumor-selective drug delivery, low therapeutic efficacy and unsustainable costs, Clinical and translational medicine, 7 (2018) 11 1-20.

[12] G. Housman, S. Byler, S. Heerboth, K. Lapinska, M. Longacre, N. Snyder, S. Sarkar, Drug resistance in cancer: an overview, Cancers, 6 (2014) 1769-1792.

[13] G.J. Kim, Cancer nanotechnology: engineering multifunctional nanostructures for targeting tumor cells and vasculatures, in, Georgia Institute of Technology, 2007.

[14] Y.H. Bae, K. Park, Targeted drug delivery to tumors: myths, reality and possibility, Journal of Controlled Release, 153 (2011) 198-205.

[15] P. Kanavos, R. Sullivan, G. Lewison, W. Schurer, S. Eckhouse, Z. Vlachopioti, The role of funding and policies on innovation in cancer drug development, ecancermedicalscience, 4 (2010) 1-139.

[16] D.J. Stewart, G. Batist, H.M. Kantarjian, J.-P. Bradford, J.H. Schiller, R. Kurzrock, The urgent need for clinical research reform to permit faster, less expensive access to new therapies for lethal diseases, in, AACR, 2015.

[17] F. Danhier, O. Feron, V. Preat, To exploit the tumor microenvironment: passive and active tumor targeting of nanocarriers for anti-cancer drug delivery, Journal of controlled release, 148 (2010) 135-146.

[18] P. Duesberg, R. Stindl, R. Hehlmann, Explaining the high mutation rates of cancer cells to drug and multidrug resistance by chromosome reassortments that are catalyzed by aneuploidy, Proceedings of the National Academy of Sciences, 97 (2000) 14295-14300.

[19] N.L. Komarova, D. Wodarz, Drug resistance in cancer: principles of emergence and prevention, Proceedings of the National Academy of Sciences, 102 (2005) 9714-9719.

[20] X. Ke, L. Shen, Molecular targeted therapy of cancer: The progress and future prospect, Frontiers in Laboratory Medicine, 1 (2017) 69-75.

[21] S.K. Sriraman, B. Aryasomayajula, V.P. Torchilin, Barriers to drug delivery in solid tumors, Tissue barriers, 2 (2014) e29528 1-10.

[22] F. Alexis, E.M. Pridgen, R. Langer, O.C. Farokhzad, Nanoparticle technologies for cancer therapy, in: Drug delivery, Springer, 2010, pp. 55-86.

[23] O.C. Farokhzad, R. Langer, Impact of nanotechnology on drug delivery, ACS nano, 3 (2009) 16-20.

[24] Z. Gao, L. Zhang, Y. Sun, Nanotechnology applied to overcome tumor drug resistance, Journal of Controlled Release, 162 (2012) 45-55.

[25] A. Gothwal, I. Khan, U. Gupta, Polymeric micelles: recent advancements in the delivery of anticancer drugs, Pharmaceutical research, 33 (2016) 18-39.

[26] U. Kedar, P. Phutane, S. Shidhaye, V. Kadam, Advances in polymeric micelles for drug delivery and tumor targeting, Nanomedicine: Nanotechnology, Biology and Medicine, 6 (2010) 714-729.

[27] Y. Luqmani, Mechanisms of drug resistance in cancer chemotherapy, Medical Principles and Practice, 14 (2005) 35-48.

[28] D. Peer, J.M. Karp, S. Hong, O.C. Farokhzad, R. Margalit, R. Langer, Nanocarriers as an emerging platform for cancer therapy, Nature nanotechnology, 2 (2007) 751-760.

[29] D. Rosenblum, N. Joshi, W. Tao, J.M. Karp, D. Peer, Progress and challenges towards targeted delivery of cancer therapeutics, Nature communications, 9 (2018) 1410 1-12.

[30] T. Lammers, W. Hennink, G. Storm, Tumour-targeted nanomedicines: principles and practice, British journal of cancer, 99 (2008) 392-397.

[31] M.L. Etheridge, S.A. Campbell, A.G. Erdman, C.L. Haynes, S.M. Wolf, J. McCullough, The big picture on nanomedicine: the state of investigational and

approved nanomedicine products, Nanomedicine: nanotechnology, biology and medicine, 9 (2013) 1-14.

[32] L.Y. Rizzo, B. Theek, G. Storm, F. Kiessling, T. Lammers, Recent progress in nanomedicine: therapeutic, diagnostic and theranostic applications, Current opinion in biotechnology, 24 (2013) 1159-1166.

[33] A. Wicki, D. Witzigmann, V. Balasubramanian, J. Huwyler, Nanomedicine in cancer therapy: challenges, opportunities, and clinical applications, Journal of controlled release, 200 (2015) 138-157.

[34] M.E. Davis, Z. Chen, D.M. Shin, Nanoparticle therapeutics: an emerging treatment modality for cancer, in: Nanoscience And Technology: A Collection of Reviews from Nature Journals, World Scientific, 2010, pp. 239-250.

[35] V. Sanna, N. Pala, M. Sechi, Targeted therapy using nanotechnology: focus on cancer, International journal of nanomedicine, 9 (2014) 467-483.

[36] K.N. Shah, Receptor-mediated targeting to enhance therapeutic efficacy of chemotherapeutic agents, The University of Akron, 2014.

[37] X. Yang, Development of Nanoparticle Systems for Therapeutic Drug Delivery, in, The Ohio State University, 2009.

[38] C.-M.J. Hu, Functionalization of nanocarriers for efficient combination drug delivery, in, UC San Diego, 2011.

[39] R. van der Meel, L.J. Vehmeijer, R.J. Kok, G. Storm, E.V. van Gaal, Ligand-targeted particulate nanomedicines undergoing clinical evaluation: current status, in: Intracellular Delivery III, Springer, 2016, pp. 163-200.

[40] P. Carmeliet, R.K. Jain, Angiogenesis in cancer and other diseases, nature, 407 (2000) 249-257.

[41] R.K. Jain, Normalization of tumor vasculature: an emerging concept in antiangiogenic therapy, Science, 307 (2005) 58-62.

[42] H. Maeda, J. Wu, T. Sawa, Y. Matsumura, K. Hori, Tumor vascular permeability and the EPR effect in macromolecular therapeutics: a review, Journal of Controlled Release, 65 (2000) 271-284.

[43] R. Bazak, M. Houri, S. El Achy, W. Hussein, T. Refaat, Passive targeting of nanoparticles to cancer: A comprehensive review of the literature, Molecular and clinical oncology, 2 (2014) 904-908.

[44] D. Banerjee, R. Harfouche, S. Sengupta, Nanotechnology-mediated targeting of tumor angiogenesis, Vascular Cell, 3 (2011) 3 1-13.

[45] H. Kobayashi, R. Watanabe, P.L. Choyke, Improving conventional enhanced permeability and retention (EPR) effects; what is the appropriate target?, Theranostics, 4 (2014) 81-90.

[46] M.J. Ernsting, M. Murakami, A. Roy, S.-D. Li, Factors controlling the pharmacokinetics, biodistribution and intratumoral penetration of nanoparticles, Journal of Controlled Release, 172 (2013) 782-794.

[47] A. Gabizon, H. Shmeeda, Y. Barenholz, Pharmacokinetics of pegylated liposomal doxorubicin, Clinical pharmacokinetics, 42 (2003) 419-436.

[48] N.T. Huynh, C. Passirani, P. Saulnier, J.-P. Benoit, Lipid nanocapsules: a new platform for nanomedicine, International journal of pharmaceutics, 379 (2009) 201-209.

[49] C. Reynolds, D. Barrera, R. Jotte, A.I. Spira, C. Weissman, K.A. Boehm, S. Pritchard, L. Asmar, Phase II trial of nanoparticle albumin-bound paclitaxel, carboplatin, and bevacizumab in first-line patients with advanced nonsquamous non-small cell lung cancer, Journal of Thoracic Oncology, 4 (2009) 1537-1543.

[50] E. Rosenthal, I. Poizot Martin, T. Saint-Marc, J. P. Spano, P. Cacoub, D.S. Group, Phase IV study of liposomal daunorubicin (DaunoXome) in AIDS-related Kaposi sarcoma, American journal of clinical oncology, 25 (2002) 57-59.

[51] B. McClune, F. Buadi, N. Aslam, D. Przepiorka, Intrathecal Liposomal Cytarabine (Depocyt) Is Safe and Effective for Prevention of Meningeal Disease in Patients with Acute Lymphoblastic Leukemia and High-Grade Lymphoma Treated with the HyperCVAD Regimen, in, Am Soc Hematology, 2005.

[52] J.A. Silverman, S.R. Deitcher, Marqibo® (vincristine sulfate liposome injection) improves the pharmacokinetics and pharmacodynamics of vincristine, Cancer chemotherapy and pharmacology, 71 (2013) 555-564.

[53] K. Mori, K. Ando, D. Heymann, Liposomal muramyl tripeptide phosphatidyl ethanolamine: a safe and effective agent against osteosarcoma pulmonary metastases, Expert review of anticancer therapy, 8 (2008) 151-159.

[54] L. Kager, U. Pötschger, S. Bielack, Review of mifamurtide in the treatment of patients with osteosarcoma, Therapeutics and clinical risk management, 6 (2010) 279-286.

[55] M. Montana, C. Ducros, P. Verhaeghe, T. Terme, P. Vanelle, P. Rathelot, Albumin-bound paclitaxel: the benefit of this new formulation in the treatment of various cancers, Journal of Chemotherapy, 23 (2011) 59-66.

[56] P.A. Dinndorf, J. Gootenberg, M.H. Cohen, P. Keegan, R. Pazdur, FDA drug approval summary: pegaspargase (Oncaspar®) for the first-line treatment of children with acute lymphoblastic leukemia (ALL), The oncologist, 12 (2007) 991-998.

[57] X. Wu, S. Chen, L. Lin, J. Liu, Y. Wang, Y. Li, Q. Li, Z. Wang, A Single Domain–Based Anti-Her2 Antibody Has Potent Antitumor Activities, Translational oncology, 11 (2018) 366-373.

[58] C.G. Murphy, S. Modi, HER2 breast cancer therapies: a review, Biologics: targets & therapy, 3 (2009) 289-301.

[59] S.D. Steichen, M. Caldorera-Moore, N.A. Peppas, A review of current nanoparticle and targeting moieties for the delivery of cancer therapeutics, European journal of pharmaceutical sciences, 48 (2013) 416-427.

[60] S.R. Fernandes, R. Fernandes, B. Sarmento, P.M. Pereira, J.P. Tome, Photoimmunoconjugates: novel synthetic strategies to target and treat cancer by photodynamic therapy, Organic & biomolecular chemistry, 17 (2019) 2579-2593.

[61] D. Kirpotin, J.W. Park, K. Hong, S. Zalipsky, W.-L. Li, P. Carter, C.C. Benz, D. Papahadjopoulos, Sterically stabilized anti-HER2 immunoliposomes: design and targeting to human breast cancer cells in vitro, Biochemistry, 36 (1997) 66-75.

[62] J.W. Park, K. Hong, D.B. Kirpotin, G. Colbern, R. Shalaby, J. Baselga, Y. Shao, U.B. Nielsen, J.D. Marks, D. Moore, Anti-HER2 immunoliposomes: enhanced efficacy attributable to targeted delivery, Clinical Cancer Research, 8 (2002) 1172-1181.

[63] J. Zhang, L.J. Medeiros, K.H. Young, Cancer Immunotherapy in Diffuse Large B-Cell Lymphoma, Frontiers in oncology, 8 (2018) 1-12.

[64] T. Suresh, L.X. Lee, J. Joshi, S.K. Barta, New antibody approaches to lymphoma therapy, Journal of hematology & oncology, 7 (2014) 58 1-12.

[65] L. Kou, Y.D. Bhutia, Q. Yao, Z. He, J. Sun, V. Ganapathy, Transporter-guided delivery of nanoparticles to improve drug permeation across cellular barriers and drug exposure to selective cell types, Frontiers in pharmacology, 9 (2018) 27 1-16.

[66] M.J. Akhtar, M. Ahamed, H.A. Alhadlaq, S.A. Alrokayan, S. Kumar, Targeted anticancer therapy: overexpressed receptors and nanotechnology, Clinica chimica acta, 436 (2014) 78-92.

[67] J.S. Suk, Q. Xu, N. Kim, J. Hanes, L.M. Ensign, PEGylation as a strategy for improving nanoparticle-based drug and gene delivery, Advanced drug delivery reviews, 99 (2016) 28-51.

[68] E.C. Dreaden, L.A. Austin, M.A. Mackey, M.A. El-Sayed, Size matters: gold nanoparticles in targeted cancer drug delivery, Therapeutic delivery, 3 (2012) 457-478.

[69] A. D Friedman, S. E Claypool, R. Liu, The smart targeting of nanoparticles, Current pharmaceutical design, 19 (2013) 6315-6329.

[70] P. Ray, R.R. White, Aptamers for targeted drug delivery, Pharmaceuticals, 3 (2010) 1761-1778.

[71] J.T. Duskey, K.G. Rice, Nanoparticle ligand presentation for targeting solid tumors, AAPS PharmSciTech, 15 (2014) 1345-1354.

[72] R. Singh, J.W. Lillard Jr, Nanoparticle-based targeted drug delivery, Experimental and molecular pathology, 86 (2009) 215-223.

[73] F. ud Din, W. Aman, I. Ullah, O.S. Qureshi, O. Mustapha, S. Shafique, A. Zeb, Effective use of nanocarriers as drug delivery systems for the treatment of selected tumors, International journal of nanomedicine, 12 (2017) 7291-7309.

[74] Z. Amoozgar, Y. Yeo, Recent advances in stealth coating of nanoparticle drug delivery systems, Wiley Interdisciplinary Reviews: Nanomedicine and Nanobiotechnology, 4 (2012) 219-233.

[75] J. W. Yoo, E. Chambers, S. Mitragotri, Factors that control the circulation time of nanoparticles in blood: challenges, solutions and future prospects, Current pharmaceutical design, 16 (2010) 2298-2307.

[76] J. Su, H. Sun, Q. Meng, Q. Yin, S. Tang, P. Zhang, Y. Chen, Z. Zhang, H. Yu, Y. Li, Long Circulation Red-Blood-Cell-Mimetic Nanoparticles with Peptide-Enhanced Tumor Penetration for Simultaneously Inhibiting Growth and Lung Metastasis of Breast Cancer, Advanced Functional Materials, 26 (2016) 1243-1252.

[77] D.A. Balazs, W. Godbey, Liposomes for use in gene delivery, Journal of drug delivery, 2011 (2011) 1-12.

[78] D.E. Owens III, N.A. Peppas, Opsonization, biodistribution, and pharmacokinetics of polymeric nanoparticles, International journal of pharmaceutics, 307 (2006) 93-102.

[79] N. Vij, T. Min, R. Marasigan, C.N. Belcher, S. Mazur, H. Ding, K.-T. Yong, I. Roy, Development of PEGylated PLGA nanoparticle for controlled and sustained drug delivery in cystic fibrosis, Journal of nanobiotechnology, 8 (2010) 22 1-18.

[80] E.L. Chambers, Extended vascular circulation of polymeric particles via erythrocyte binding, (2005).

[81] E. Blanco, H. Shen, M. Ferrari, Principles of nanoparticle design for overcoming biological barriers to drug delivery, Nature biotechnology, 33 (2015) 941-951.

[82] N. Hoshyar, S. Gray, H. Han, G. Bao, The effect of nanoparticle size on in vivo pharmacokinetics and cellular interaction, Nanomedicine, 11 (2016) 673-692.

[83] C.D. Walkey, J.B. Olsen, H. Guo, A. Emili, W.C. Chan, Nanoparticle size and surface chemistry determine serum protein adsorption and macrophage uptake, Journal of the American Chemical Society, 134 (2012) 2139-2147.

[84] A. Albanese, P.S. Tang, W.C. Chan, The effect of nanoparticle size, shape, and surface chemistry on biological systems, Annual review of biomedical engineering, 14 (2012) 1-16.

[85] J. Lu, X. Chuan, H. Zhang, W. Dai, X. Wang, X. Wang, Q. Zhang, Free paclitaxel loaded PEGylated-paclitaxel nanoparticles: preparation and comparison with other paclitaxel systems in vitro and in vivo, International journal of pharmaceutics, 471 (2014) 525-535.

[86] S. Movassaghian, V.P. Torchilin, Long-Circulating Therapies for Cancer Treatment, in: Novel Approaches and Strategies for Biologics, Vaccines and Cancer Therapies, Elsevier, 2015, pp. 433-462.

[87] B. Romberg, W.E. Hennink, G. Storm, Sheddable coatings for long-circulating nanoparticles, Pharmaceutical research, 25 (2008) 55-71.

[88] Q. Yang, Exploring and harnessing PEG-immune system interactions to engineer targeted stealth nanoparticles, in, The University of North Carolina at Chapel Hill, 2016.

[89] J.V. Jokerst, T. Lobovkina, R.N. Zare, S.S. Gambhir, Nanoparticle PEGylation for imaging and therapy, Nanomedicine, 6 (2011) 715-728.

[90] H. Otsuka, Y. Nagasaki, K. Kataoka, PEGylated nanoparticles for biological and pharmaceutical applications, Advanced drug delivery reviews, 64 (2012) 246-255.

[91] K. Shiraishi, M. Hamano, H. Ma, K. Kawano, Y. Maitani, T. Aoshi, K.J. Ishii, M. Yokoyama, Hydrophobic blocks of PEG-conjugates play a significant role in the accelerated blood clearance (ABC) phenomenon, Journal of Controlled Release, 165 (2013) 183-190.

[92] K. Shiraishi, M. Yokoyama, Polymeric micelles possessing polyethyleneglycol as outer shell and their unique behaviors in accelerated blood clearance phenomenon, Biological and Pharmaceutical Bulletin, 36 (2013) 878-882.

[93] V. Gaberc-Porekar, I. Zore, B. Podobnik, V. Menart, Obstacles and pitfalls in the PEGylation of therapeutic proteins, Current Opinion in Drug Discovery and Development, 11 (2008) 242-250.

[94] R. Saadati, S. Dadashzadeh, Z. Abbasian, H. Soleimanjahi, Accelerated blood clearance of PEGylated PLGA nanoparticles following repeated injections: effects of polymer dose, PEG coating, and encapsulated anticancer drug, Pharmaceutical research, 30 (2013) 985-995.

[95] M.G. Saifer, L.D. Williams, M.A. Sobczyk, S.J. Michaels, M.R. Sherman, Selectivity of binding of PEGs and PEG-like oligomers to anti-PEG antibodies induced by methoxyPEG-proteins, Molecular immunology, 57 (2014) 236-246.

[96] T. Suzuki, M. Ichihara, K. Hyodo, E. Yamamoto, T. Ishida, H. Kiwada, H. Ishihara, H. Kikuchi, Accelerated blood clearance of PEGylated liposomes containing

doxorubicin upon repeated administration to dogs, International journal of pharmaceutics, 436 (2012) 636-643.

[97] T. Suzuki, M. Ichihara, K. Hyodo, E. Yamamoto, T. Ishida, H. Kiwada, H. Kikuchi, H. Ishihara, Influence of dose and animal species on accelerated blood clearance of PEGylated liposomal doxorubicin, International journal of pharmaceutics, 476 (2014) 205-212.

[98] J.J. Verhoef, J.F. Carpenter, T.J. Anchordoquy, H. Schellekens, Potential induction of anti-PEG antibodies and complement activation toward PEGylated therapeutics, Drug discovery today, 19 (2014) 1945-1952.

[99] Y. Zhao, L. Wang, M. Yan, Y. Ma, G. Zang, Z. She, Y. Deng, Repeated injection of PEGylated solid lipid nanoparticles induces accelerated blood clearance in mice and beagles, International journal of nanomedicine, 7 (2012) 2891-2900.

[100] A.R. Kirtane, Strategies to Improve Plasma Circulation of Nanoparticles, (2014).

[101] J.-W. Yoo, D.J. Irvine, D.E. Discher, S. Mitragotri, Bio-inspired, bioengineered and biomimetic drug delivery carriers, Nature reviews Drug discovery, 10 (2011) 521-535.

[102] N.M. Gulati, P.L. Stewart, N.F. Steinmetz, Bioinspired shielding strategies for nanoparticle drug delivery applications, Molecular pharmaceutics, 15 (2018) 2900-2909.

[103] A.C. Anselmo, V. Gupta, B.J. Zern, D. Pan, M. Zakrewsky, V. Muzykantov, S. Mitragotri, Delivering nanoparticles to lungs while avoiding liver and spleen through adsorption on red blood cells, ACS nano, 7 (2013) 11129-11137.

[104] A.C. Anselmo, S. Kumar, V. Gupta, A.M. Pearce, A. Ragusa, V. Muzykantov, S. Mitragotri, Exploiting shape, cellular-hitchhiking and antibodies to target

nanoparticles to lung endothelium: Synergy between physical, chemical and biological approaches, Biomaterials, 68 (2015) 1-8.

[105] A.C. Anselmo, M. Zhang, S. Kumar, D.R. Vogus, S. Menegatti, M.E. Helgeson, S. Mitragotri, Elasticity of nanoparticles influences their blood circulation, phagocytosis, endocytosis, and targeting, ACS nano, 9 (2015) 3169-3177.

[106] J.S. Brenner, D.C. Pan, J.W. Myerson, O.A. Marcos-Contreras, C.H. Villa, P. Patel, H. Hekierski, S. Chatterjee, J.-Q. Tao, H. Parhiz, Red blood cell-hitchhiking boosts delivery of nanocarriers to chosen organs by orders of magnitude, Nature communications, 9 (2018) 2684 1-14.

[107] E. Chambers, S. Mitragotri, Prolonged circulation of large polymeric nanoparticles by non-covalent adsorption on erythrocytes, Journal of Controlled Release, 100 (2004) 111-119.

[108] E. Chambers, S. Mitragotri, Long circulating nanoparticles via adhesion on red blood cells: mechanism and extended circulation, Experimental biology and medicine, 232 (2007) 958-966.

[109] N. Doshi, A.S. Zahr, S. Bhaskar, J. Lahann, S. Mitragotri, Red blood cell-mimicking synthetic biomaterial particles, Proceedings of the National Academy of Sciences, 106 (2009) 21495-21499.

[110] R.H. Fang, C.-M.J. Hu, L. Zhang, Nanoparticles disguised as red blood cells to evade the immune system, in, Taylor & Francis, 2012 385-389.

[111] J. Lahann, S. Mitragotri, S. Bhaskar, N. Doshi, A.A. Zahr, Red blood cell-mimetic particles and methods for making use thereof, in, Google Patents, 2010.

[112] S.M. Moghimi, A.C. Hunter, J.C. Murray, Long-circulating and target-specific nanoparticles: theory to practice, Pharmacological reviews, 53 (2001) 283-318.

[113] V.R. Muzykantov, Drug delivery by red blood cells: vascular carriers designed by mother nature, Expert opinion on drug delivery, 7 (2010) 403-427.

[114] D. Pan, O. Vargas-Morales, B. Zern, A.C. Anselmo, V. Gupta, M. Zakrewsky, S. Mitragotri, V. Muzykantov, The effect of polymeric nanoparticles on biocompatibility of carrier red blood cells, PloS one, 11 (2016) e0152074.

[115] L. Rao, L.L. Bu, J.H. Xu, B. Cai, G.T. Yu, X. Yu, Z. He, Q. Huang, A. Li, S.S. Guo, Red blood cell membrane as a biomimetic nanocoating for prolonged circulation time and reduced accelerated blood clearance, Small, 11 (2015) 6225-6236.

[116] C.H. Villa, A.C. Anselmo, S. Mitragotri, V. Muzykantov, Red blood cells: Supercarriers for drugs, biologicals, and nanoparticles and inspiration for advanced delivery systems, Advanced drug delivery reviews, 106 (2016) 88-103.

[117] P.P. Wibroe, A.C. Anselmo, P.H. Nilsson, A. Sarode, V. Gupta, R. Urbanics, J. Szebeni, A.C. Hunter, S. Mitragotri, T.E. Mollnes, Bypassing adverse injection reactions to nanoparticles through shape modification and attachment to erythrocytes, Nature Nanotechnology, 12 (2017) 589-594.

[118] Z. Wu, B.E.F. de Avila, A. Martín, C. Christianson, W. Gao, S.K. Thamphiwatana, A. Escarpa, Q. He, L. Zhang, J. Wang, RBC micromotors carrying multiple cargos towards potential theranostic applications, Nanoscale, 7 (2015) 13680-13686.

[119] I. Bernhardt, J.C. Ellory, Red cell membrane transport in health and disease, Springer Science & Business Media, 2013.

[120] Q. Xia, Y. Zhang, Z. Li, X. Hou, N. Feng, Red blood cell membrane-camouflaged nanoparticles: A novel drug delivery system for antitumor application, Acta Pharmaceutica Sinica B, (2019) 1-15.

[121] J.G. Piao, L. Wang, F. Gao, Y.-Z. You, Y. Xiong, L. Yang, Erythrocyte membrane is an alternative coating to polyethylene glycol for prolonging the circulation lifetime of gold nanocages for photothermal therapy, ACS nano, 8 (2014) 10414-10425.

[122] N. Yan, A Glimpse of Membrane Transport through Structures—Advances in the Structural Biology of the GLUT Glucose Transporters, Journal of molecular biology, 429 (2017) 2710-2725.

[123] M. Zheng, D. Librizzi, A. Kılıç, Y. Liu, H. Renz, O.M. Merkel, T. Kissel, Enhancing in vivo circulation and siRNA delivery with biodegradable polyethylenimine-graft-polycaprolactone-block-poly (ethylene glycol) copolymers, Biomaterials, 33 (2012) 6551-6558.

[124] A.N. Koo, K.H. Min, H.J. Lee, S.-U. Lee, K. Kim, I.C. Kwon, S.H. Cho, S.Y. Jeong, S.C. Lee, Tumor accumulation and antitumor efficacy of docetaxel-loaded core-shell-corona micelles with shell-specific redox-responsive cross-links, Biomaterials, 33 (2012) 1489-1499.

[125] H.D. Han, A. Lee, T. Hwang, C.K. Song, H. Seong, J. Hyun, B.C. Shin, Enhanced circulation time and antitumor activity of doxorubicin by comblike polymer-incorporated liposomes, Journal of Controlled Release, 120 (2007) 161-168.

[126] L. Ye, Y. Zhang, B. Yang, X. Zhou, J. Li, Z. Qin, D. Dong, Y. Cui, F. Yao, Zwitterionic-modified starch-based stealth micelles for prolonging circulation time

and reducing macrophage response, ACS applied materials & interfaces, 8 (2016) 4385-4398.

[127] H. Su, Y. Wang, S. Liu, Y. Wang, Q. Liu, G. Liu, Q. Chen, Emerging transporter-targeted nanoparticulate drug delivery systems, Acta Pharmaceutica Sinica B, (2018) 1-10.

[128] W. Wu, S. Zhao, Metabolic changes in cancer: beyond the Warburg effect, Acta biochimica et biophysica Sinica, 45 (2013) 18-26.

[129] A.N. McCracken, A.L. Edinger, Nutrient transporters: the Achilles' heel of anabolism, Trends in Endocrinology & Metabolism, 24 (2013) 200-208.

[130] L. Lin, Characterization of Influx Transporters in the Blood-Brain Barrier: Implications for Drug Delivery, in, UCSF, 2015.

[131] M.A. Hediger, B. Clemencon, R.E. Burrier, E.A. Bruford, The ABCs of membrane transporters in health and disease (SLC series): introduction, Molecular aspects of medicine, 34 (2013) 95-107.

[132] G. You, M.E. Morris, Drug transporters: molecular characterization and role in drug disposition, John Wiley and Sons, 2006.

[133] M.L. Rives, J.A. Javitch, A.D. Wickenden, Potentiating SLC transporter activity: emerging drug discovery opportunities, Biochemical pharmacology, 135 (2017) 1-11.

[134] M.H. Saier Jr, C.V. Tran, R.D. Barabote, TCDB: the Transporter Classification Database for membrane transport protein analyses and information, Nucleic acids research, 34 (2006) D181-D186.

[135] S. Jalgaonkar, ABC Membrane Transporters: Target for Drugs and Diseases, Global J Pharmc, 4 (2010) 75-82.

[136] Y.-L. Sun, A. Patel, P. Kumar, Z.-S. Chen, Role of ABC transporters in cancer chemotherapy, Chinese journal of cancer, 31 (2012) 51-57.

[137] T. Nakanishi, I. Tamai, Solute carrier transporters as targets for drug delivery and pharmacological intervention for chemotherapy, Journal of pharmaceutical sciences, 100 (2011) 3731-3750.

[138] V. Ganapathy, M. Thangaraju, P.D. Prasad, Nutrient transporters in cancer: relevance to Warburg hypothesis and beyond, Pharmacology & therapeutics, 121 (2009) 29-40.

[139] B.M. Burt, J.L. Humm, D.A. Kooby, O.D. Squire, S. Mastorides, S.M. Larson, Y. Fong, Using positron emission tomography with [$^{18}$F] FDG to predict tumor behavior in experimental colorectal cancer, Neoplasia, 3 (2001) 189-195.

[140] J.R. Oh, B.C. Ahn, False-positive uptake on radioiodine whole-body scintigraphy: physiologic and pathologic variants unrelated to thyroid cancer, American journal of nuclear medicine and molecular imaging, 2 (2012) 362-385.

[141] D. Deng, N. Yan, GLUT, SGLT, and SWEET: Structural and mechanistic investigations of the glucose transporters, Protein Science, 25 (2016) 546-558.

[142] M.B. Calvo, A. Figueroa, E.G. Pulido, R.G. Campelo, L.A. Aparicio, Potential role of sugar transporters in cancer and their relationship with anticancer therapy, International journal of endocrinology, 2010 (2010) 1-15.

[143] L.Szablewski, Glucose transporters in healthy heart and in cardiac disease, International journal of cardiology, 230 (2017) 70-75.

[144] M.L. Macheda, S. Rogers, J.D. Best, Molecular and cellular regulation of glucose transporter (GLUT) proteins in cancer, Journal of cellular physiology, 202 (2005) 654-662.

[145] K.C. Carvalho, I.W. Cunha, R.M. Rocha, F.R. Ayala, M.M. Cajaíba, M.D. Begnami, R.S. Vilela, G.R. Paiva, R.G. Andrade, F.A. Soares, GLUT1 expression in malignant tumors and its use as an immunodiagnostic marker, Clinics, 66 (2011) 965-972.

[146] R.E. Airley, A. Mobasheri, Hypoxic regulation of glucose transport, anaerobic metabolism and angiogenesis in cancer: novel pathways and targets for anticancer therapeutics, Chemotherapy, 53 (2007) 233-256.

[147] R.A. Medina, G.I. Owen, Glucose transporters: expression, regulation and cancer, Biological research, 35 (2002) 9-26.

[148] Y. Nakayama, T. Torigoe, Y. Inoue, N. Minagawa, H. Izumi, K. Kohno, K. Yamaguchi, Prognostic significance of monocarboxylate transporter 4 expression in patients with colorectal cancer, Experimental and therapeutic medicine, 3 (2012) 25-30.

[149] H. Reis, S. Tschirdewahn, T. Szarvas, H. Rübben, K. Werner Schmid, F. Grabellus, Expression of GLUT1 is associated with increasing grade of malignancy in non-invasive and invasive urothelial carcinomas of the bladder, Oncology letters, 2 (2011) 1149-1153.

[150] M. Yu, H. Yongzhi, S. Chen, X. Luo, Y. Lin, Y. Zhou, H. Jin, B. Hou, Y. Deng, L. Tu, The prognostic value of GLUT1 in cancers: a systematic review and meta-analysis, Oncotarget, 8 (2017) 43356-43367.

[151] C. Barron, E. Tsiani, T. Tsakiridis, Expression of the glucose transporters GLUT1, GLUT3, GLUT4 and GLUT12 in human cancer cells, in: BMC proceedings, BioMed Central, 2012, pp. P4.

[152] K. Reinicke, P. Sotomayor, P. Cisterna, C. Delgado, F. Nualart, A. Godoy, Cellular distribution of Glut-1 and Glut-5 in benign and malignant human prostate tissue, Journal of cellular biochemistry, 113 (2012) 553-562.

[153] A. Godoy, V. Ulloa, F. Rodríguez, K. Reinicke, A.J. Yanez, M.d.l.A. Garcia, R.A. Medina, M. Carrasco, S. Barberis, T. Castro, Differential subcellular distribution of glucose transporters GLUT1–6 and GLUT9 in human cancer: ultrastructural localization of GLUT1 and GLUT5 in breast tumor tissues, Journal of cellular physiology, 207 (2006) 614-627.

[154] S. Oh, H. Kim, K. Nam, I. Shin, Glut1 promotes cell proliferation, migration and invasion by regulating epidermal growth factor receptor and integrin signaling in triple-negative breast cancer cells, BMB reports, 50 (2017) 132-137.

[155] Y.R. Hussein, S. Bandyopadhyay, A. Semaan, Q. Ahmed, B. Albashiti, T. Jazaerly, Z. Nahleh, R. Ali-Fehmi, Glut-1 expression correlates with basal-like breast cancer, Translational oncology, 4 (2011) 321-327.

[156] S.S. Kang, Y.K. Chun, M.H. Hur, H.K. Lee, Y.J. Kim, S.R. Hong, J.H. Lee, S.G. Lee, Y.K. Park, Clinical significance of glucose transporter 1 (GLUT1) expression in human breast carcinoma, Japanese Journal of Cancer Research, 93 (2002) 1123-1128.

[157] E.A. Wellberg, S. Johnson, J. Finlay-Schultz, A.S. Lewis, K.L. Terrell, C.A. Sartorius, E.D. Abel, W.J. Muller, S.M. Anderson, The glucose transporter GLUT1

is required for ErbB2-induced mammary tumorigenesis, Breast Cancer Research, 18 (2016) 131 1-15.

[158] R. Cooper, S. Sarioğlu, S. Sokmen, M. Füzün, A. Küpelioğlu, H. Valentine, I. Görken, R. Airley, C. West, Glucose transporter-1 (GLUT-1): a potential marker of prognosis in rectal carcinoma?, British journal of cancer, 89 (2003) 870-876.

[159] R. Oliver, R. Woodwards, P. Sloan, N. Thakker, I. Stratford, R. Airley, Prognostic value of facilitative glucose transporter Glut-1 in oral squamous cell carcinomas treated by surgical resection: results of EORTC Translational Research Fund studies, European Journal of Cancer, 40 (2004) 503-507.

[160] P. Effert, A. Beniers, Y. Tamimi, S. Handt, G. Jakse, Expression of glucose transporter 1 (Glut-1) in cell lines and clinical specimens from human prostate adenocarcinoma, Anticancer research, 24 (2004) 3057-3064.

[161] M. Patra, T.C. Johnstone, K. Suntharalingam, S.J. Lippard, A potent glucose–platinum conjugate exploits glucose transporters and preferentially accumulates in cancer cells, Angewandte Chemie, 128 (2016) 2596-2600.

[162] H.G. Joost, G.I. Bell, J.D. Best, M.J. Birnbaum, M.J. Charron, Y. Chen, H. Doege, D.E. James, H.F. Lodish, K.H. Moley, Nomenclature of the GLUT/SLC2A family of sugar/polyol transport facilitators, American Journal of Physiology-Endocrinology And Metabolism, 282 (2002) E974-E976.

[163] R.S. Haber, A. Rathan, K.R. Weiser, A. Pritsker, S.H. Itzkowitz, C. Bodian, G. Slater, A. Weiss, D.E. Burstein, GLUT1 glucose transporter expression in colorectal carcinoma: a marker for poor prognosis, Cancer, 83 (1998) 34-40.

[164] C.P. Rojas, S.M. Castle, C.A. Llanos, J.A.S. Cortes, V. Bird, S. Rodriguez, I.M. Reis, W. Zhao, C. Gomez-Fernandez, R.J. Leveillee, Low biopsy volume in ureteroscopy does not affect tumor biopsy grading in upper tract urothelial carcinoma, in: Urologic Oncology: Seminars and Original Investigations, Elsevier, 2013, pp. 1696-1700.

[165] K. Nemejcova, J. Rosmusova, M. Bartu, M. Dura, I. Ticha, P. Dundr, Expression of Glut-1 in Normal Endometrium and Endometrial Lesions: Analysis of 336 Cases, International journal of surgical pathology, 25 (2017) 389-396.

[166] M. Younes, J. Lechago, S. Chakraborty, M. Ostrowski, M. Bridges, F. Meriano, D. Solcher, A. Barroso, D. Whitman, J. Schwartz, Relationship between dysplasia, p53 protein accumulation, DNA ploidy, and Glut1 overexpression in Barrett metaplasia, Scandinavian journal of gastroenterology, 35 (2000) 131-137.

[167] K. Higashi, Y. Ueda, A. Sakurai, X. MingWang, L. Xu, M. Murakami, H. Seki, M. Oguchi, S. Taki, Y. Nambu, Correlation of Glut-1 glucose transporter expression with [18 F] FDG uptake in non-small cell lung cancer, European journal of nuclear medicine, 27 (2000) 1778-1785.

[168] T. Yamamoto, Y. Seino, H. Fukumoto, G. Koh, H. Yano, N. Inagaki, Y. Yamada, K. Inoue, T. Manabe, H. Imura, Over-expression of facilitative glucose transporter genes in human cancer, Biochemical and biophysical research communications, 170 (1990) 223-230.

[169] S. Simoes-Sousa, S. Granja, C. Pinheiro, D. Fernandes, A. Longatto-Filho, A.C. Laus, C.D.C. Alves, J. Suarez-Penaranda, M. Pérez-Sayans, A. Lopes Carvalho,

Prognostic significance of monocarboxylate transporter expression in oral cavity tumors, Cell Cycle, 15 (2016) 1865-1873.

[170] T. Amann, U. Maegdefrau, A. Hartmann, A. Agaimy, J. Marienhagen, T.S. Weiss, O. Stoeltzing, C. Warnecke, J. Schölmerich, P.J. Oefner, GLUT1 expression is increased in hepatocellular carcinoma and promotes tumorigenesis, The American journal of pathology, 174 (2009) 1544-1552.

[171] J. Wang, X. Ying, L. Wang, Prognostic merit of glucose transporter GLUT1 expression status in gastric cancer, Annals of Oncology, 28 (2017) mdx653. 027.

[172] H. Xiao, J. Wang, W. Yan, Y. Cui, Z. Chen, X. Gao, X. Wen, J. Chen, GLUT1 regulates cell glycolysis and proliferation in prostate cancer, The Prostate, 78 (2018) 86-94.

[173] L.E. Mendez, N. Manci, G. Cantuaria, O. Gomez-Marin, M. Penalver, P. Braunschweiger, M. Nadji, Expression of glucose transporter-1 in cervical cancer and its precursors, Gynecologic oncology, 86 (2002) 138-143.

[174] S.N. Reske, K.G. Grillenberger, G. Glatting, M. Port, M. Hildebrandt, F. Gansauge, H.-G. Beger, Overexpression of glucose transporter 1 and increased FDG uptake in pancreatic carcinoma, Journal of Nuclear Medicine, 38 (1997) 1344-1348.

[175] S. Ramanathan, B. Qiu, S. Pooyan, G. Zhang, S. Stein, M.J. Leibowitz, P.J. Sinko, Targeted PEG-based bioconjugates enhance the cellular uptake and transport of a HIV-1 TAT nonapeptide, Journal of Controlled Release, 77 (2001) 199-212.

[176] S. Lee, K. Kim, T.S. Kumar, J. Lee, S.K. Kim, D.Y. Lee, Y.-k. Lee, Y. Byun, Synthesis and Biological Properties of Insulin−Deoxycholic Acid Chemical Conjugates, Bioconjugate chemistry, 16 (2005) 615-620.

[177] Y.K. Lee, J.H. Nam, H.-C. Shin, Y. Byun, Conjugation of low-molecular-weight heparin and deoxycholic acid for the development of a new oral anticoagulant agent, Circulation, 104 (2001) 3116-3120.

[178] L. Kou, Q. Yao, M. Sun, C. Wu, J. Wang, Q. Luo, G. Wang, Y. Du, Q. Fu, J. Wang, Cotransporting Ion is a Trigger for Cellular Endocytosis of Transporter-Targeting Nanoparticles: A Case Study of High-Efficiency SLC22A5 (OCTN2)-Mediated Carnitine-Conjugated Nanoparticles for Oral Delivery of Therapeutic Drugs, Advanced healthcare materials, 6 (2017) 1700165.

[179] D. Barbaro, L. Di Bari, V. Gandin, C. Evangelisti, G. Vitulli, E. Schiavi, C. Marzano, A.M. Ferretti, P. Salvadori, Glucose-coated superparamagnetic iron oxide nanoparticles prepared by metal vapour synthesis are electively internalized in a pancreatic adenocarcinoma cell line expressing GLUT1 transporter, PloS one, 10 (2015) e0123159 1-13.

[180] A. Bukchin, G. Pascual-Pasto, M. Cuadrado-Vilanova, H. Castillo-Ecija, C. Monterrubio, N.G. Olaciregui, M. Vila-Ubach, L. Ordeix, J. Mora, A.M. Carcaboso, Glucosylated nanomicelles target glucose-avid pediatric patient-derived sarcomas, Journal of controlled release, 276 (2018) 59-71.

[181] X. Jiang, H. Xin, Q. Ren, J. Gu, L. Zhu, F. Du, C. Feng, Y. Xie, X. Sha, X. Fang, Nanoparticles of 2-deoxy-D-glucose functionalized poly (ethylene glycol)-co-poly (trimethylene carbonate) for dual-targeted drug delivery in glioma treatment, Biomaterials, 35 (2014) 518-529.

[182] R. Liu, Z. Fu, M. Zhao, X. Gao, H. Li, Q. Mi, P. Liu, J. Yang, Z. Yao, Q. Gao, GLUT1-mediated selective tumor targeting with fluorine containing platinum (II) glycoconjugates, Oncotarget, 8 (2017) 39476-39496.

[183] C.-X. Zhang, W.-Y. Zhao, L. Liu, R.-J. Ju, L.-M. Mu, Y. Zhao, F. Zeng, H.-J. Xie, Y. Yan, W.-L. Lu, A nanostructure of functional targeting epirubicin liposomes dually modified with aminophenyl glucose and cyclic pentapeptide used for brain glioblastoma treatment, Oncotarget, 6 (2015) 32681-32700.

[184] M. Zhang, Z. Zhang, D. Blessington, H. Li, T.M. Busch, V. Madrak, J. Miles, B. Chance, J.D. Glickson, G. Zheng, Pyropheophorbide 2-deoxyglucosamide: a new photosensitizer targeting glucose transporters, Bioconjugate chemistry, 14 (2003) 709-714.

[185] R. Liu, H. Li, X. Gao, Q. Mi, H. Zhao, Q. Gao, Mannose-conjugated platinum complexes reveals effective tumor targeting mediated by glucose transporter 1, Biochemical and biophysical research communications, 487 (2017) 34-40.

[186] X.H. Shan, H. Hu, F. Xiong, N. Gu, X.D. Geng, W. Zhu, J. Lin, Y.F. Wang, Targeting Glut1-overexpressing MDA-MB-231 cells with 2-deoxy-d-g1ucose modified SPIOs, European journal of radiology, 81 (2012) 95-99.

[187] Y. Guo, Y. Zhang, J. Li, Y. Zhang, Y. Lu, X. Jiang, X. He, H. Ma, S. An, C. Jiang, Cell microenvironment-controlled antitumor drug releasing-nanomicelles for GLUT1-targeting hepatocellular carcinoma therapy, ACS applied materials & interfaces, 7 (2015) 5444-5453.

[188] N. Bertrand, J. Wu, X. Xu, N. Kamaly, O.C. Farokhzad, Cancer nanotechnology: the impact of passive and active targeting in the era of modern cancer biology, Advanced drug delivery reviews, 66 (2014) 2-25.

[189] S. Bhaskar, F. Tian, T. Stoeger, W. Kreyling, J.M. de la Fuente, V. Grazu, P. Borm, G. Estrada, V. Ntziachristos, D. Razansky, Multifunctional Nanocarriers for diagnostics, drug delivery and targeted treatment across blood-brain barrier: perspectives on tracking and neuroimaging, Particle and fibre toxicology, 7 (2010) 3 1-25.

[190] M. Ferrari, Cancer nanotechnology: opportunities and challenges, Nature Reviews Cancer, 5 (2005) 161-171.

[191] S. Chapman, M. Dobrovolskaia, K. Farahani, A. Goodwin, A. Joshi, H. Lee, T. Meade, M. Pomper, K. Ptak, J. Rao, Nanoparticles for cancer imaging: The good, the bad, and the promise, Nano Today, 8 (2013) 454-460.

[192] S. Harmsen, R. Huang, M.A. Wall, H. Karabeber, J.M. Samii, M. Spaliviero, J.R. White, S. Monette, R. O'Connor, K.L. Pitter, Surface-enhanced resonance Raman scattering nanostars for high-precision cancer imaging, Science translational medicine, 7 (2015) 1-22.

[193] A.R. Mehdipour, M. Hamidi, Brain drug targeting: a computational approach for overcoming blood–brain barrier, Drug discovery today, 14 (2009) 1030-1036.

[194] J. Panyam, V. Labhasetwar, Biodegradable nanoparticles for drug and gene delivery to cells and tissue, Advanced drug delivery reviews, 55 (2003) 329-347.

[195] Y. Liu, Y.c. Tseng, L. Huang, Biodistribution studies of nanoparticles using fluorescence imaging: a qualitative or quantitative method?, Pharmaceutical research, 29 (2012) 3273-3277.

[196] F. Alexis, E. Pridgen, L.K. Molnar, O.C. Farokhzad, Factors affecting the clearance and biodistribution of polymeric nanoparticles, Molecular pharmaceutics, 5 (2008) 505-515.

[197] M. Longmire, P.L. Choyke, H. Kobayashi, Clearance properties of nano-sized particles and molecules as imaging agents: considerations and caveats, (2008).

[198] E.A. Sykes, Q. Dai, C.D. Sarsons, J. Chen, J.V. Rocheleau, D.M. Hwang, G. Zheng, D.T. Cramb, K.D. Rinker, W.C. Chan, Tailoring nanoparticle designs to target cancer based on tumor pathophysiology, Proceedings of the National Academy of Sciences, 113 (2016) E1142-E1151.

[199] H. Hatakeyama, H. Akita, H. Harashima, A multifunctional envelope type nano device (MEND) for gene delivery to tumours based on the EPR effect: a strategy for overcoming the PEG dilemma, Advanced drug delivery reviews, 63 (2011) 152-160.

[200] X. Zhang, H.M. Burt, G. Mangold, D. Dexter, D.H. Von, L. Mayer, W.L. Hunter, Anti-tumor efficacy and biodistribution of intravenous polymeric micellar paclitaxel, Anti-cancer drugs, 8 (1997) 696-701.

[201] E.A. Sykes, J. Chen, G. Zheng, W.C. Chan, Investigating the impact of nanoparticle size on active and passive tumor targeting efficiency, ACS nano, 8 (2014) 5696-5706.

[202] C. Jiang, H. Wang, X. Zhang, Z. Sun, F. Wang, J. Cheng, H. Xie, B. Yu, L. Zhou, Deoxycholic acid-modified chitooligosaccharide/mPEG-PDLLA mixed micelles

loaded with paclitaxel for enhanced antitumor efficacy, International journal of pharmaceutics, 475 (2014) 60-68.

[203] H. Hatakeyama, H. Akita, H. Harashima, The polyethyleneglycol dilemma: advantage and disadvantage of PEGylation of liposomes for systemic genes and nucleic acids delivery to tumors, Biological and Pharmaceutical Bulletin, 36 (2013) 892-899.

[204] L.E. Hoelzle, M. Zeder, K.M. Felder, K. Hoelzle, Pathobiology of Mycoplasma suis, The Veterinary Journal, 202 (2014) 20-25.

[205] I.R. Peters, C.R. Helps, T.J. Gruffydd-Jones, M.J. Day, S. Tasker, Antigen specificity of the humoral immune response to Mycoplasma haemofelis infection, Clinical and Vaccine Immunology, 17 (2010) 1238-1243.

[206] Y. Zhang, Y. Zou, P. Ma, H.M. Muhammad, Y. Li, P. Jiang, Identification of Mycoplasma suis MSG1 interaction proteins on porcine erythrocytes, Archives of microbiology, 197 (2015) 277-283.

[207] P.P. Wibroe, A.C. Anselmo, P.H. Nilsson, A. Sarode, V. Gupta, R. Urbanics, J. Szebeni, A.C. Hunter, S. Mitragotri, T.E. Mollnes, Bypassing adverse injection reactions to nanoparticles through shape modification and attachment to erythrocytes, Nature Nanotechnology, 12 (2017) 589-294.

[208] H. Tummala, P. Muley, Enhancing the in-vivo efficiency of particle delivery through non-covalent interaction with red blood cell surface proteins, in, Google Patents, 2016.

[209] L. Szablewski, Expression of glucose transporters in cancers, Biochimica et Biophysica Acta (BBA)-Reviews on Cancer, 1835 (2013) 164-169.

[210] E. Roulet-Perez, D. Ballhausen, L. Bonafe, S. Cronel-Ohayon, M. Maeder-Ingvar, Glut-1 deficiency syndrome masquerading as idiopathic generalized epilepsy, Epilepsia, 49 (2008) 1955-1958.

[211] S.J. Gatley, Labeled glucose analogs in the genomic era, The Journal of Nuclear Medicine, 44 (2003) 1082-1086.

[212] S.R. Popielarski, S. Hu-Lieskovan, S.W. French, T.J. Triche, M.E. Davis, A nanoparticle-based model delivery system to guide the rational design of gene delivery to the liver. 2. In vitro and in vivo uptake results, Bioconjugate chemistry, 16 (2005) 1071-1080.

[213] M. Yokoyama, S. Fukushima, R. Uehara, K. Okamoto, K. Kataoka, Y. Sakurai, T. Okano, Characterization of physical entrapment and chemical conjugation of adriamycin in polymeric micelles and their design for in vivo delivery to a solid tumor, Journal of Controlled Release, 50 (1998) 79-92.

[214] S. Kumar, S.S. Kesharwani, B. Kuppast, M.A. Bakkari, H. Tummala, Pathogen-mimicking vaccine delivery system designed with a bioactive polymer (inulin acetate) for robust humoral and cellular immune responses, Journal of Controlled Release, 261 (2017) 263-274.

[215] S. Kumar, S.S. Kesharwani, B. Kuppast, M. Rajput, M.A. Bakkari, H. Tummala, Discovery of inulin acetate as a novel immune-active polymer and vaccine adjuvant: synthesis, material characterization, and biological evaluation as a toll-like receptor-4 agonist, Journal of Materials Chemistry B, 4 (2016) 7950-7960.

[216] P. Muley, S. Kumar, F. El Kourati, S.S. Kesharwani, H. Tummala, Hydrophobically modified inulin as an amphiphilic carbohydrate polymer for micellar delivery of

paclitaxel for intravenous route, International journal of pharmaceutics, 500 (2016) 32-41.

[217] M.K. Rajput, S.S. Kesharwani, S. Kumar, P. Muley, S. Narisetty, H. Tummala, Dendritic Cell-Targeted Nanovaccine Delivery System Prepared with an Immune-Active Polymer, ACS applied materials & interfaces, 10 (2018) 27589-27602.

[218] R. Dachineni, D.R. Kumar, E. Callegari, S.S. Kesharwani, R. Sankaranarayanan, T. Seefeldt, H. Tummala, G.J. Bhat, Salicylic acid metabolites and derivatives inhibit CDK activity: Novel insights into aspirin's chemopreventive effects against colorectal cancer, International journal of oncology, 51 (2017) 1661-1673.

[219] R. Sankaranarayanan, C.K. Valiveti, D.R. Kumar, S.S. Kesharwani, T. Seefeldt, J. Scaria, H. Tummala, G.J. Bhat, The Flavonoid Metabolite 2, 4, 6-Trihydroxybenzoic Acid Is a CDK Inhibitor and an Anti-Proliferative Agent: A Potential Role in Cancer Prevention, Cancers, 11 (2019) 427 1-18.

[220] W.J. Smith, G. Wang, H. Gaikwad, V.P. Vu, E. Groman, D.W. Bourne, D. Simberg, Accelerated Blood Clearance of Antibodies by Nanosized Click Antidotes, ACS nano, 12 (2018) 12523-12532.

[221] Q. Yan, Y. Lu, L. Zhou, J. Chen, H. Xu, M. Cai, Y. Shi, J. Jiang, W. Xiong, J. Gao, Mechanistic insights into GLUT1 activation and clustering revealed by super-resolution imaging, Proceedings of the National Academy of Sciences, 115 (2018) 7033-7038.

[222] D.M. Blodgett, J.K. De Zutter, K.B. Levine, P. Karim, A. Carruthers, Structural basis of GLUT1 inhibition by cytoplasmic ATP, The Journal of general physiology, 130 (2007) 157-168.

[223] S. Rungaldier, W. Oberwagner, U. Salzer, E. Csaszar, R. Prohaska, Stomatin interacts with GLUT1/SLC2A1, band 3/SLC4A1, and aquaporin-1 in human erythrocyte membrane domains, Biochimica et Biophysica Acta (BBA)-Biomembranes, 1828 (2013) 956-966.

[224] J.C. Vera, A.M. Reyes, J.G. Cárcamo, F.V. Velásquez, C.I. Rivas, R.H. Zhang, P. Strobel, R. Iribarren, H.I. Scher, J.C. Slebe, Genistein is a natural inhibitor of hexose and dehydroascorbic acid transport through the glucose transporter, GLUT1, Journal of Biological Chemistry, 271 (1996) 8719-8724.

[225] R. Krupka, R. Deves, Evidence for allosteric inhibition sites in the glucose carrier of erythrocytes, Biochimica et Biophysica Acta (BBA)-Biomembranes, 598 (1980) 127-133.

[226] E. Meram, B.D. Yilmaz, C. Bas, N. Atac, O. Yalcin, H.J. Meiselman, O.K. Baskurt, Shear stress-induced improvement of red blood cell deformability, Biorheology, 50 (2013) 165-176.

[227] S. Liu, Y. Han, R. Qiao, J. Zeng, Q. Jia, Y. Wang, M. Gao, Investigations on the interactions between plasma proteins and magnetic iron oxide nanoparticles with different surface modifications, The Journal of Physical Chemistry C, 114 (2010) 21270-21276.

[228] Y.K. Lee, E.-J. Choi, T.J. Webster, S.-H. Kim, D. Khang, Effect of the protein corona on nanoparticles for modulating cytotoxicity and immunotoxicity, International journal of nanomedicine, 10 (2015) 97-113.

[229] A. Gessner, B.-R. Paulke, R. Muller, T. Goppert, Protein rejecting properties of PEG-grafted nanoparticles: Influence of PEG-chain length and surface density evaluated

by two-dimensional electrophoresis and bicinchoninic acid (BCA)-proteinassay, Die Pharmazie-An International Journal of Pharmaceutical Sciences, 61 (2006) 293-297.

[230] I. Capjak, S.S. Goreta, D.D. Jurasin, I.V. Vrcek, How protein coronas determine the fate of engineered nanoparticles in biological environment, Archives of Industrial Hygiene and Toxicology, 68 (2017) 245-253.

[231] J.D. Brain, R.M. Molina, M.M. DeCamp, A.E. Warner, Pulmonary intravascular macrophages: their contribution to the mononuclear phagocyte system in 13 species, American Journal of Physiology-Lung Cellular and Molecular Physiology, 276 (1999) L146-L154.

[232] T.J. Kindt, R.A. Goldsby, B.A. Osborne, J. Kuby, Kuby immunology, Macmillan, 2007.

[233] K.I Ogawara, K. Furumoto, Y. Takakura, M. Hashida, K. Higaki, T. Kimura, Surface hydrophobicity of particles is not necessarily the most important determinant in their in vivo disposition after intravenous administration in rats, Journal of Controlled Release, 77 (2001) 191-198.

[234] K.I. Ogawara, M. Yoshida, K. Higaki, T. Kimura, K. Shiraishi, M. Nishikawa, Y. Takakura, M. Hashida, Hepatic uptake of polystyrene microspheres in rats: effect of particle size on intrahepatic distribution, Journal of Controlled Release, 59 (1999) 15-22.

[235] S. Stolnik, L. Illum, S. Davis, Long circulating microparticulate drug carriers, Advanced drug delivery reviews, 16 (1995) 195-214.

[236] K.I. Ogawara, M. Yoshida, Y. Takakura, M. Hashida, K. Higaki, T. Kimura, Interaction of polystyrene microspheres with liver cells: roles of membrane receptors and serum proteins, Biochimica et Biophysica Acta (BBA)-General Subjects, 1472 (1999) 165-172.

[237] K.I. Ogawara, M. Yoshida, J.-i. Kubo, M. Nishikawa, Y. Takakura, M. Hashida, K. Higaki, T. Kimura, Mechanisms of hepatic disposition of polystyrene microspheres in rats: effects of serum depend on the sizes of microspheres, Journal of Controlled Release, 61 (1999) 241-250.

[238] T. Yamaoka, Y. Tabata, Y. Ikada, Blood clearance and organ distribution of intravenously administered polystyrene microspheres of different sizes, Journal of bioactive and compatible polymers, 8 (1993) 220-235.

[239] J. Rao, Shedding light on tumors using nanoparticles, ACS nano, 2 (2008) 1984-1986.

[240] M.F. Kircher, U. Mahmood, R.S. King, R. Weissleder, L. Josephson, A multimodal nanoparticle for preoperative magnetic resonance imaging and intraoperative optical brain tumor delineation, Cancer research, 63 (2003) 8122-8125.

[241] S.M. Moghimi, A.J. Andersen, S.H. Hashemi, B. Lettiero, D. Ahmadvand, A. Hunter, T.L. Andresen, I. Hamad, J. Szebeni, Complement activation cascade triggered by PEG–PL engineered nanomedicines and carbon nanotubes: The challenges ahead, Journal of Controlled Release, 146 (2010) 175-181.

[242] A. Chanan-Khan, J. Szebeni, S. Savay, L. Liebes, N. Rafique, C. Alving, F. Muggia, Complement activation following first exposure to pegylated liposomal doxorubicin

(Doxil®): possible role in hypersensitivity reactions, Annals of Oncology, 14 (2003) 1430-1437.

[243] S.M. Moghimi, I. Hamad, T.L. Andresen, K. Jørgensen, J. Szebeni, Methylation of the phosphate oxygen moiety of phospholipid-methoxy (polyethylene glycol) conjugate prevents PEGylated liposome-mediated complement activation and anaphylatoxin production, The FASEB journal, 20 (2006) 2591-2593.

[244] A. Luciani, J.C. Olivier, O. Clement, N. Siauve, P.-Y. Brillet, B. Bessoud, F. Gazeau, I.F. Uchegbu, E. Kahn, G. Frija, Glucose-receptor MR imaging of tumors: study in mice with PEGylated paramagnetic niosomes, Radiology, 231 (2004) 135-142.

[245] C. He, Y. Hu, L. Yin, C. Tang, C. Yin, Effects of particle size and surface charge on cellular uptake and biodistribution of polymeric nanoparticles, Biomaterials, 31 (2010) 3657-3666.

[246] S.A. Kulkarni, S.-S. Feng, Effects of particle size and surface modification on cellular uptake and biodistribution of polymeric nanoparticles for drug delivery, Pharmaceutical research, 30 (2013) 2512-2522.

[247] R. Toy, P.M. Peiris, K.B. Ghaghada, E. Karathanasis, Shaping cancer nanomedicine: the effect of particle shape on the in vivo journey of nanoparticles, Nanomedicine, 9 (2014) 121-134.

[248] J. Lazarovits, Y.Y. Chen, E.A. Sykes, W.C. Chan, Nanoparticle–blood interactions: the implications on solid tumour targeting, Chemical Communications, 51 (2015) 2756-2767.

[249] T. Galochkina, M.N.F. Chong, L. Challali, S. Abbar, C. Etchebest, New insights into GluT1 mechanics during glucose transfer, Scientific reports, 9 (2019) 998 1-14.

[250] C.M.J. Hu, L. Zhang, S. Aryal, C. Cheung, R.H. Fang, L. Zhang, Erythrocyte membrane-camouflaged polymeric nanoparticles as a biomimetic delivery platform, Proceedings of the National Academy of Sciences, 108 (2011) 10980-10985.

[251] C.-M.J. Hu, R.H. Fang, B.T. Luk, L. Zhang, Polymeric nanotherapeutics: clinical development and advances in stealth functionalization strategies, Nanoscale, 6 (2014) 65-75.

[252] W. Gao, L. Zhang, Engineering red-blood-cell-membrane–coated nanoparticles for broad biomedical applications, AIChE Journal, 61 (2015) 738-746.

[253] J.D. Chandler, E.D. Williams, J.L. Slavin, J.D. Best, S. Rogers, Expression and localization of GLUT1 and GLUT12 in prostate carcinoma, Cancer, 97 (2003) 2035-2042.

[254] A. Krzeslak, K. Wojcik-Krowiranda, E. Forma, P. Jozwiak, H. Romanowicz, A. Bienkiewicz, M. Brys, Expression of GLUT1 and GLUT3 glucose transporters in endometrial and breast cancers, Pathology & Oncology Research, 18 (2012) 721-728.

[255] L. Venturelli, S. Nappini, M. Bulfoni, G. Gianfranceschi, S. Dal Zilio, G. Coceano, F. Del Ben, M. Turetta, G. Scoles, L. Vaccari, Glucose is a key driver for GLUT1-mediated nanoparticles internalization in breast cancer cells, Scientific reports, 6 (2016) 21629 1-14.

[256] P. Carmeliet, R. Jain, Angiogenesis in cancer and other diseases. Nature 407, Vivo Assay of Human Angiogenesis, 267 (2000) 249-257.

[257] A.C. Anselmo, S. Mitragotri, Nanoparticles in the clinic, Bioengineering & translational medicine, 1 (2016) 10-29.

[258] J. Meng, V. Agrahari, I. Youm, Advances in targeted drug delivery approaches for the central nervous system tumors: the inspiration of nanobiotechnology, Journal of Neuroimmune Pharmacology, 12 (2017) 84-98.

[259] J.M. Lajoie, E.V. Shusta, Targeting receptor-mediated transport for delivery of biologics across the blood-brain barrier, Annual review of pharmacology and toxicology, 55 (2015) 613-631.

[260] R. Bazak, M. Houri, S. El Achy, S. Kamel, T. Refaat, Cancer active targeting by nanoparticles: a comprehensive review of literature, Journal of cancer research and clinical oncology, 141 (2015) 769-784.

[261] V. Tambe, S. Thakkar, N. Raval, D. Sharma, K. Kalia, R.K. Tekade, Surface engineered dendrimers in siRNA delivery and gene silencing, Current pharmaceutical design, 23 (2017) 2952-2975.

[262] J. Chen, L. Cao, Z. Li, Y. Li, SIRT1 promotes GLUT1 expression and bladder cancer progression via regulation of glucose uptake, Human cell, (2019) 1-9.

[263] L. Venturelli, S. Nappini, M. Bulfoni, G. Gianfranceschi, S. Dal Zilio, G. Coceano, F. Del Ben, M. Turetta, G. Scoles, L. Vaccari, Glucose is a key driver for GLUT1-mediated nanoparticles internalization in breast cancer cells, Scientific reports, 6 (2016) srep21629.

[264] G. Sahay, E.V. Batrakova, A.V. Kabanov, Different internalization pathways of polymeric micelles and unimers and their effects on vesicular transport, Bioconjugate chemistry, 19 (2008) 2023-2029.

[265] A.I. Ivanov, Pharmacological inhibition of endocytic pathways: is it specific enough to be useful?, in: Exocytosis and Endocytosis, Springer, 2008, pp. 15-33.

[266] F. Gu, R. Langer, O.C. Farokhzad, Formulation/preparation of functionalized nanoparticles for in vivo targeted drug delivery, in: Micro and Nano Technologies in Bioanalysis, Springer, 2009, pp. 589-598.

[267] S.S. Kesharwani, R. Ahmad, M.A. Bakkari, M.K. Rajput, R. Dachineni, C.K. Valiveti, S. Kapur, G.J. Bhat, A.B. Singh, H. Tummala, Site-directed non-covalent polymer-drug complexes for inflammatory bowel disease (IBD): Formulation development, characterization and pharmacological evaluation, Journal of Controlled Release, 290 (2018) 165-179.

[268] D. Dutta, J.G. Donaldson, Search for inhibitors of endocytosis: Intended specificity and unintended consequences, Cellular logistics, 2 (2012) 203-208.

[269] L. Kou, J. Sun, Y. Zhai, Z. He, The endocytosis and intracellular fate of nanomedicines: Implication for rational design, Asian Journal of Pharmaceutical Sciences, 8 (2013) 1-10.

[270] G.M.N. Neubi, Y. Opoku-Damoah, X. Gu, Y. Han, J. Zhou, Y. Ding, Bio-inspired drug delivery systems: an emerging platform for targeted cancer therapy, Biomaterials science, 6 (2018) 958-973.

[271] S. Muro, Challenges in design and characterization of ligand-targeted drug delivery systems, Journal of Controlled Release, 164 (2012) 125-137.

[272] D.E. Large, J.R. Soucy, J. Hebert, D.T. Auguste, Advances in Receptor-Mediated, Tumor-Targeted Drug Delivery, Advanced Therapeutics, 2 (2019) 1800091.

[273] K.M. Huttunen, M. Gynther, J. Huttunen, E. Puris, J.A. Spicer, W.A. Denny, A Selective and Slowly Reversible Inhibitor of l-Type Amino Acid Transporter 1

(LAT1) Potentiates Antiproliferative Drug Efficacy in Cancer Cells, Journal of medicinal chemistry, 59 (2016) 5740-5751.

[274] L. Li, X. Di, M. Wu, Z. Sun, L. Zhong, Y. Wang, Q. Fu, Q. Kan, J. Sun, Z. He, Targeting tumor highly-expressed LAT1 transporter with amino acid-modified nanoparticles: toward a novel active targeting strategy in breast cancer therapy, Nanomedicine: Nanotechnology, Biology and Medicine, 13 (2017) 987-998.

[275] L. Napolitano, M. Scalise, M. Koyioni, P. Koutentis, M. Catto, I. Eberini, C. Parravicini, L. Palazzolo, L. Pisani, M. Galluccio, Potent inhibitors of human LAT1 (SLC7A5) transporter based on dithiazole and dithiazine compounds for development of anticancer drugs, Biochemical pharmacology, 143 (2017) 39-52.

[276] E.C. Calvaresi, P.J. Hergenrother, Glucose conjugation for the specific targeting and treatment of cancer, Chemical science, 4 (2013) 2319-2333.

[277] R.S. Santos, C. Figueiredo, N.F. Azevedo, K. Braeckmans, S.C. De Smedt, Nanomaterials and molecular transporters to overcome the bacterial envelope barrier: Towards advanced delivery of antibiotics, Advanced drug delivery reviews, 136 (2018) 28-48.

[278] D. Xu, G. You, Loops and layers of post-translational modifications of drug transporters, Advanced drug delivery reviews, 116 (2017) 37-44.

[279] R.S. Brown, J.Y. Leung, P.V. Kison, K.R. Zasadny, Glucose transporters and FDG uptake in untreated primary human non-small cell lung cancer, The Journal of Nuclear Medicine, 40 (1999) 556-565.

[280] H.K. Makadia, S.J. Siegel, Poly lactic-co-glycolic acid (PLGA) as biodegradable controlled drug delivery carrier, Polymers, 3 (2011) 1377-1397.

[281] D. Lombardo, M.A. Kiselev, M.T. Caccamo, Smart Nanoparticles for Drug Delivery Application: Development of Versatile Nanocarrier Platforms in Biotechnology and Nanomedicine, Journal of Nanomaterials, 2019 (2019) 1-26.

[282] J. Wang, J.D. Byrne, M.E. Napier, J.M. DeSimone, More effective nanomedicines through particle design, Small, 7 (2011) 1919-1931.

[283] P. Belchetz, J. Crawley, I. Braidman, G. Gregoriadis, Treatment of Gaucher's disease with liposome-entrapped glucocerebroside: β-glucosidase, The Lancet, 310 (1977) 116-117.

[284] P. Chen, Z. Wang, S. Zong, D. Zhu, H. Chen, Y. Zhang, L. Wu, Y. Cui, pH-sensitive nanocarrier based on gold/silver core–shell nanoparticles decorated multi-walled carbon manotubes for tracing drug release in living cells, Biosensors and Bioelectronics, 75 (2016) 446-451.

[285] W. Hao, D. Liu, Y. Shang, J. Zhang, S. Xu, H. Liu, pH-triggered copolymer micelles as drug nanocarriers for intracellular delivery, RSC Advances, 6 (2016) 29149-29158.

[286] A. Parodi, C. Corbo, A. Cevenini, R. Molinaro, R. Palomba, L. Pandolfi, M. Agostini, F. Salvatore, E. Tasciotti, Enabling cytoplasmic delivery and organelle targeting by surface modification of nanocarriers, Nanomedicine, 10 (2015) 1923-1940.

[287] L. Tang, X. Yang, Q. Yin, K. Cai, H. Wang, I. Chaudhury, C. Yao, Q. Zhou, M. Kwon, J.A. Hartman, Investigating the optimal size of anticancer nanomedicine, Proceedings of the National Academy of Sciences, 111 (2014) 15344-15349.

[288] S.T. Jahan, S. Sadat, M. Walliser, A. Haddadi, Targeted therapeutic nanoparticles: an immense promise to fight against cancer, Journal of drug delivery, 2017 (2017) 1-24.

[289] F. Xiong, Z.-y. Zhu, C. Xiong, X.-q. Hua, X.-h. Shan, Y. Zhang, N. Gu, Preparation, characterization of 2-deoxy-D-glucose functionalized dimercaptosuccinic acid-coated maghemite nanoparticles for targeting tumor cells, Pharmaceutical research, 29 (2012) 1087-1097.